5101-177
Flat-Plate
Solar Array Project

DOE/JPL-1012-60
Distribution Category UC-63b

Photovoltaic Module Encapsulation Design and Materials Selection: Volume I

E. Cuddihy
W. Carroll
C. Coulbert
A. Gupta
R. Liang

June 1, 1982

Prepared for
U.S Department of Energy
Through an Agreement with
National Aeronautics and Space Administration
by
Jet Propulsion Laboratory
California Institute of Technology
Pasadena, California

(JPL PUBLICATION 81-102)

TECHNICAL REPORT STANDARD TITLE PAGE

1. Report No. JPL Pub. 81-102	2. Government Accession No.	3. Recipient's Catalog No.
4. Title and Subtitle PHOTOVOLTAIC MODULE ENCAPSULATION DESIGN AND MATERIALS SELECTION: Volume 1		5. Report Date June 1, 1982 6. Performing Organization Code
7. Author(s) E.Cuddihy, W.Carroll, C.Coulbert, A.Gupta, R.Liang		8. Performing Organization Report No.
9. Performing Organization Name and Address JET PROPULSION LABORATORY California Institute of Technology 4800 Oak Grove Drive Pasadena, California 91109		10. Work Unit No. 11. Contract or Grant No. NAS 7-100 13. Type of Report and Period Covered JPL Publication
12. Sponsoring Agency Name and Address NATIONAL AERONAUTICS AND SPACE ADMINISTRATION Washington, D.C. 20546		14. Sponsoring Agency Code

15. Supplementary Notes
Also sponsored by U.S. Department of Energy under Interagency Agreement DE-AI01-76ET20356, identified as DOE/JPL-1012-60, and JPL Project Document 5101-177. (RTOP #776-52-61)

16. Abstract

Encapsulation-material system requirements, material-selection criteria, and the status and properties of encapsulation materials and processes available to the module manufacturer are presented in detail. Technical and economic goals established for photovoltaic modules and encapsulation systems and their status are described for material suppliers to assist them in assessing the suitability of materials in their product lines and the potential of new-material products.

A comprehensive discussion of available encapsulation technology and data is presented to facilitate design and material selection for silicon flat-plate photovoltaic modules, using the best materials available and processes optimized for specific power applications and geographic sites.

Section II provides a basis for specifying the operational and environmental loads that encapsulation material systems must resist.

Section III describes encapsulation-system functional requirements and candidate design concepts and materials that have been identified and analyzed as having the best potential to meet the cost and performance goals for the Flat-Plate Solar Array Project. Sections IV, V, and VI present the available data on encapsulant material properties, fabrication processing, and module life and durability characteristics.

17. Key Words (Selected by Author(s))	18. Distribution Statement
Energy Production Economics Power Sources	Unclassified - Unlimited

19. Security Classif. (of this report)	20. Security Classif. (of this page)	21. No. of Pages	22. Price
Unclassified	Unclassified	170	

JPL 0184 1180

5101-177
Flat-Plate
Solar Array Project

DOE/JPL-1012-60
Distribution Category UC-63b

Photovoltaic Module Encapsulation Design and Materials Selection: Volume I

E. Cuddihy
W. Carroll
C. Coulbert
A. Gupta
R. Liang

June 1, 1982

Prepared for
U S Department of Energy
Through an Agreement with
National Aeronautics and Space Administration
by
Jet Propulsion Laboratory
California Institute of Technology
Pasadena, California

(JPL PUBLICATION 81-102)

Prepared by the Jet Propulsion Laboratory, California Institute of Technology, for the Department of Energy through an agreement with the National Aeronautics and Space Administration.

The JPL Flat-Plate Solar Array Project is sponsored by the Department of Energy (DOE) and forms part of the Photovoltaic Energy Systems Program to initiate a major effort toward the development of cost-competitive solar arrays.

ABSTRACT

Encapsulation-material system requirements, material-selection criteria, and the status and properties of encapsulation materials and processes available to the module manufacturer are presented in detail. Technical and economic goals established for photovoltaic modules and encapsulation systems and their status are described for material suppliers to assist them in assessing the suitability of materials in their product lines and the potential of new-material products.

A comprehensive discussion of available encapsulation technology and data is presented to facilitate design and material selection for silicon flat-plate photovoltaic modules, using the best materials available and processes optimized for specific power applications and geographic sites.

Section II provides a basis for specifying the operational and environmental loads that encapsulation material systems must resist. Potential deployment sites for which cost effectiveness may be achieved at a module price much greater than $\$0.70/W_p$, are also considered; data on higher-cost encapsulant materials and processes that may be in use and other material candidates that may be justified for special application are discussed.

Section III describes encapsulation-system functional requirements and candidate design concepts and materials that have been identified and analyzed as having the best potential to meet the cost and performance goals for the Flat-Plate Solar Array Project. Sections IV, V, and VI present the available data on encapsulant material properties, fabrication processing, and module life and durability characteristics.

FOREWORD

This document (Volume I) describes the detailed functional requirements and the status of candidate material systems and processes for photovoltaic modules. A summary of this report, outlining the basic encapsulation system requirements and the characteristics of the most promising candidate systems identified and evaluated under the Flat-Plate Solar Array Project, will be published as Volume II within two months of this document's release.

ACKNOWLEDGMENT

The authors gratefully acknowledge the assistance and encouragement of the many members of the Encapsulation Task of the Flat-Plate Solar Array Projects for their contributions to this report.

This work was sponsored by the U.S. Department of Energy through an interagency agreement, DE-AI01-76ET-20356, with the National Aeronautics and Space Administration (Task RD152, Amendment 66).

CONTENTS

Tables

Figures

SECTION I

INTRODUCTION

A. PURPOSE

This report is for photovoltaic (PV) module manufacturers, designers, and the material supply industry who may be developing and selling module encapsulant materials. The encapsulation system for a flat-plate PV module is a configuration of selected materials required to provide electrical isolation, structural support, and environmental protection for an assembly of active PV solar cells and associated electrical circuitry. The encapsulation protects the solar cells during operation, handling, shipping, installation, and maintenance. Protection is also provided for those working near modules in arrays that may be operating at electrical potentials of 1000 V above ground.

This report is a detailed summary of the encapsulation-material system requirements and material-selection criteria, and the status and properties of encapsulation materials and processes available to the module manufacturer. It is a status report and a description of the technical and economic goals established for PV modules and encapsulation systems, so that material suppliers, may assess the suitability of materials in their product lines and the potential of new-material products.

B. FLAT-PLATE SOLAR ARRAY PROJECT

The Flat-Plate Solar Array Project (FSA) of the U.S. Department of Energy (DOE) was established at the Jet Propulsion Laboratory (JPL) in 1975 to: (1) develop the technology for low-cost PV flat-plate solar arrays; and (2) stimulate industry to produce, market, and distribute PV systems for widespread residential, commercial, and governmental use. A specific goal of the FSA Project is the establishment of technologies that, if scaled up to commercial levels, would allow production of PV modules at a price of no more than $\$0.70/W_p$ (1980$). The allocation for the cost of the encapsulation material as a part of the FSA module price objective is $\$14/m^2$ (about $\$0.12/W_p$) of completed module, including any required edge seal or frame. The FSA objective for module life is 20 yr, as shown in Table 1-1.

C. SCOPE

This report will always be subject to additions and updates because progress in solar technology areas is rapid. Activities within the FSA Project and within private industry are continually providing new data on the properties and characteristics of available materials and processes and are developing new and improved ones.

This report is a comprehensive summary of available encapsulation technology and data to facilitate the design and material selection for silicon flat-plate PV modules, using the best materials available and processes optimized for specific power applications. Therefore, Section II provides the basis for specifying the operational and environmental loads that encapsulation material systems must resist.

Table 1-1. Objectives and Plans

Objectives	Plans[a]
Develop flat-module and array technology for industry use to achieve: (1) Module prices >$0.70/$W_p$ FOB (plus marketing and distribution costs) (2) Production rates sufficient to attain economies of scale (3) Operating lifetimes: ~20 yr (4) Module efficiency: >10%	Develop: (1) Selected, long-lead-time, high-payoff potential manufacturing technology for the flat-module and array manufacturing process (2) Technology through cooperation, with industry, government, and universities, relying primarily on contracts to industry (3) Module and array specifications and technology for various project application requirements Develop and use analytical and test capabilities to verify technology performance and reliability Achieve module technical readiness in 1982-1984: $0.70/$W_p$ FOB (1980$), 20-yr lifetime, >10% efficiency Transfer technology to stimulate use by industry Continue assessment of advanced module and array performance and reliability in operational environments Continue assessment of advanced technology for potentially lower-cost, higher-efficiency modules

[a]Plans and schedules are subject to change pending DOE Program approval.

It is also recognized that there will always be a wide diversity of solar-array applications and potential deployment sites for which cost effectiveness may be achieved at a module price much greater than $0.70/W_p$. Therefore, this report also includes data on higher-cost encapsulant materials and processes that may be in use, and other material candidates that may be justified for special applications. Such special applications may include remote stand-alone power sources for navigational aids, cathodic protection, electrical fences, communications, portable battery charging, irrigation pumps, etc.

The apparent emphasis on the specific pottant material ethylene vinyl acetate (EVA) reflects the extensive development and characterization already accomplished with FSA Project support. The data on EVA are presented to disseminate its characteristics as a baseline encapsulant material with the potential to meet FSA Project goals. These data are also a basis for evaluating other pottant candidates proposed by industry, and serve as guidelines for the improvement of EVA or the development of new materials. (The orderly progression of design activities required to proceed from the general PV-array operational requirements to the final selection of encapsulant materials and configuration is discussed in Section II.)

Section III describes the encapsulation system functional requirements and the candidate design concepts and materials that have been identified and analyzed as having the best potential to meet the cost and performance goals for the FSA Program. Sections IV, V, and VI summarize the available data on encapsulant material properties, fabrication processing, and module life and durability characteristics.

The technical information on encapsulation applies primarily to crystalline silicon solar cells from either sliced or ribbon-cell processes. Application of this technology to alternative PV systems must be governed by differences in cell-protection requirements, module configurations, and application environments.

Separate reports on various aspects of PV-module design have already been published; the results of which are only summarized here. References are made to the published reports for those seeking greater detail or background material.

SECTION II

PHOTOVOLTAIC SYSTEM AND MODULE FUNCTIONAL REQUIREMENTS

The one all purpose of a PV system is to produce and deliver electrical power. The purpose of encapsulation is to provide the necessary mechanical support and environmental isolation for the cells and electrical wiring system to assure their electrical performance.

As indicated in Figure 2-1, the requirements imposed on the encapsulation are defined by the specifics of the PV system, array, and module for any single or group of similar applications. Some of the key requirements, both general and system-specific, are discussed in the following sections.

There are many special applications for PV systems. However, during the next few years, two types of systems, each with certain special requirements, are expected to be the major markets for PV: (1) intermediate-load applications (25 kW to 1000 kW), analogous to past installations at Mead, Nebraska, and Mount Laguna, California, and (2) residential applications (3 kW to 20 kW) similar to the John Long Residence in Phoenix, Arizona.

The principal differences between module requirements for these two major market segments are temperature, operating voltage, and safety. Intermediate-load systems will generally be rack-mounted, free to cool from both sides, and thus will have typical maximum temperatures of $\approx 60^{\circ}C$; residential modules will typically be roof-mounted, will cool primarily from one side, and will have typical maximum temperatures of $\approx 85^{\circ}C$. Intermediate-load systems may be designed to operate at ~1000 Vdc, residential at 300 Vdc. Safety concerns with intermediate-load systems (commercial-industrial) are typically protection of workers and of the system itself; for residential systems, safety concerns are in the context of the PV modules as an integral part of a dwelling; protection of occupants and contents is the dominant concern.

The quantitative requirements described in this section and the following sections reflect these differences.

A. OPERATIONAL AND SAFETY REQUIREMENTS

1. Electrical

Efficient production of useful electrical power from PV systems frequently requires relatively high voltage, accomplished by series-parallel electrical interconnection within and between modules in the array. To prevent power loss, to preclude resistive heating damage, and to protect persons working in the vicinity, all electrically active elements (cells, interconnects, wiring, terminals) must be effectively insulated from ground and external surfaces.

Voltage isolation must be maintained under all operating conditions for the life of the module and must not be destroyed by aging, cycling, mechanical damage (e.g., from hail) or as the result of hot-spot heating (see Section VI).

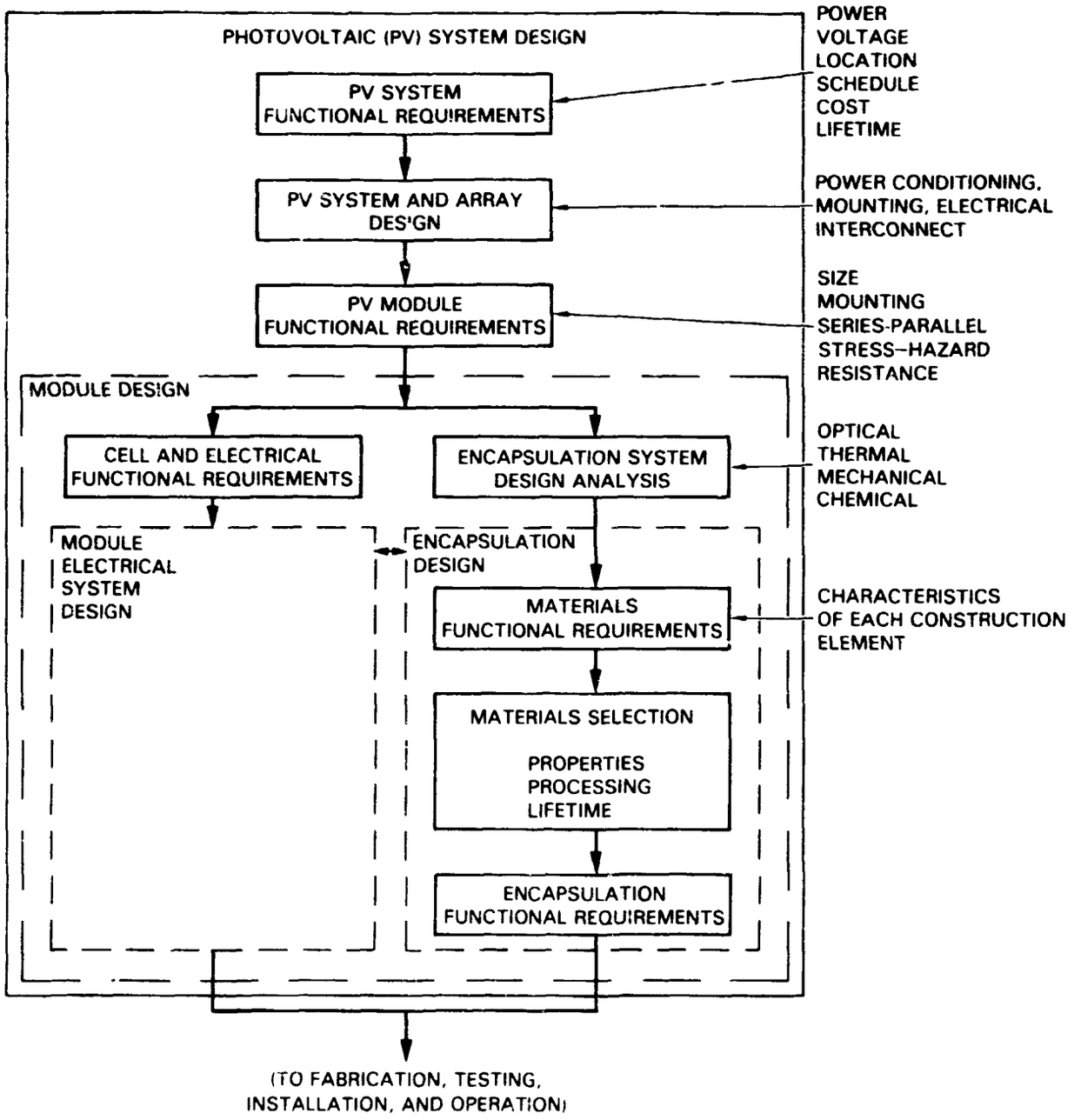

Figure 2-1. Design Activities Required for Final Selection of Encapsulant Materials

The required isolation depends on the system voltage. For residential installations, operating requirements are 300 Vdc,[1] with a design and qualification test requirement of 1500 Vdc; for intermediate-load applications, the operating requirements are 1000 Vdc, and the design and qualification test requirements are 3000 Vdc. Interim standards for achieving adequate electrical isolation have been published in Reference 1.

2. Mechanical

Considerations of fabrication, transportation, supporting structure, mechanics of installation, cost, and wind-load deflection combine to determine module size. For residential and intermediate-load applications, an upper limit of 1.2 x 1.2 m (4 x 4 ft) has been established. Modules may be assembled into larger panels before field installation.

The practical limits of conventional low-cost support construction and long-term foundation stability have led to the requirement that the modules survive and operate satisfactorily when mounted on a surface after twisting by 20 mm/m (0.25 in./ft). Brittle tensile fracture of the silicon defines the limits of stress transferred to the cells as a result of wind-load deflection of the modules. Assignment of stress limits for silicon and the implications of these limits for encapsulation materials selection and design are discussed in Section III.

3. Thermal

The voltage, and thus the power, of a silicon solar cell is temperature-dependent. The efficiency decreases with increasing temperature at the rate of about 0.5%/°C. Thus, the module encapsulation design must remove energy absorbed and converted into thermal energy by the cells, by dissipating it to the environment by radiation and convection. That is, the encapsulation system must enhance module cooling and should not itself be detrimental in causing or contributing to module heating (see Section III).

There are three characteristic temperatures for potential pottant materials:

(1) Cell temperature for rack-mounted modules (convection and radiation from both sides).

(2) Cell temperature for roof-mounted modules (constricted radiation and convection, back side).

(3) Hot-spot heating.

The range of temperatures for each of these and the resulting implications for thermal and photothermal stability are discussed in Sections III and VI.

---

[1]Worst-case, open-circuit system voltage at 100 MW/m^2 irradiance and 0°C cell temperature.

4. Codes and Regulations

Building, fire, and other safety codes are applicable to PV modules and systems, specifically where the results of failure, malfunction, or response (e.g., to fire, vandalism, etc.) may be hazardous to persons or property. Interim standards for safety (see Reference 1) have been established. Additional work on development of standards is in progress.

Federal, state, and local governmental agencies may impose standards for future PV installations, with requirements dependent on the type of system. For example, rooftop systems may be required to include only materials that:

(1) Have ignition temperatures >400°C.

(2) Do not melt during combustion.

(3) Are self-extinguishing.

(4) Produce no toxic fumes on burning, nor thermal degradation at 300°C.

5. Miscellaneous

A variety of other system or module requirements can affect encapsulation in rigorous or incidental ways. For example:

(1) Aesthetics is important for visible residential applications. Appearance and maintenance may be far more important than efficiency, cost, or other considerations.

(2) Size and weight restrictions may be imposed by limitations on transportation to remote sites.

(3) Mechanical ruggedness and durability are required for transportable military systems.

(4) Reliability in military, remote, etc., applications is required for reliability of available power and infrequent replacement.

B. ENVIRONMENTAL STRESSES AND HAZARDS

The diversity of environmental stresses and hazards to which a PV module is exposed is shown in Figure 2-2.

As with most commercial products, the approach with PV modules will be to design for survival under probable stresses and hazards, and to plan for repair or replacement in case of an extreme stress level. As indicated in Figures 2-3 and 2-4, the level of stresses and hazards vary significantly within the continental United States. This could lead to regionalized designs for specific applications.

ORIGINAL PAGE
BLACK AND WHITE PHOTOGRAPH

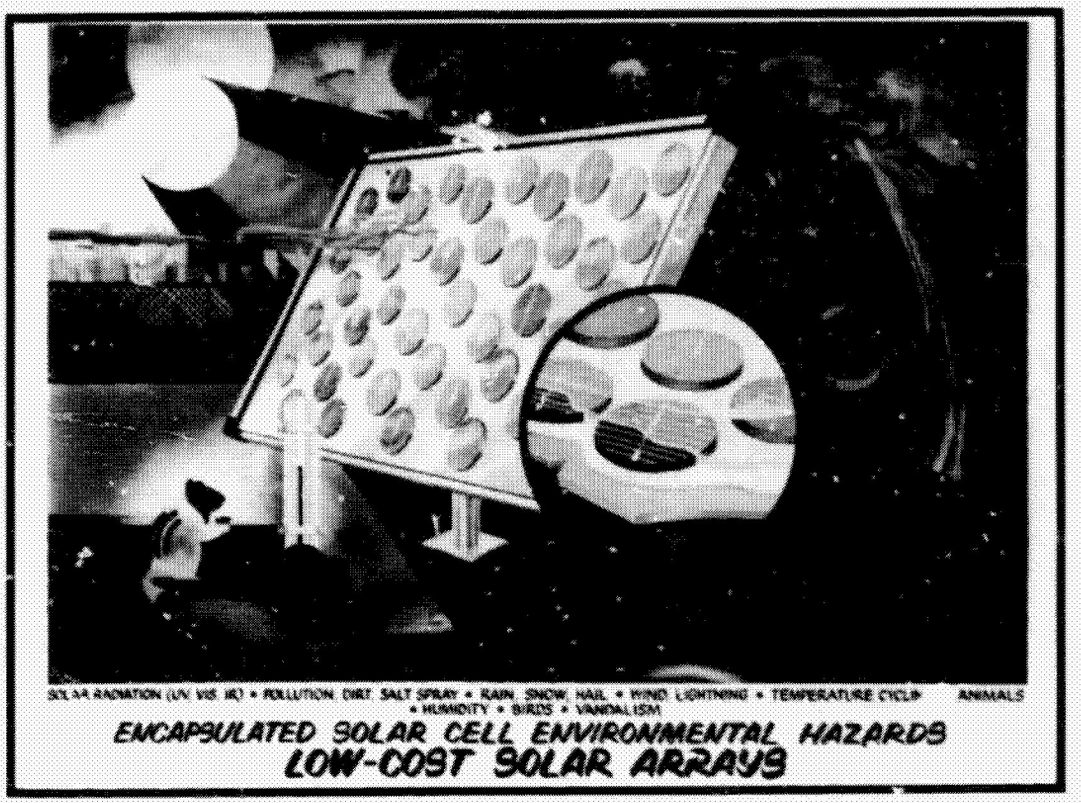

Figure 2-2. Encapsulated Solar Cell Environmental Hazards

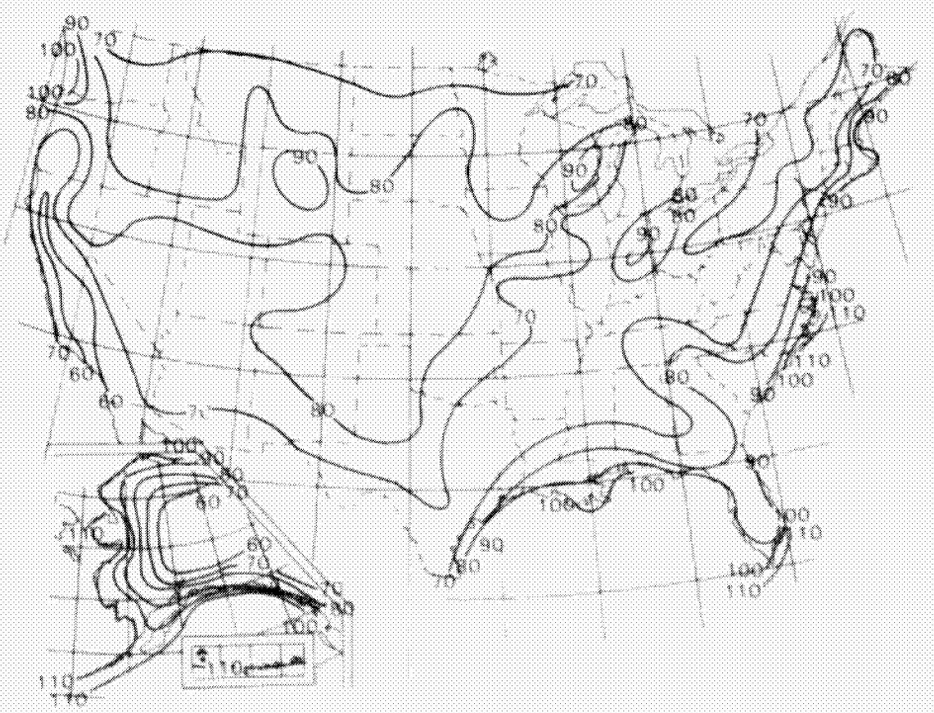

Figure 2-3. Annual Extreme Wind, 30 ft Above Ground, 50-yr Recurrence Interval (mph)

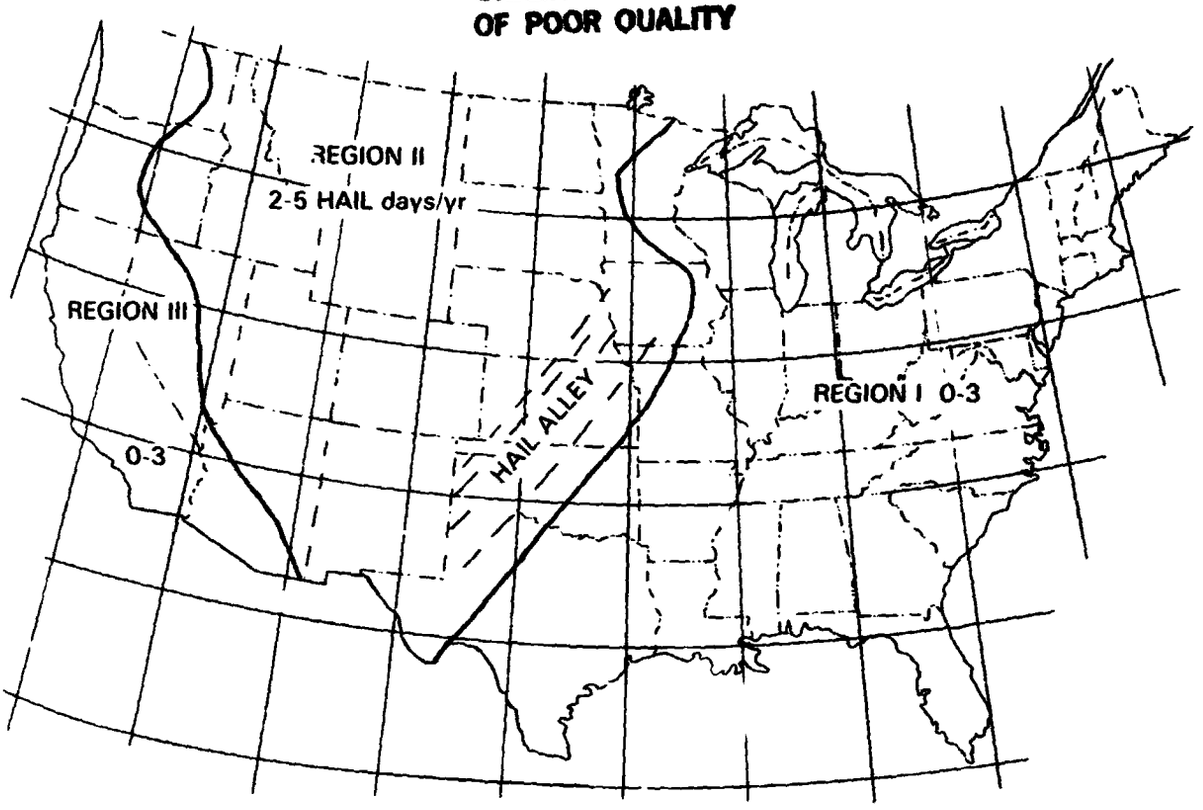

Figure 2-4. Hail Regions of the United States

The expected environmental stresses and hazards are the basis for many of the presently imposed qualification tests (see Section II, D). The simulation of specific environmental conditions in these tests is intended to identify life-limiting failure modes that are primarily mechanical and thermomechanical. Because it is impractical to simulate interactive effects of environmental stresses in these tests, successful completion of the qualification sequence does not ensure long-term performance.

In considering interactive effects, it is important to note that simultaneous combinations of environmental stress extremes (e.g., high temperature and high humidity) occur very infrequently (Reference 2).

Stresses and hazards are described in narrative form as a sequence that includes: identification, magnitude, temporal and geographic distribution, nature, key effects, and selected key interactions.

1. Temperature and Thermal Cycles

Ambient air temperatures range from -50°C to +47°C in the United States and vary daily, seasonally, and with local weather conditions (Reference 2). The temperature of the cells in PV modules may be 20°C to 30°C above ambient for rack-mounted and above 50°C or more above ambient for roof-mounted modules. Night temperatures may be well below ambient temperatures because of radiant cooling on clear, windless nights.

The two major effects of temperature are chemical-reaction rate and mechanical stress due to differential thermal expansion. In addition, the mechanical properties of many polymeric encapsulation materials are temperature-dependent.

2. Ultraviolet

Solar ultraviolet (UV) radiation can be a major cause or initiator of detrimental changes in properties of polymeric materials. The solar spectrum outside the Earth's atmosphere includes about 10% of its total energy in the UV wavelength range that is shorter than 400 nm. The shorter-wavelength portion of this is strongly absorbed by the atmosphere so that no radiation at wavelengths shorter than 290 nm reaches the Earth's surface on a clear day. The quantity, spectral energy distribution, and spatial distribution of 290 nm to 400 nm of UV rays that reach the surface are highly variable and are affected by scattering and absorption (Reference 2).

Atmospheric moisture is a major contributor to UV scattering but is also non-absorbing, so that frequently, in many locations, the global UV radiation outside the direct solar beam is equal to or greater than that in the direct beam.

Shorter-wavelength UV is typically most damaging to organic materials and is also the most susceptible to absorption and scattering, and is therefore the most variable.

3. Water: Liquid and Vapor

Water can interact in a variety of mechanical and chemical ways to affect adversely the performance of encapsulation and the electrically active components of modules.

Condensed liquid-phase moisture can be present on surfaces even at relative humidity considerably less than 100% due to radiation subcooling or the presence of deliquescent salts.

Many polymer encapsulation materials (including wood) absorb some available moisture (liquid or vapor). In so doing, these materials may undergo dimensional and mechanical property change(s), with the magnitude dependent on moisture content.

Moisture can participate directly in thermochemical and photochemical reactions with polymer encapsulation materials. An electrolyte of condensed-phase moisture and dissolved salts can participate in corrosion of electrical conductors.

The primary effect of rainfall on PV modules is the removal of part of the accumulated soil on the optical surface (see Section IV, H). Potential degradation by pollution-contaminated rain (e.g., acid rain) has been postulated, but is yet to be evaluated.

4. Wind

Wind loads are the dominant factor in mechanical design of PV modules and foundations. The effects of wind on PV installations have been studied experimentally and analytically (Reference 3).

Wind speed and the resulting force are highly variable with time and location. National distribution of wind velocities and frequencies is shown in Figure 2-3.

As described in Section III, C, deflection of a module by wind load can cause mechanical failure of the cells. A qualification test load of 50 lb/ft^2, corresponding to a wind speed of 100 mi/h, has been used for modules for several years.

5. Hail

Hailstones, falling at terminal velocity and frequently with an added wind-driven velocity vector, have caused moderate to severe impact damage to PV modules, just as they have to automobiles and other equipment.

The most severe and frequent hailstorms in the United States occur in a region along the eastern slopes of the Rocky Mountains from Texas to South Dakota, sometimes called Hail Alley.

Design and qualification-test levels of 25.4-mm (1-in.)-dia ice balls at a terminal velocity of 23.2 m/s (52 mi/h) have been adopted for modules as representative of a reasonable hazard survival (Reference 4). Because hail severity and frequency are highly variable with geographical area, alternative higher or lower levels might be appropriate, depending on the area of intended deployment.

Results of hail tests on various module designs and a range of simulated hail sizes and recommendations for improved hail resistance are described in Reference 4.

6. Snow

Mechanical loads because of accumulated snow are significantly lower than survival wind loads used for module design. Therefore, typical snow loads are not a controlling environmental stress for design. For mounting angles typical of the United States, snow will tend to slide off rather than to accumulate to a significant depth.

For roof-mounted residential applications, however, ice dams associated with rooftop snow accumulations may lead to ice damage or water incursion similar to that experienced by conventional roofing materials, with damage to the electrical functioning of modules. This has not been studied.

7. Ice

The increase in volume associated with the liquid-to-solid-phase change of water destructively manifests itself in many ways, from cracked engine blocks on poorly protected automobiles to burst water pipes. Water that can accumulate and then freeze in a constrained volume, because of either flawed module design or degradation (e.g., delamination), can produce serious damage.

8. Birds and Rodents

Animal life can cause a variety of damage by gnawing, scratching, peeling, etc., in search of food or nesting materials, or in other activi Animal excrement on the optical surface can cause loss of power output by obscuration and may react chemically with surface materials.

9. Pollutants (Soiling)

A variety of natural and man-made pollutants, solids, liquids, and gases, in varying amounts and locations, may have effects on PV modules.

The effects of light obscuration by surface contamination (soiling) are well documented (Reference 5). Module power losses up to 60% have occurred for modules with soft surface materials in a high-pollution city environment.

Pollution effects other than light obscuration and certain specifics (e.g., salt, fog) have not been examined in detail.

10. Hazards: Hurricanes and Tornadoes

At some level of intensity, it becomes economically impractical to design and construct PV modules for hurricane or tornado survival. Planned repair or replacement is more practical for the statistically rare occurrence of such severe hazards.

11. Earthquakes

The technology to analyze, design, and build structures for earthquake survival is well established but has not yet been systematically applied to PV module arrays and installations.

12. Vandalism

Road signs, billboards, and telephone-line insulators have always been attractive targets for a certain group of hunters or marksmen. It is unlikely that PV modules in remote locations will escape a similar fate. Installing hardened-design (bullet-proof) vs replace-as-required modules will become an economic and power-available reliability decision.

In urban areas, windows, skylights, walls, etc., are attractive targets for rocks, bricks, bottles, and paint-spray cans. Commercial and residential installations in certain areas may require module designs to withstand thrown objects, and installation logistics which would keep throwers and spray-can wielders at a distance.

C. MODULE LIFE AND LIFE-CYCLE ENERGY COST

The initial Project-defined objective of a 20-yr life (associated with the cost objective) was recognized at the time as an oversimplification. Since that time, the engineering definition has been clarified, as discussed in Section VI.

Though other criteria (e.g., capacity cost, aesthetics) are important for some applications of photovoltaics, the life-cycle energy cost is the most dominant for most applications.

The life-cycle cost of a PV system is the initial plant cost (including interest during construction) and the present value of operating and maintenance costs that are distributed throughout the life of the plant. The life-cycle energy cost is the life-cycle-system cost divided by the life-cycle useful energy produced.

Life-cycle energy cost is a vital tool for module- and system-design optimization. The method and details of calculating this quantity are given in FSA reports (References 6 and 7).

D. CHARACTERIZATION AND QUALIFICATION TESTS

A series of module tests have been developed at JPL and are used to characterize the thermal and electrical behavior of module designs and to qualify those designs. The environmental qualification tests demontrate the initial absence of specific design-related failure modes. There are, at this time, no simple tests to verify satisfactory lifetime.

1. Characterization Tests

The nominal operating cell temperature (NOCT) measures the thermal design and performance of the module. Because cell efficiency is temperature-dependent, the NOCT is important to module performance. Furthermore, NOCT can be used to estimate the expected temperature conditions to which encapsulation materials will be subjected. Module thermal design and design analysis are discussed in Section III, C.

Electrical characterization tests (I-V curve) reflect the electrical design and construction of the module, and are described in References 8 and 9.

2. Qualification Tests

A set of tests have been developed to ensure that modules satisfy general design requirements and provide a level of confidence that they will function within performance requirements.

The set of qualification tests falls into two groups: (1) those that specify elements of the performance, safety, and reliability of the module design, and (2) those that ensure the absence of design-related failures in response to individual specific environmental stresses.

Tests in the first group are:

(1) Baseline electrical measurement and visual inspection, to be used as a baseline for the effects of qualification tests.

(2) Ground continuity, to ensure that external conductive surfaces or components have electrical continuity to ground for safety.

(3) Electrical isolation, to ensure that cell strings are adequately isolated from the module exterior and from the ground.

(4) Hot-spot endurance, to ensure that hot-spot heating from reversed bias does not propagate beyond the initial fault and does not cause electrical safety hazards.

Tests in the second group are:

(1) Thermal cycle.

(2) Humidity-freezing cycle.

(3) Mechanical load.

(4) Twist-mounting surface.

(5) Hail impact.

The significance of these tests to encapsulation design is discussed in Section III.

E. MANUFACTURING

The manufacturing-related system and module requirements include: economical, reliable, high-volume producibility; the commercial availability of encapsulation materials, and appropriate quality assurance (QA) for all phases from incoming material to finished product.

1. Producibility

End-product cost limitations preclude the use of labor-intensive manufacturing processes used by many module manufacturers. Automation

may not be at the optimum in the foreseeable future, but processes approaching full automation will probably be required.

Expected production volume will preclude the use of relatively long cure-cycle batch processes presently in use. A production rate of 500 MW/yr, for example, translates into about 5×10^7 ft^2/yr, or about 96 ft^2 (6 modules, 4 x 4 ft each)/min, 24 h/day, 365 days/yr. A 1-h cure time would require capacity for about 180 modules to be curing at all times.

2. Material Availability

Like any design for large-scale production, the design of PV modules must be based on reliable commercial availability of encapsulation materials in suitable size, form, quantity, and quality. At a production rate of 500 MW/yr (5×10^7 ft^2), a 5-mil polymer film encapsulant would require more than 1 million lb/yr of the polymer.

3. Quality Assurance

Quality assurance procedures for large-scale commercial products will be required for all phases. Accommodation to QA requirements is a consideration in module and encapsulation system design.

SECTION III

ENCAPSULATION REQUIREMENTS AND ENGINEERING ANALYSIS

Section II describes PV array and module requirements. This section focuses on the module encapsulation system as it evolves from module requirements. To be described are, basic module designs, construction elements and functional requirements of module encapsulation systems, tabulation of potential encapsulation materials, and encapsulation design engineering are presented.

A. ENCAPSULATION CONSTRUCTION ELEMENTS

PV modules contain strings of electrically interconnected solar cells capable of producing practical quantities of electricity when illuminated with sunlight. Silicon solar cells are fragile and are especially sensitive to brittleness failure in tension and bending. The electrically conductive metallization materials (functioning as grids, interconnects, bus bars, and terminals) must be protected from excessive flexing and corrosion or other deteriorating interaction with the terrestrial environment. In short, the silicon solar cells must be mechanically supported, and the electrically conductive metallization materials must be isolated from environmental exposure.

Encapsulation materials are defined as all construction materials (excluding cells and electrical conductors) required in a PV module to provide mechanical support and environmental isolation. Early encapsulation efforts to identify a single material that could satisfy all of the encapsulation requirements and needs were unsuccessful (References 10 and 11). The understanding evolved that more than one material would have to be assembled in a composite package to fabricate an encapsulated module satisfying all of the requirements.

After an examination of all commercial and experimental flat-plate module designs, it was observed that these designs could be separated into two basic classes (see Figure 3-1). These are designated as substrate-bonded and superstrate-bonded designs, referring to the method by which the solar cells are mechanically supported. In the substrate design, the cells are bonded to a structural substrate, and in the superstrate design, the cells are bonded to a transparent structural superstrate.

From these two design options, nine basic encapsulation construction elements can be identified, which are illustrated in Figure 3-2 with their designations and encapsulation function. Fabricated modules do not need to use all nine of these construction elements, but combinations of these basic elements are incorporated in most module designs. Cross-sectional views of representative superstrate and substrate designs are illustrated in Figure 3-3, and typical industrial designs are shown in Figure 3-4.

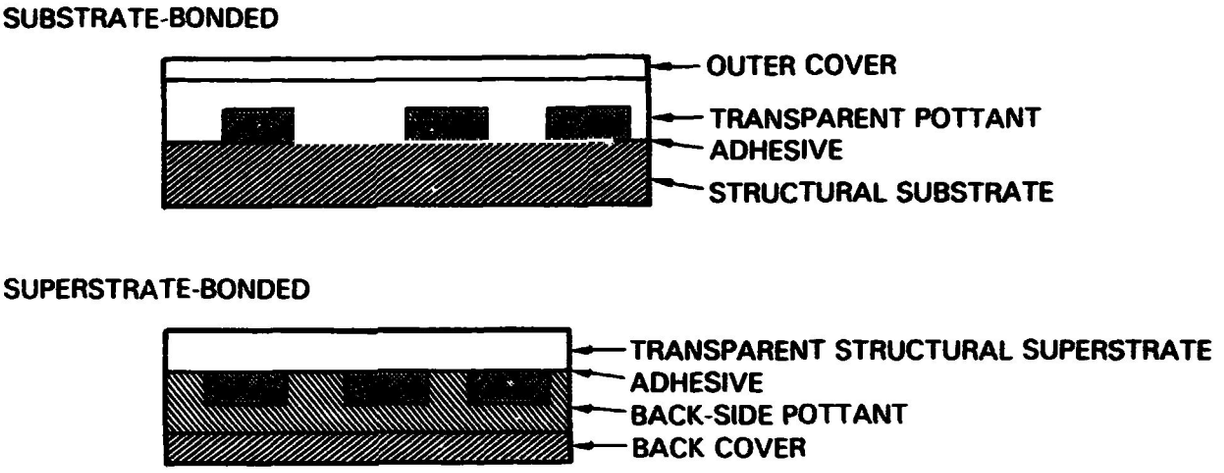

Figure 3-1. Flat-Plate Module Design Classifications

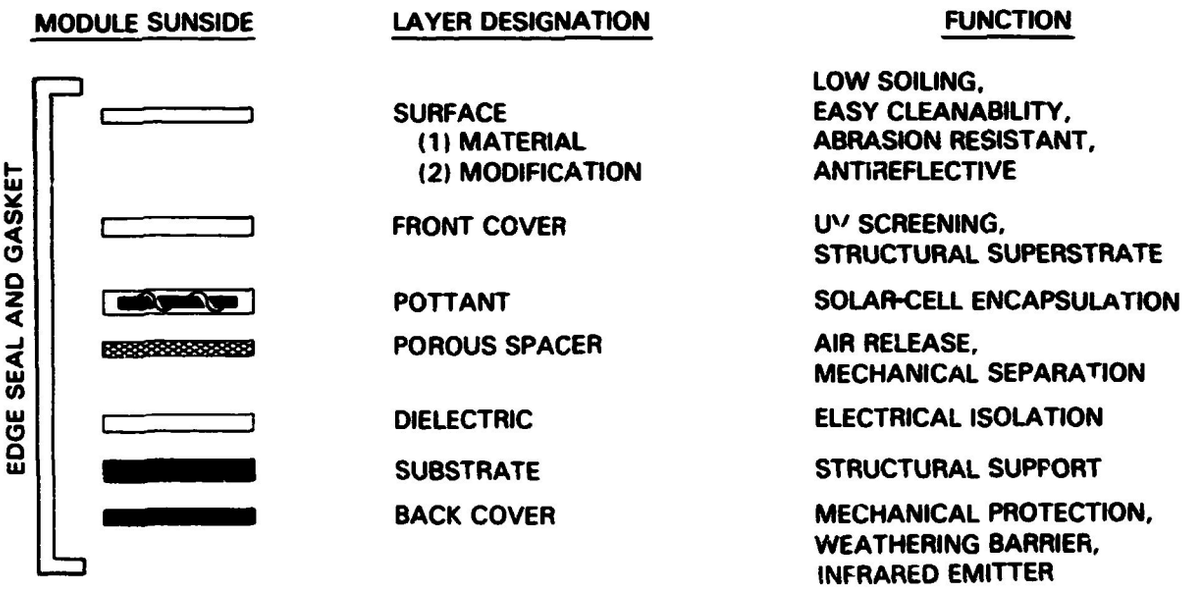

Figure 3-2. Encapsulation Materials: Module Construction Elements

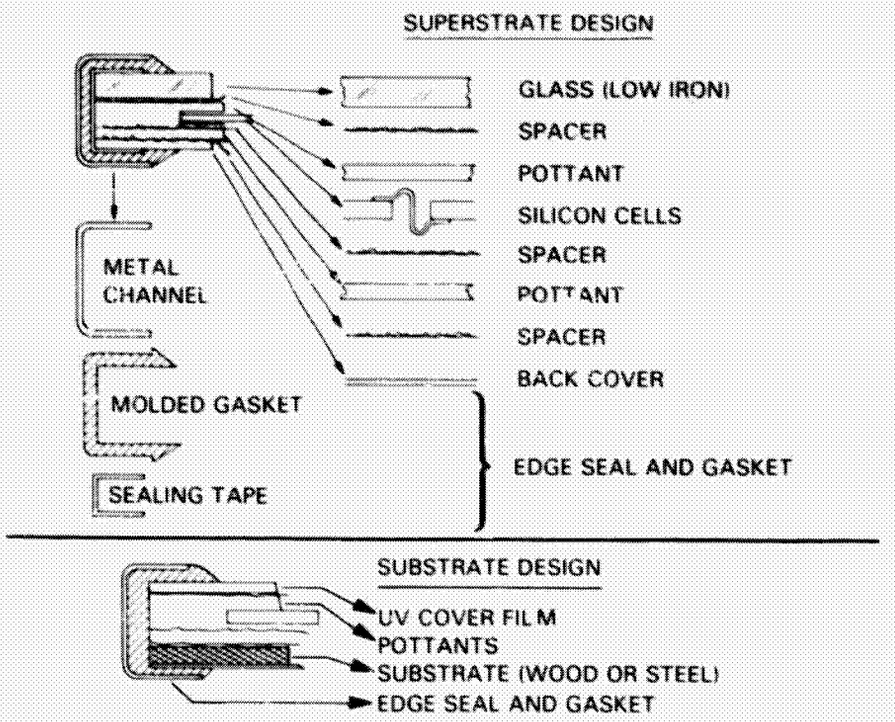

Figure 3-3. Cross-Sectional Views of Representative Superstrate and Substrate Designs

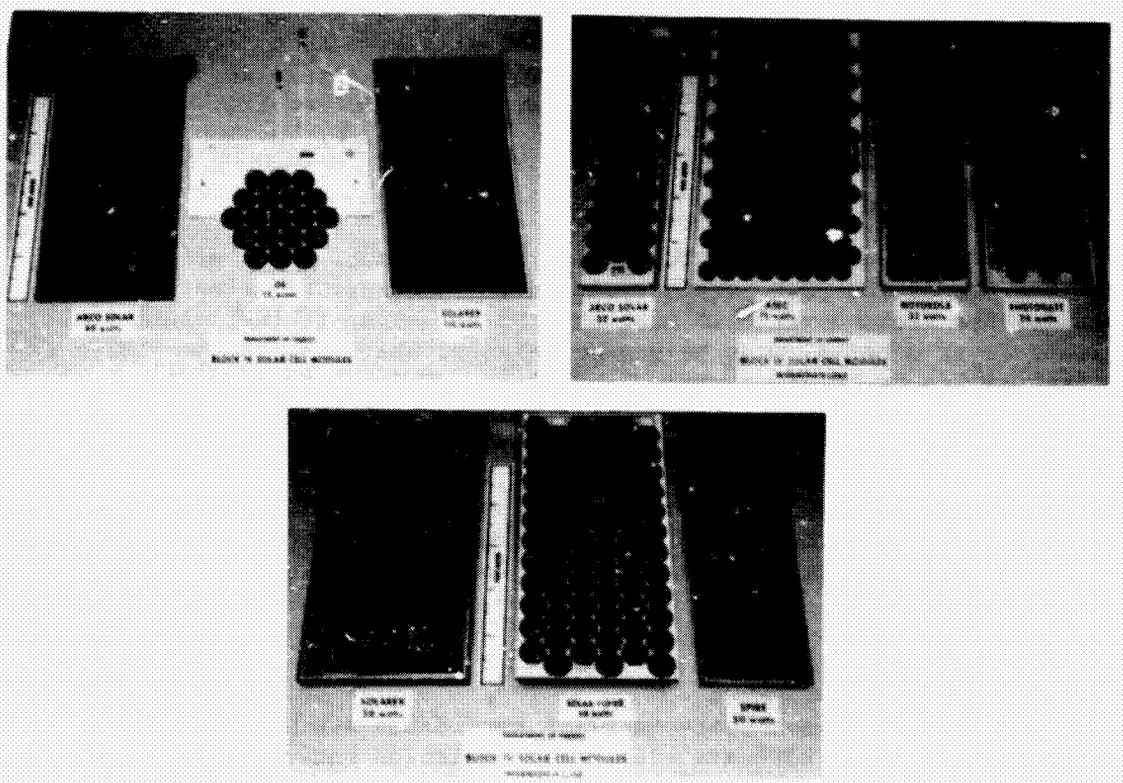

Figure 3-4. Typical Industrial Designs

1. Pottants

The central core of an encapsulation package is the pottant, a transparent material that is the actual solar-cell encapsulating medium in a module. This material totally encloses and embeds all of the solar cells and their associated electrical circuitry. The demands on a pottant material are numerous, and some of the more significant requirements are that they must:

(1) Be highly transparent in the silicon solar-cell wavelength response region of 0.4 to 1.1 μm.

(2) Be elastomeric.

(3) Function as electrical insulation for isolating high-voltage circuitry.

(4) Provide mechanical cushioning and stress relief for fragile solar cells.

(5) Be readily processible in automated module fabrication.

A more expanded discussion of pottants will be found in Section IV.

2. Superstrate and Substrate

The cells and circuitry encapsulated within an elastomeric pottant must be supported mechanically by either a structural-substrate panel or a transparent structural-superstrate panel. If supported by a substrate panel, the top surface of the soft, elastomeric pottant will have to be covered with a hard, durable front-cover film to reduce soil accumulation, as soft surfaces retain soil more easily than do hard surfaces (see Section IV).

3. Front Cover

To provide weathering protection for the pottant, and therefore to enable the use of low-cost, weather-sensitive, transparent, elastomeric materials, the front-cover film must be a UV-screening filter. Additionally, the front-cover material must be weather-stable, which limits the choice to acrylics, silicones, fluorocarbons, and glass. Thick, structurally stiff, transparent slabs or sheets of materials from these four generic weatherable-material families could also function as structural superstrates. Of these four materials, glass is the lowest in cost for structural applications. For thin-film, non-structural front-cover application (substrate design), acrylics cost less and fluorocarbons cost more. Expanded discussions of front covers, substrates, and superstrates are presented in Section IV.

4. Dielectric

Another class of substrate-material candidates are metals such as steel or aluminum. If used, adequate electrical isolation between the electrically

active cell circuitry and the metal-substrate panels must be ensured. The dielectric film shown in Figure 3-2 (with the pottant) is intended to provide adequate electrical insulation.

5. Back Cover

The back cover is a back-surface material layer that should be weatherable, hard, mechanically durable, and tough. For reasons that will be presented in Section V, the color of the back surface of the back cover layer should be white. Back covers function primarily to provide necessary back-side protection for substrates, such as corrosion protection for low-cost, mild-steel panels, or humidity barriers for moisture-sensitive panels. For superstrate designs, the back cover provides a tough overlay on the back surface of the soft, elastomeric pottant. Again, for the superstrate design, if the back cover is selected to be a metal foil, a dielectric film would be used to provide adequate electrical isolation on the back-side of the solar cells. Expanded descriptions of back covers will be found in Section IV.

6. Porous Spacer

The porous spacer indicated in Figure 3-2 is primarily an air-release mat that is inserted at various interfaces in the module to facilitate air removal (e.g., for module processing by vacuum-bag lamination). The mat is permanently retained in the fabricated module. The lowest-costing, most suitable mat materials identified are non-woven, E-glass mats, manufactured by Crane & Co., Inc., Dalton, Massachusetts. Mat materials will be discussed in greater detail in Section IV.

7. Edge Seal and Gasket, Adhesives and Primers, Surfacing Materials and Treatments

The three remaining construction elements are edge seals and gaskets, necessary primers and adhesives, and surfacing materials for (or surfacing modifications of) structural and non-structural front covers.

The functional requirements for these encapsulation construction elements enable identification of low-cost candidate materials. Functional requirements, selection criteria, and specific material candidates and costs are described in greater detail in Section IV.

B. MATERIALS INVENTORY

Table 3-1 summarizes the state-of-the-art inventory (to March 1981) of encapsulation materials, by construction element, that are being developed or identified by the FSA Encapsulation Task. The table includes those materials that are or have been used by the PV manufacturing industry. The list of materials is further subdivided into those materials still being actively considered by the FSA Encapsulation Task, and those materials that were once considered but have been deleted from FSA R&D activities.

Table 3-1. Inventory of Encapsulation Materials

	Commercial Materials		FSA Materials Still in Evaluation		Materials Assessed and Deleted from FSA List
Front Covers	Low-iron, tempered, soda-lime glass Borosilicate glass Plexiglas, lucite acrylic sheet Lexan (polycarbonate) Tedlar 400 XRB 160 SE film Llumar weatherized polyester film Korad 212 acrylic film	Front Covers	X-22416 acrylic film (3M) X-22417 acrylic film (3M) Tedlar 100 BG 30 UT (Du Pont) Tedlar 200 SRB 160 SE (Du Pont)	Front Covers	Korad 212 acrylic film Silicone/acrylic copolymer film
Pottants	Polyvinyl butyral (PVB) Silicone rubber (RTV-614, Sylgard 184) Silicone gels Ethylene vinyl acetate (EVA)	Pottants	Ethylene vinyl acetate Ethylene methyl acrylate Poly-n-butyl acrylate Aliphatic polyether urethanes	Pottants	Polyvinyl chloride plastisol Ethylene propylene rubber Q1-2577 silicone resin Silicone/acrylic copolymer liquid Ethylene methyl acrylate Ionomer (Du Pont)
Substrates	Glass, tempered or annealed Lexan (polycarbonate) Porcelainized steel Glass-fiber-reinforced polyester Pressed paper board (shingle design) Aluminum NEMA-G10 epoxy board	Substrates	Hardboards (wood) Mild steel Glass-reinforced concrete	Substrates	Strandboards Galvanized steel Kraft paper honeycombs Paper boards Plywood
Back Covers	Mylar (clear) White-pigmented Tedlar Aluminum foil/Tedlar Tedlar/aluminum foil/Tedlar Tedlar/stainless-steel foil/Tedlar Black polyethylene	Back Covers	Scotchpar-20CP-white polyester (3M) White Korad (XCEL) Polyester/aluminum foil/polyester White melamine formaldehydes (for wood) 3M white acrylic film (being developed) Corrosion-prevention coatings for mild steel (see Table 4-12) White pigmented pottants	Back Covers	Stainless-steel foil
Spacer	Craneglas non-woven glass mats	Spacer	Craneglas non-woven glass mats	Spacer	Non-woven polyester glass mats Paper tissue
Dielectric Film	White Korad acrylic film (XCEL)	Dielectric Films	White Korad acrylic (XCEL) Scotchpar-20CP-white polyester		
Edge Gaskets	Silicone rubber Neoprene	Edge Gaskets	See text		
Edge Seals	Silicones Polysulfides Butyls	Edge Seals	See text		
Edge Frames	Aluminum extrusion Cor-Ten steel extrusion Pultrusion fiber-reinforced polyester	Surface	See text for surfacing materials and modifications		
Surface-Dirt Cover	Q1-2577 silicone resin (Dow Corning)				

Specific materials for edge gaskets, edge seals, surface treatments and mild-steel corrosion-protection coatings are being identified by the Encapsulation Task. (Refer to Section IV for a description of these material activities and present trends.)

For a description of the engineering performance and outdoor-exposure behavior of commercial and experimental modules made with some of the encapsulation materials listed in Table 3-1, refer to Section VI.

C. ENGINEERING ANALYSIS

1. Objectives and Approach

PV modules fabricated with a combination of the construction elements have attendant requirements that must be satisfied jointly. The requirements are:

Materials and Fabrication

(1) Identification of materials that will fulfill the functions of each of the construction elements.

(2) Materials and designs amenable to high-speed automated fabrication.

Engineering

(3) Structural adequacy of the module to resist mechanical failure from wind loads, ice layers, hail, etc.

(4) Electrical isolation (insulation) of the electrically-active components for safety considerations, with a 3000-Vdc breakdown requirement.

(5) Maximum-possible optical transmission to the solar cells through the transparent material layers situated above the solar cells.

(6) Lowest-possible module operating temperature in its service environments.

Life

(7) Long service life, with an objective of 20 yr outdoors.

(8) Resistance to interfacial debonding or delamination.

(9) Isolation of the solar cells and metallic conductors from the deteriorating action of the terrestrial environment.

Cost

(10) Accomplish all of the above at the lowest possible materials cost, preferably within the FSA cost objective of $\approx \$1.40/ft^2$ ($\$14/m^2$).

An engineering analysis of encapsulation systems is being conducted to achieve a reliable and practical engineering design, involving the previously mentioned engineering features:

(1) Structural adequacy.

(2) Electrical isolation (safety).

(3) Maximum optical transmission.

(4) Minimum module operating temperature.

A major part of this analysis is being conducted by Spectrolab, Inc., under an FSA contract, with the following objectives:

(1) Development and verification of general analytical methods and techniques, employing material costs and physical properties as data inputs, to generate for any combination of materials an optimized module design involving the following:

   (a) Minimum thickness of the structural panel satisfying FSA load requirements.

   (b) Solar cells stress to no higher than mechanical stress limits allowed.

   (c) Minimum material thicknesses required for electrical isolation (safety).

   (d) Maximum module power output as a function of module operating temperature and optical transmission to solar cells.

   (e) Mimimum life-cycle energy cost.

(2) Identification of the specific combinations of materials and associated module designs to achieve the above objectives.

(3) Generation, where possible, of encapsulation design generalities and principles and design guidelines to avoid engineering problems and failures.

The contract activity is divided into three technical phases. Phase I involves computer analysis and simulation modeling and includes experimental work only to the extent of measurement of critical material properties where the needed data did not exist and could not be estimated with the accuracy required for the computer analysis (Reference 12).

A major effort of Phase I was to identify the relevant properties of encapsulation materials needed to do the various technical analyses, such as thermal conductivities for module operating-temperature analysis, tensile modulus and strength for structural analysis, etc. The sensitivity of system response to variations in a relevant property was assessed, and predictions of the performance of specific encapsulation designs were made.

Phase I was generally done by describing real encapsulation materials in terms of the magnitude of relevant properties, rather than by chemical name, such as ethylene vinyl acetate. The impact, if any, of the interchangeability of encapsulation materials can be assessed, because the property(ies) required for comparison is known, and the system sensitivity of that property(ies) has been determined. Also, this approach identifies optimum magnitudes of relevant properties, material thicknesses, and call-outs for specifications and recommendations of candidate encapsulation materials, and the penalties to be paid for deviations from the optimum magnitudes.

Phase II of the contract will be an experimental activity that will measure the properties and performance of fabricated modules, for which properties and performance were predicted during Phase I. Necessary refinements and modifications to the computer programs and/or analytical models will be performed, depending on the deviations encountered between prediction and measurement.

Phase III will constitute preparation of engineering drawings of the most cost-effective encapsulation design. This section will describe the initial findings of the Phase I analytical work, but these findings must be treated as preliminary or indicative, awaiting Phase II validation. The computer programs will not be described nor an in-depth report made on the analytical models (see Reference 12 for those details).

2. Thermo-Optical Analysis

Thermal and optical models describing encapsulated modules were generated separately and then were combined to do the thermo-optical analysis. This was done because the incoming solar flux is partitioned between that optically transmitted to the solar cells for electrical conversion and that converted to heat. The partitioning is related to the thermal and optical properties of the encapsulation system, which is dictated by the specific combination of encapsulation materials.

The thermal model is shown in Figure 3-5. The solar cells are treated as a thin plate with an infinite area, and of uniform temperature through their thickness (no temperature gradients from front to back of the silicon). This is because the thermal conductivity of silicon is high, compared with the thermal conductivity of the organic encapsulation materials on either side of the cells. Solar flux that is absorbed by the solar cells is proportioned between electrical and heat generation. Electrical generation is calculated from knowledge of the spectral response curve for silicon solar cells and the solar-cell temperature t_c (the latter is really an iteration variable in the program).

The remaining portion of the solar flux absorbed by the cells that is not converted to electrical power is considered to be converted to heat. This heat (originating in the cells) is conducted away from the cells (H_F and H_B in Figure 3-5) through the front- and back-side encapsulation-material layers and to the surfaces for heat dissipation to the atmosphere by radiation and convection.

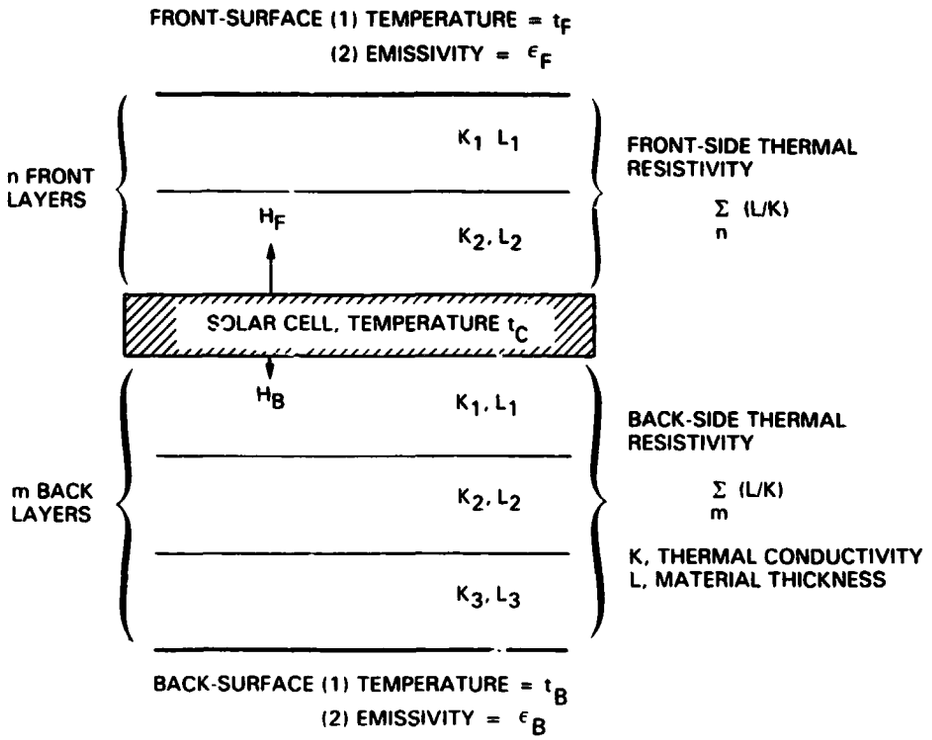

Figure 3-5. Thermal C nduction Model

The encapsulation material layers can be described by the sum of their individual thermal resistivities, which is the thickness L of the layer, divided by the thermal conductivity K of the material in the layer. Representative thermal-resistivity values for encapsulation materials are given in Table 3-2. The sum of front and back thermal resistivities of encapsulation layers for a glass-superstrate design and a wooden (hardboard)-substrate design are given in Table 3-3. For these examples, the thickness of the glass and the wood is 1/8 in. (125 mils), and are the dominant contributors to the thermal resistivity on their respective side of the module. A mild-steel substrate design would have a back-side thermal-resistivity sum less than that of the wooden-substrate design. The surfaces of the thermal model are described by the magnitude of the infrared emissivity that is involved in regulating the dissipation of heat from the surface by radiation.

For a module, this thermal model is assumed to be located in an outdoor environment, as shown in Figure 3-6. The solar-flux input to this module, direct and diffused, is algebraically distributed into the quantities that are reflected at surfaces and interfaces (absorbed by the encapsulation layers) and into the quantity that is absorbed by the solar cell for conversion to electricity and heat. The algebraic distribution is accomplished by computer solution of a set of algebraic expressions generated by a radiosity-network analysis as shown in Figure 3-7 for a single material layer, and Figure 3-8 for multiple layers. The quantity of solar flux, absorbed by the cell and converted into

Table 3-2. Thermal Resistivities

Material	K, $\frac{\text{Watts-mils}}{\text{ft}^2 - {}^{o}\text{C}}$	Representative Thickness L, mils	Thermal Resistance, L/K
Acrylic film	7×10^2	3	4.3×10^{-3}
Glass	3×10^3	125	41.6×10^{-3}
EVA	9×10^2	10	11.1×10^{-3}
Steel	2×10^5	28	0.14×10^{-3}
Wood (hardboard)	7×10^2	125	178×10^{-3}
Mylar	6×10^2	3	5×10^{-3}
Aluminum foil	7×10^5	2	0.003×10^{-3}
Stainless-steel foil	2×10^5	2	0.01×10^{-3}

Table 3-3. Thermal Resistivity Sums for Glass-Superstrate and Wooden-Substrate Module Designs

Module Design	Thermal Resistivity
Glass, EVA,[a] Mylar	$(L/K)_{Front} = 52.7 \times 10^{-3}$ $(L/K)_{Back} = 16.1 \times 10^{-3}$
Acrylic, EVA,[a] Wood, Mylar	$(L/K)_{Front} = 15.4 \times 10^{-3}$ $(L/K)_{Back} = 194.1 \times 10^{-3}$

[a]This example assumes that the EVA layer in front of the cells, and the EVA layer behind the cells are each 10 mils thick.

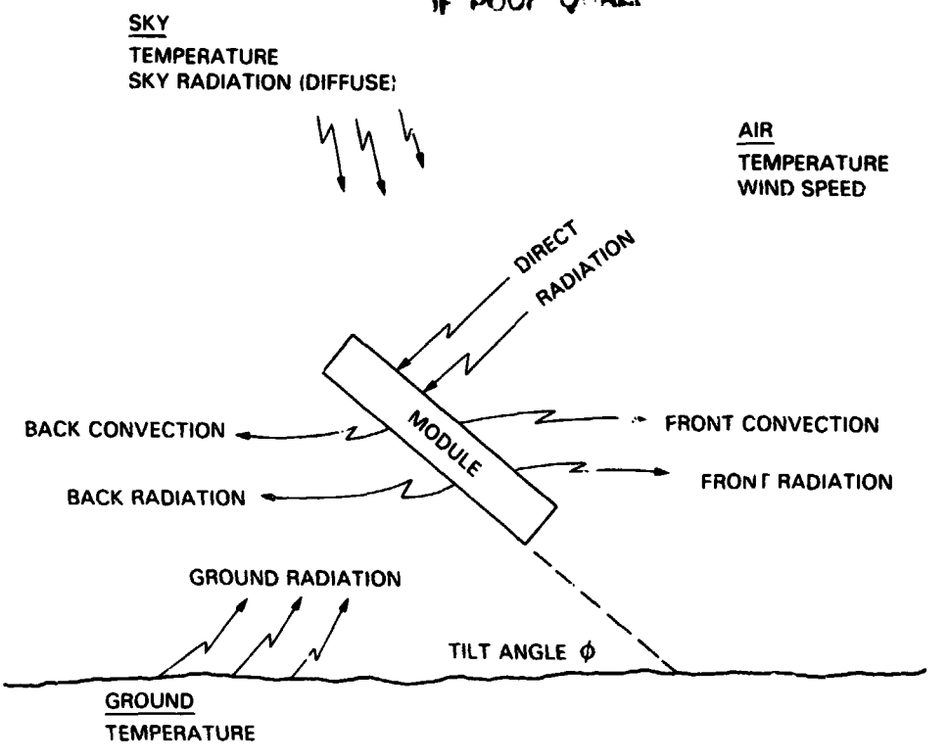

Figure 3-6. Thermo-Optical Analysis

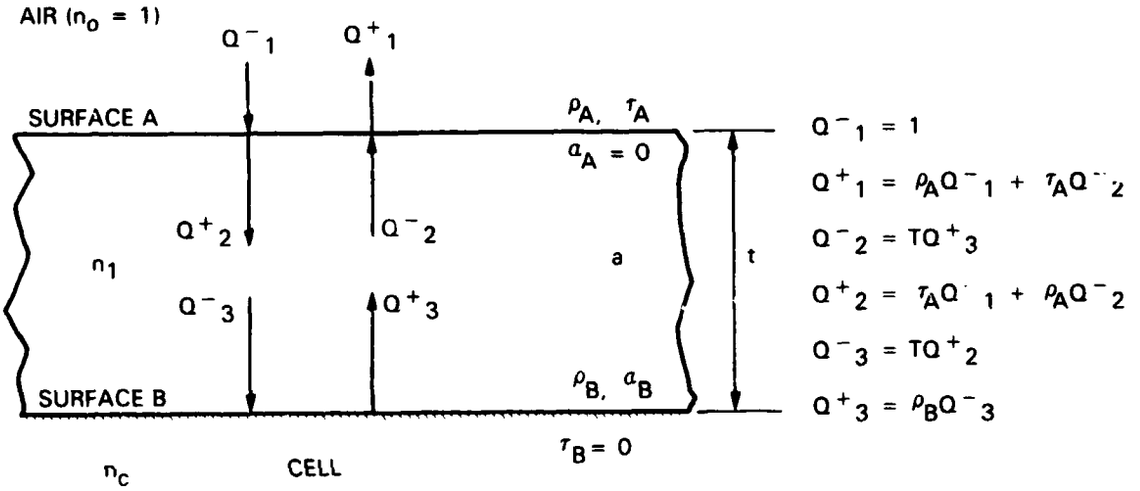

n = INDEX OF REFRACTION
ρ = REFLECTANCE OF SURFACE
a = ABSORPTANCE OF SURFACE
τ = TRANSMITTANCE OF SURFACE
a = ATTENUATION COEFFICIENT
T = TRANSMITTANCE OF LAYER = e^{-at}

Figure 3-7. Optical Model Radiosity-Network Concept: Single-Layer System

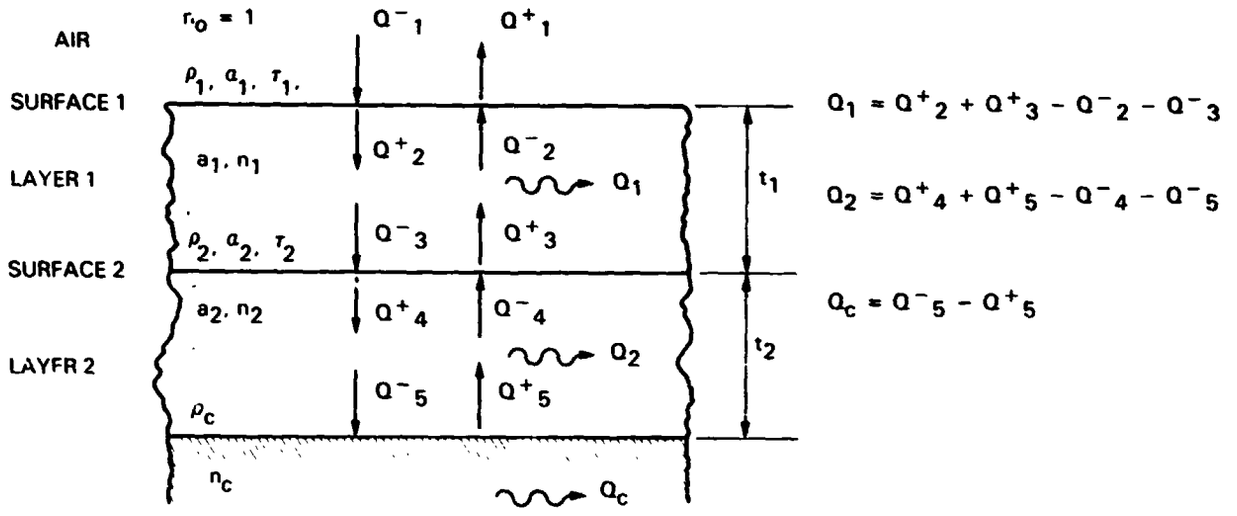

Figure 3-8. Optical Model Radiosity-Network Concept: Three-Layer System

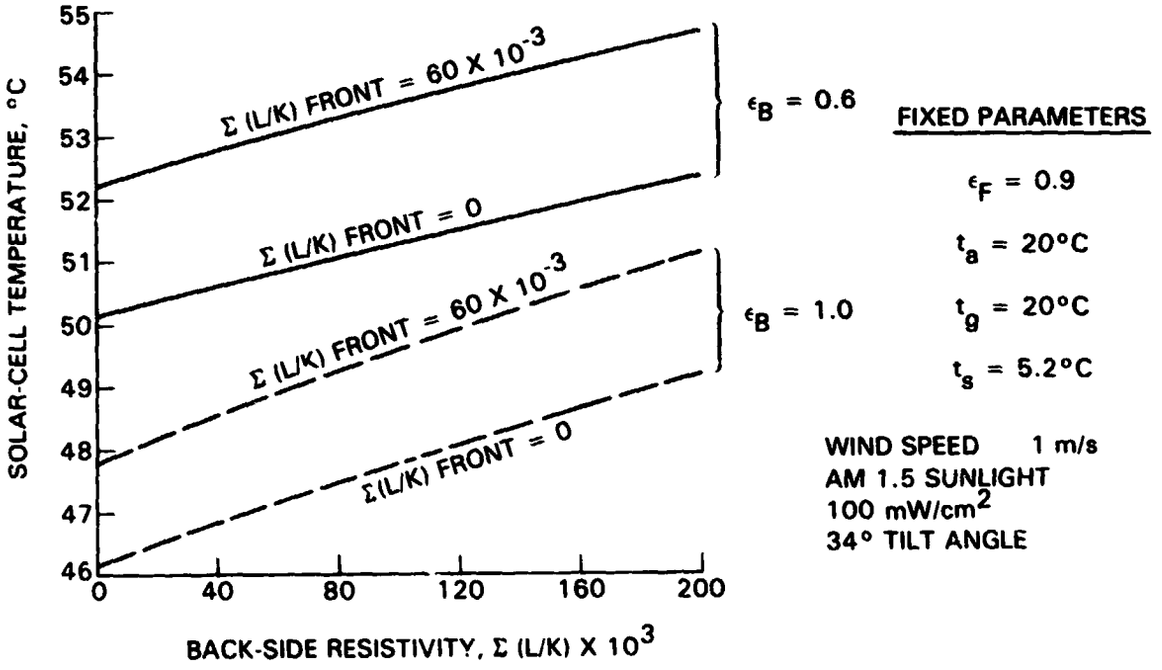

Figure 3-9. Solar-Cell Temperature: Illustrative Trend as Function of Thermal Resistivities and Back-Side Emissivity

electricity and heat, is indicated by the symbol Q_c in Figure 3-8. An expanded and detailed discussion of this optical model is reported in Reference 12. As an illustration of the computer output for the combined thermo-optical model, Figure 3-9 is a plot of solar-cell temperature t_c vs the back-side resistivity for two parametric conditions of back-side emissivity (ϵ_B) and front-side resistivity. Fixed parameters and environmental inputs for this analysis are indicated in Figure 3-9. Because the front surface of a module will be either glass or a plastic film, the front-side emissivity (ϵ_F) in the infrared will be in the order of 0.9. (The AM1.5 solar spectrum was provided by Roger Estey of JPL.)

The range of values selected for the front- and back-side thermal resistivities includes the extreme values calculated for the module designs indicated in Table 3-3.

Examining the temperature curves in Figure 3-9 for $\epsilon_B = 1.0$ indicates that a 1/8-in.-thick (3.175/ m) wooden-substrate design would have a solar-cell temperature of about 49°C for the associated fixed parameters and environmental inputs. But a glass-superstrate design would have a solar-cell temperature about 48°F, about 1°C less than a wooden-substrate module, a surprising result considering the popular expectation that a wooden-substrate module would run hotter than either a glass-superstrate design or a metal-substrate design.

Further examination of these curves in Figure 3-9 reveals that back-side surface emissivity (ϵ_B) affects the solar-cell temperature (t_c) significantly more than the front- and back-side thermal resistivities.

A major finding from the thermo-optical analysis in the Phase I program is that heat dissipation from modules, and therefore the level of module operating temperature, is regulated primarily by radiation and convection losses from the front and back surfaces, and secondarily by bulk thermal conduction through the encapsulation layers.

The singular thermal property over which there is control by material selection is the infrared emissivity of the back-cover material. The strong dependence of solar-cell temperature on back-side emissivity (ϵ_B) for a glass-superstrate design is shown in Figure 3-10. Because it is also desirable to minimize back-side absorption of any scattered or reflected solar flux, in order to prevent such absorption from becoming an added heat load entering the module, it seems best that the back cover be a white, non-metallic material. A white-pigmented plastic film or pottant will have maximum infrared emissivity and minimum solar absorptivity.

For the outdoor environment tabulated in the legend of Figure 3-9, a thermal calculation was done for the case of zero heat dissipation from the back-side of the module. All heat generated in the module from the absorbed solar flux is forced to be dissipated only from the front surface of the module. This situation may describe, for example, an integral rooftop-mounting application. In general, for all three designs, glass-superstrate, and wooden- and mild-steel substrate, the module operating temperature averaged between 75°C and 80°C. Although the temperatures for rooftop-mounting are higher, the range of temperature for the three design options are no greater than that for racking mounting.

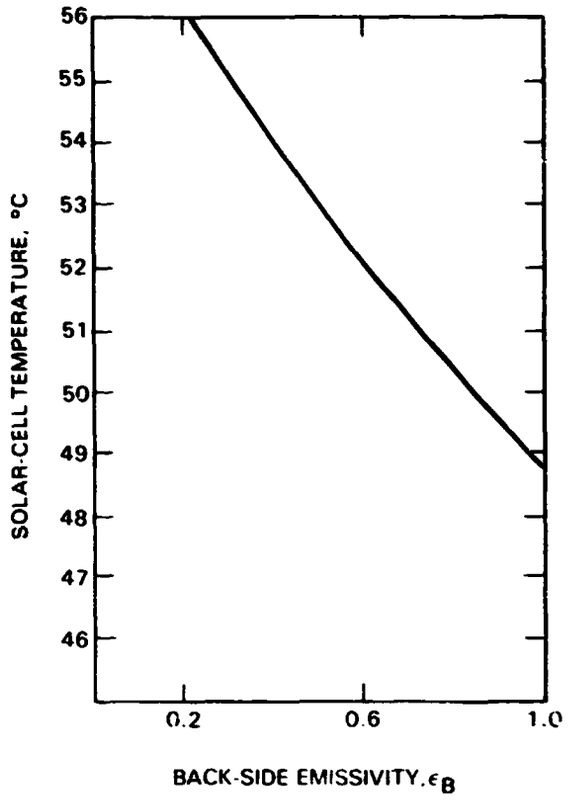

Figure 3-10. Solar-Cell Temperature vs Back-Side Emissivity, Glass-Superstrate Design (Same Fixed Parameter as Used for Figure 3-9)

The thermo-optical analysis has resulted in identifying three important findings for encapsulation:

(1) Heat dissipation from modules is limited primarily by radiation and by convection from surfaces, and to a lesser and almost trivial extent, by internal bulk thermal conduction through the front and back encapsulation layers.

(2) Lower module operating temperature is achieved primarily by maximizing surface emissivities and accessibility of both front and back surfaces to circulating air. Fins on the back surface may help lower temperature, but the reduction is small compared to maximizing the back-side surface emissivity. The major encapsulation material contribution to lower module temperature is made by a white, non-metallic back cover.

(3) With the exception of the white back covers, module operating temperature is affected negligibly by most other choices of encapsulation materials and thicknesses.

The effect of wind speed and wind direction on heat convection from the surfaces, and therefore on the operating temperature of a glass-superstrate module, was recently reported (Reference 13). For a glass module facing due

south and experiencing a constant wind speed, the lowest module temperature occurred when the winds were from either the east or west, the highest module temperatures occurred when the winds were from due south, and a north wind resulted in an intermediate temperature. This study demonstrated and reinforced the Spectrolab finding that maximizing the accessibility of the front and back surface to air, which occurs when winds blow from either east or west on a south-facing module, results in the lowest module operating temperature. When winds blow from the north or south and impinge on one surface only, cooling efficiency by convection is reduced, and the module operating temperature increases. Under conditions of north and south winds, the effect of the bulk-thermal conductivity of the front-side and back-side encapsulation layers of a glass-superstrate design is revealed. As indicated in Table 3-1, glass reduces the front-side thermal conduction compared to that of the back side; thus the efficiency of module cooling by a north wind is observed to be better than that of a south wind. Although not experimentally studied, it is interesting to speculate that a south wind would cool a wooden-substrate module more efficiently than a north wind, the opposite of the effect on a glass-superstrate module.

3. Structural Analysis

Phase I structural analysis at Spectrolab consisted of two parts: prediction of stress distribution throughout a module when deflected by a 100-mi/h wind (50 lb/ft^2 loading pressure), and prediction of stress distribution throughout a module set-up by thermal-expansion differences when a module is heated or cooled over a temperature range of 100°C. For both cases, a zero-stress state was assumed to exist throughout the module before deflection or thermal stressing. Also, the two cases have been only separately analyzed; the combined action of wind deflection and thermal stressing has not yet been analyzed.

Details of the module construction that was analyzed are:

(1) Module dimension: 1.2-m square (4 x 4-ft square).

(2) Solar cells: 10 x 10-cm square (4 x 4-in. x 0.015-in.-thick).

(3) Spacing between solar cells: 1.3 mm (0.050 in.).

For the deflection analysis, the perimeter of the module is assumed to be constrained and restricted from being twisted or deflected out of planarity. Thus, as the module deflects under a uniform wind-pressure load, the edges always remain in the plane of the undeflected, initially flat module.

Structural analysis was done on three encapsulation systems: glass-superstrate, and wooden- and mild-steel-substrate designs. The structural properties of the glass, wood, and mild steel were fixed-input data. The pottant was treated as a variable, expressed in terms of its Young's modulus. Output data consisted of the stress distribution throughout the module, calculated as a function of pottant modulus, and pottant thickness between the cells and the structural panel. The structural analysis model is summarized in Figure 3-11.

INPUT PROPERTIES

- MODULUS
- TENSILE STRENGTH
- THERMAL-EXPANSION COEFFICIENT
- PANEL THICKNESS
- SOLAR-CELL ALLOWABLE STRESSES
  - (a) DEFLECTION, 8000 lb in.^{2}
  - (b) LINEAR (THERMAL), 5000 lb in.^{2}

PRIMARY OUTPUT

GENERATED STRESS IN SOLAR CELLS AS A FUNCTION OF POTTANT THICKNESS BETWEEN CELLS AND STRUCTURAL PANEL

MODULE DESIGN FEATURES

- 1.2 x 1.2-m SQUARE
- 10 x 10-cm SQUARE CELLS
- 1.3-mm CELL SPACING

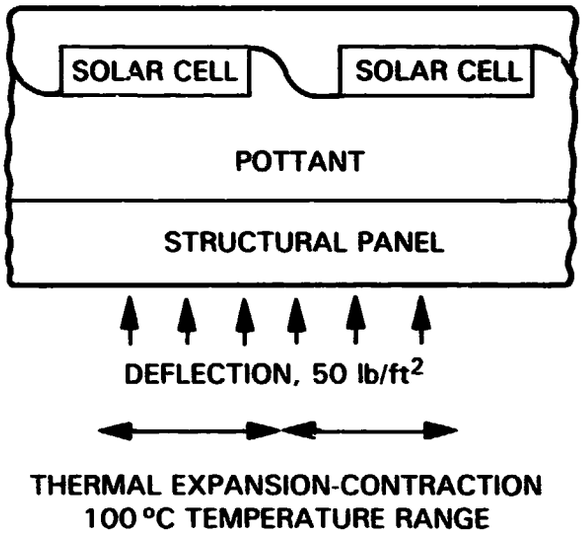

Figure 3-11. Structural Analysis, Deflection, and Thermal Stress

The calculated critical stresses are tensile stresses established in the structural panel, pottant, and solar cells. The allowable tensile stress design limit for organic polymers is a function of the Young's modulus of the polymer. The relationship between Young's modulus and tensile stress limit for polymers and the safe design stress region is given in Figure 3-12. The allowable tensile-stress design limits for glass (tempered and annealed), wood (hardboard products), and mild steel, with their Young's modulus and thermal-expansion coefficient data, are given in Table 3-4. The allowable tensile-stress design limit for 4-in.-square, single-crystal, silicon solar cells has been estimated to be 8000 lb/in.^{2} in bending, and 5000 lb/in.^{2} in tension (in-plane thermal stressing). Part of the basis for establishing these estimates was derived from a JPL report on the strength of single-crystal, silicon solar cells (Reference 14). These allowable stress limits for the cells, and the values of Young's modulus and the thermal-expansion coefficient used in the structural analysis, are also given in Table 3-4.

Details of the computer programs and a more in-depth description of the structural models are given in Reference 12. Key findings and trends are reported for each of the three designs, classified according to the structural panel: glass, wood, or mild steel.

a. Glass-Superstrate Design. Structural analysis, coupled with cost and optical analysis, reveals that the preferred glass candidate is a tempered low-iron, soda-lime glass (tempered low-iron float glass). The low iron refers

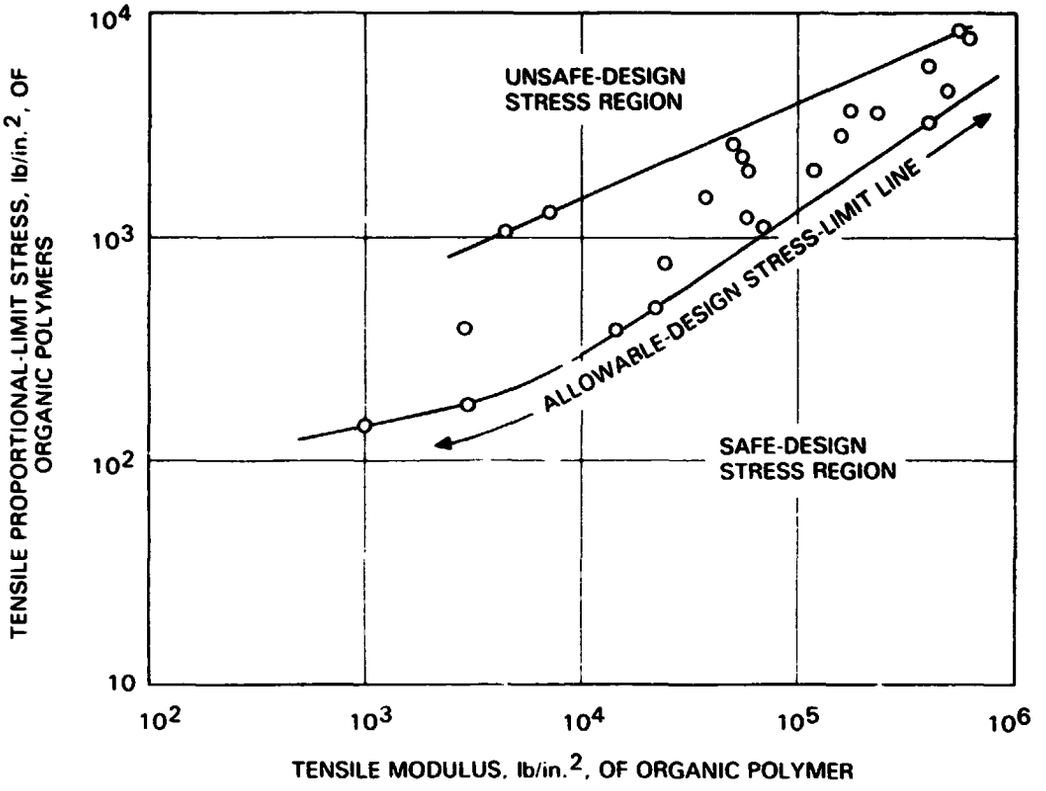

Figure 3-12. Allowable Design Stress (Tension) Limit for Organic Polymers

Table 3-4. Structural Analysis: Material Properties

Material	Modulus	Thermal-Expansion Coefficient	Allowable Stress
	lb/in.^{2}	in./in./°C	klb/in.^{2}
Glass			
Tempered	10×10^6	9.2×10^{-6}	13[a]
Annealed	10×10^6	9.2×10^{-6}	1 - 3.6[a]
Wood	$0.8\text{-}1.2 \times 10^6$	7.2×10^{-6}	2.5
Silicon	17×10^6	4.4×10^{-6}	5 - 8
Steel	30×10^6	10.8×10^{-6}	28

[a]Conservative values are based on glass-superstrate design guidelines and requirements, published as JPL reports, and discussed in Section VI-B.

specifically to the concentration of ferrous ions (Fe^{++}), which absorbs light within the solar cell operating range of 0.4 to 1.1 μm. Tempering substantially increases the allowable tensile-stress design limit, compared with other glass treatments, such as annealing (see Table 3-4). Also, soda lime as the basic glass composition is the lowest in cost, compared with other glass-composition candidates such as borosilicate.

Deflection of a 4-ft-square, 1/8-in.-thick glass plate, (Young's modulus of 10 x 10^6 lb/in.^{2} under a uniform load of 50 lb/ft^2), results in a peak bending stress in the glass of 5,340 lb/in.^{2} (<13 klb/in.^{2}, but 3.6 klb/in.^{2}) (see Table 3-4). Therefore, 1/8-in.-thick tempered glass, but not annealed glass, will handle the wind-load specifications.

In a module with a superstrate of 1/8-in.-thick, 4-ft-square tempered glass, under a wind pressure load of 50 lb/ft^2, the tensile stresses generated in the 4-in.-square solar cells (due to glass deflection) are directly related to the Young's modulus and thickness of the pottant (between the glass and the cells). For a constant Young's modulus of the pottant, the tensile stresses developed in the cells increase with decreasing pottant thickness.

Calculated relationships between solar-cell tensile stress and pottant thickness for four levels of pottant modulus E are shown in Figure 3-13 for the condition of 50 lb/ft^2 pressure loading on the glass side of the module. Assuming that 8 klb/in.^{2} is the allowable solar-cell stress in deflection, the calculated stress curves indicate that the solar cells must be separated from the glass by a pottant thickness of at least 2 to 3 mils for a pottant material having a Young's modulus of 0.5 klb/in.^{2}, which is typical of room-temperature vulcanized (RTV) silicones. For pottant modulus of 1 klb/in.^{2}, the solar-cell separation distance or pottant thickness must be >4 to 5 mils, and the thickness must be about 11 mils for a pottant modulus of 2.5 klb/in.^{2}. Using a pottant with a modulus >50 klb/in.^{2}, the tensile stress in the solar cell will exceed 8 klb/in.^{2} for any thickness.

The value of 8 klb/in.^{2} allowable cell stress is an estimate, and this estimated value does not influence mathematically the calculated solid-line relationships between cell stress and pottant modulus and thickness. When future investigation of the mechanical properties of solar cells results in a better value for the allowable cell stress, the dotted line in Figure 3-13 can be moved up or down as necessary. More important, the modulus and thickness of the pottant are structurally significant parameters that cannot be ignored in a glass module design, and that have influence on the level of the tensile stress developed in the solar cells and the cell size and thickness.

For thermal-expansion stressing (ΔT rise = 100°C), the calculated relationship between solar-cell tensile stress and pottant thickness and modulus are plotted in Figure 3-14. The effect of pottant thickness and modulus is the same as observed for the deflection analysis.

Comparing Figure 3-14 for thermal stressing with Figure 3-13 for deflection stressing reveals that the deflection stressing of the glass-superstrate module determines the minimum pottant thickness required, assuming that the allowable cell stress in tension is 5 klb/in.^{2}. Again, as with deflection stressing, if a better value of the allowable cell stress in tension is provided, the dotted line can be moved up or down.

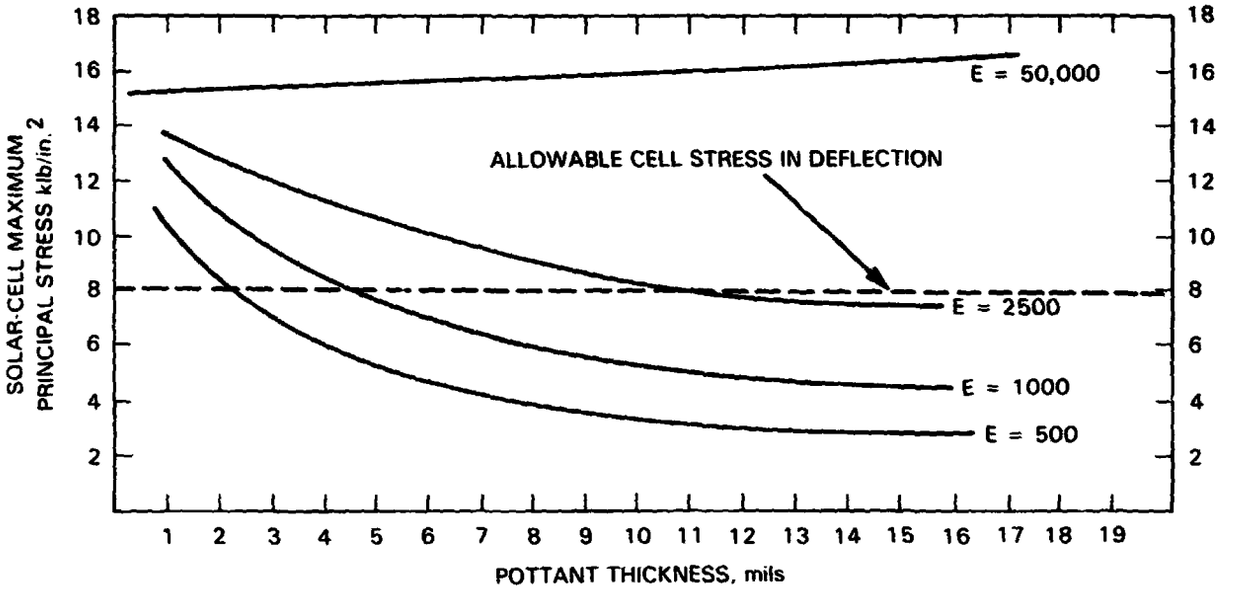

1/8-in.-THICK TEMPERED GLASS

E = POTTANT MODULUS, lb/in.^{2}

SILICON SOLAR CELL DIMENSIONS = 4 X 4 X 0.010-in. SQUARE

Figure 3-13. Deflection Analysis: Glass-Superstrate Design

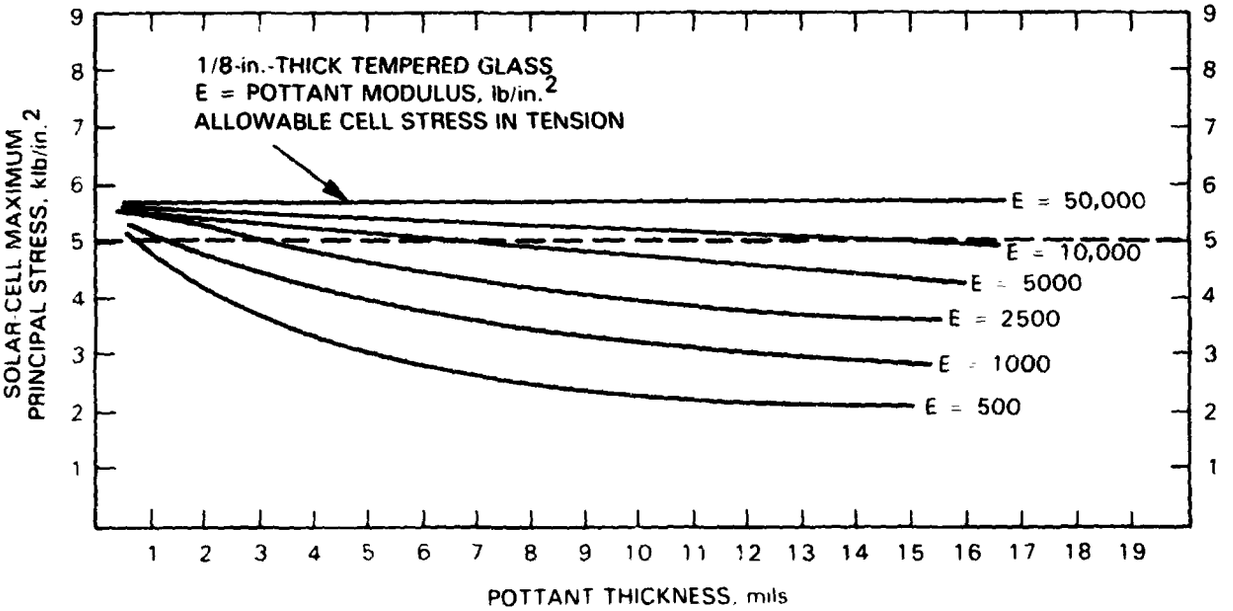

SILICON SOLAR-CELL DIMENSIONS = 4 X 4 X 0.010-in. SQUARE

Figure 3-14. Thermal Stress Analysis (ΔT = 100°C): Glass-Superstrate Design

It is important to recognize that the modulus and thickness of the pottant have structural significance relative to regulating the level of stresses in the solar cells from thermal expansion of the glass-superstrate module.

For deflection and thermal stressing of the glass module, the level of stresses developed in the pottant never exceeded the allowable design limit for polymers.

b. Mild-Steel Substrate Design. In thermal stressing over a 100°C-temperature range, preliminary results indicate that the tensile stresses developed in the pottant (and the solar cells) are independent of the thickness of the mild-steel panel. As observed for the glass-superstrate design, the tensile stresses in the cells are a function of the thickness and modulus of the pottant.

The calculated relationship between solar-cell tensile stress and pottant thickness resulting from thermal stressing is shown in Figure 3-15, for a single case of a pottant with a Young's modulus equal to 1 klb/in.^{2} (more data for other modulus levels was not available at time of publication). Assuming an allowable cell stress in tension of 5 klb/in.^{2}, the minimum pottant thickness required between the cells and the steel plate is about 4 mils. At this thickness, the tensile stresses developed in the pottant are well within the safe design limit for a polymer having a Young's modulus of 1 klb/in.^{2}. It is expected that the solid line in Figure 3-15 will generally move up as pottant modulus is increased. Thus, 4 mils of any pottant with a modulus less than 1 klb/in.^{2}, such as P-n-BA or RTV silicones, would be more than adequate.

The deflection analysis for 50-lb/ft^2 wind loading on an unribbed panel has been analyzed for a single pottant with a modulus of 1 klb/in.^{2}, and for three different thicknesses of a steel plate: 0.168 in., 0.087 in., and 0.028 in. The peak bending stress developed in a 4-ft square plate of these thicknesses under 50 lb/ft^2 of wind load are 5 klb/in.^{2} for 0.168 in., 15 klb/in.^{2} for 0.087 in., and 28 klb/in.^{2} for 0.028 in. A steel-plate thickness of less than 0.028 will experience a peak bending stress exceeding its allowable stress limit of 28 klb/in.^{2}.

For a 1-klb/in.^{2} pottant module, the calculated relationship between solar-cell tensile stress and pottant thickness for each of the three steel-plate thicknesses are plotted in Figure 3-16. Because the level of the out-of-plane deflection at constant pressure loading increases with decreasing plate thickness, the bending stresses imposed on the solar cells increase with decreasing plate thickness. For a plate thickness of 0.028 in., almost 12 mils of pottant are required between the cells and the steel plate to have the deflection stress in the cells just at 8 klb/in.^{2}, the allowable cell-stress estimate in deflection.

Increasing the plate thickness to about 0.087 in. reduces the pottant thickness demand to about 4 mils, which coincidentally matches the pottant thickness requirement for thermal stressing (see Figure 3-15). Lastly, a plate thickness of 0.168 in. is so stiff against 50 lb/ft^2 wind load that the bending stresses imposed on the solar cells are always below the allowable cell stress, down to a pottant thickness of 1 mil, which was the lower bound in the computer calculation.

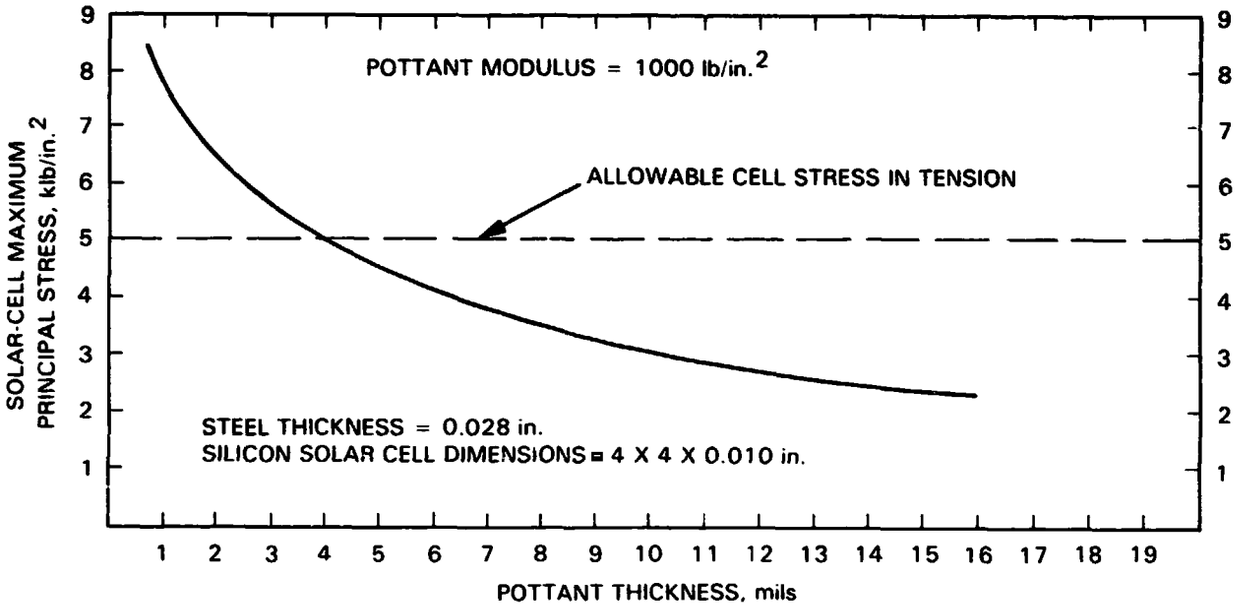

Figure 3-15. Thermal Stress Analysis (ΔT = 100°C): Steel-Substrate Design

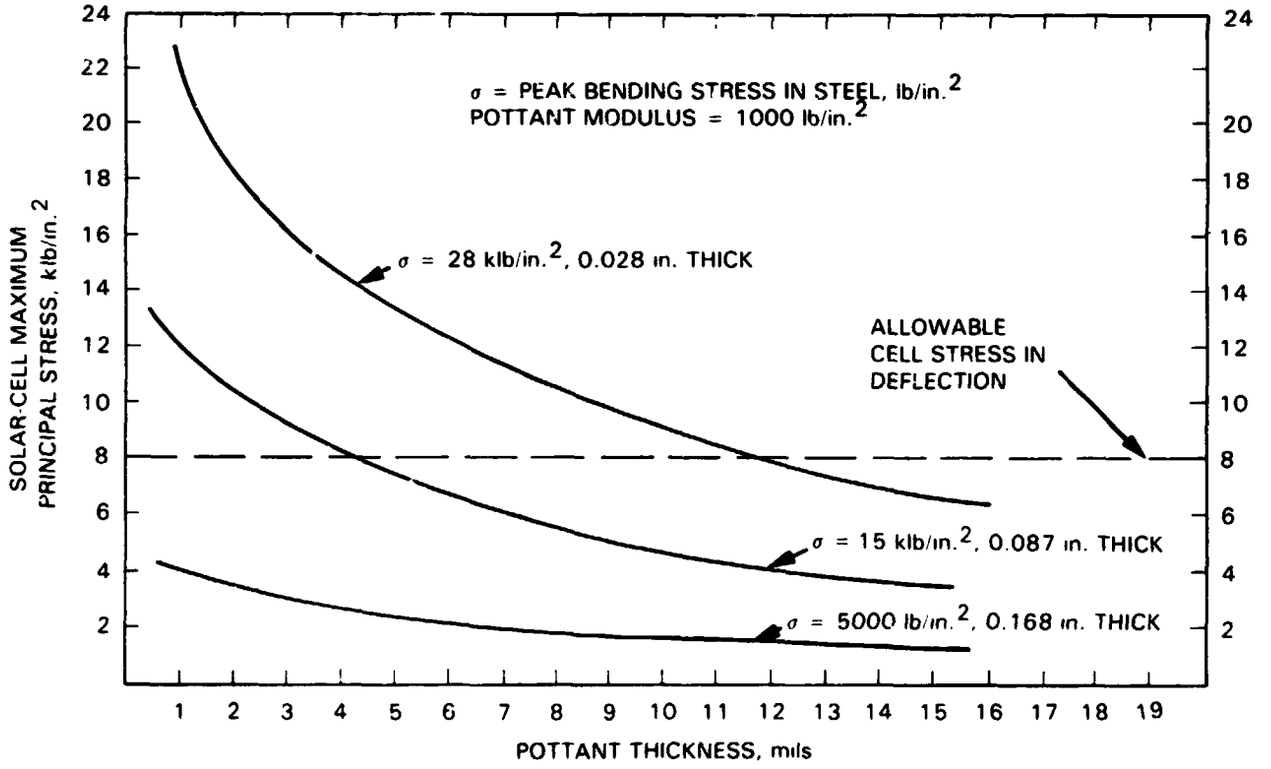

Figure 3-16. Deflection Analysis: Steel-Substrate Design

A cost-structure relationship can be explored from these computer results. The cost of mild steel averages about $\$0.007/ft^2/mil$ of thickness (see Table 4-11), therefore, the cost of 0.168-in. (168 mil)-thick mild-steel plate will be about $\$1.17/ft^2$. The cost of a 0.087-in.-thick plate would be about $\$0.61/ft^2$.

The 0.087-in. plate in deflection imposes the same thickness requirements for a pottant with a modulus of 1 klb/in.^{2}, $\approx$4 mils, as do thermal stresses (see Figure 3-15) developed over a 100°C-temperature range. If the pottant costs about \$1.00/lb (the projected cost for EVA is about \$0.95/lb), which is equivalent to about $\$0.005/ft^2/mil$ of pottant thickness, then the combined cost of a 0.087-in.-thick plate and 4 mils of pottant is about $\$0.63/ft^2$. To use the 0.028-in.-thick thinner steel plate requires a minimum 12 mils of pottant for a combined cost of $\$0.30/ft^2$.

Another way to reduce cost and the total weight of mild steel is to use stiffening ribs on the mild-steel plate. The computer program for deflection analysis (see Reference 12) can accommodate rib-design concepts. This study has not yet been done.

c. Wooden-Substrate Design. The minimum thickness of commercial hardboards is typically about 1/8 in. Thermo-optical analysis indicated that the use of 1/8-in.-thick hardboards as substrates would result in module operating temperatures comparable to those of mild-steel-substrate and glass-superstrate designs, but thicker wood panels would result in progressively higher operating temperatures.

Deflection analysis for a 50-lb/ft^2 wind load indicated that the peak bending stress in an edge-supported, 4-ft-square, 1/8-in.-thick hardboard would exceed the material's allowable design stress limit of 2.5 klb/in.^{2} (see Table 3-4). On the other hand, an unribbed 1/4-in.-thick hardboard would be deflected to a peak bending stress of 1.6 klb/in.^{2}, and therefore, has the minimum thickness permitted for an unribbed design.

For 1/4-in. hardboard, the calculated relationship between solar-cell tensile-stress-in-deflection vs thickness of a pottant with a modulus of 1 klb/in.^{2} is shown in Figure 3-17. This analysis indicates that a minimum thickness of 13 to 14 mils of pottant would be required to reduce the solar-cell bending stress to 8 klb/in.^{2}. This thick pottant requirement, and the use of a 1/4-in.-thick hardboard, is not a structurallyand thermally-efficient design.

Approaches to develop rib-design concepts for 1/8-in. hardboard to reduce the peak bending stress are described in the Phase I report (see Reference 12). For a specific rib design with a peak bending stress of 0.5 klb/in.^{2}, the calculated relationship between solar-cell bending stress and thickness of a pottant with a modulus of 1 klb/in.^{2} is also plotted in Figure 3-17. Analysis indicates that this ribbed 1/8-in. hardboard panel would be sufficiently stiff so that the peak solar-cell bending stress would be well under 4 klb/in.^{2} and virtually independent of thickness of a pottant with a modulus of 1 klb/in.^{2}.

The calculated results of the thermal-stress analysis for a wooden-substrate design are shown in Figure 3-18. The thermal-stress characteristics of a wood design are virtually independent of wooden-panel thickness, but unlike

glass and mild steel, the tensile stresses developed in the silicon solar cells are also virtually independent of pottant thickness (for pottant modulus levels up to 50 klb/in.^{2}). Thus, the magnitude of the solar-cell tensile stresses is well under the allowable solar-cell stress-design limit of 5 klb/in.^{2} for pottants with modulus up to 50 klb/in.^{2}.

The deflection analysis (Figure 3-17) has only been done for a pottant modulus of 1 klb/in.^{2}, and additional calculations involving other pottant modulus levels of ribbed-wood designs are forthcoming. The ribs on the hardboard run in one direction only, with no cross-ribbing, to facilitate back-side air circulation for module cooling.

The computer predictions for the ribbed wooden-substrate indicate that the stresses developed in the solar cell from deflection and thermal stresses are well under the allowable design stress limits, and essentially independent of pottant modulus and thickness. These findings greatly enhance the attractiveness of wood as a substrate candidate, especially when low cost is considered. Also, the thermal analysis found that the temperature of a 1/8-in.-thick wooden-substrate module would be typically only 1°C higher than a glass-superstrate or mild-steel substrate module in the same environment.

The major problem with wood is associated with humidity. The hygroscopic-expansion coefficient of wooden hardboard is $\simeq 5 \times 10^{-5}$ in./in./1% RH, and when compared with its thermal-expansion coefficient, 1% RH has the same expanding and contracting action as 7°C to 8°C. Without proper packaging, the wooden panel will dry out and shrink during vacuum lamination, as illustrated in Figure 3-19, and when reexposed to the atmosphere, the completed module will expand as moisture is slowly reabsorbed.

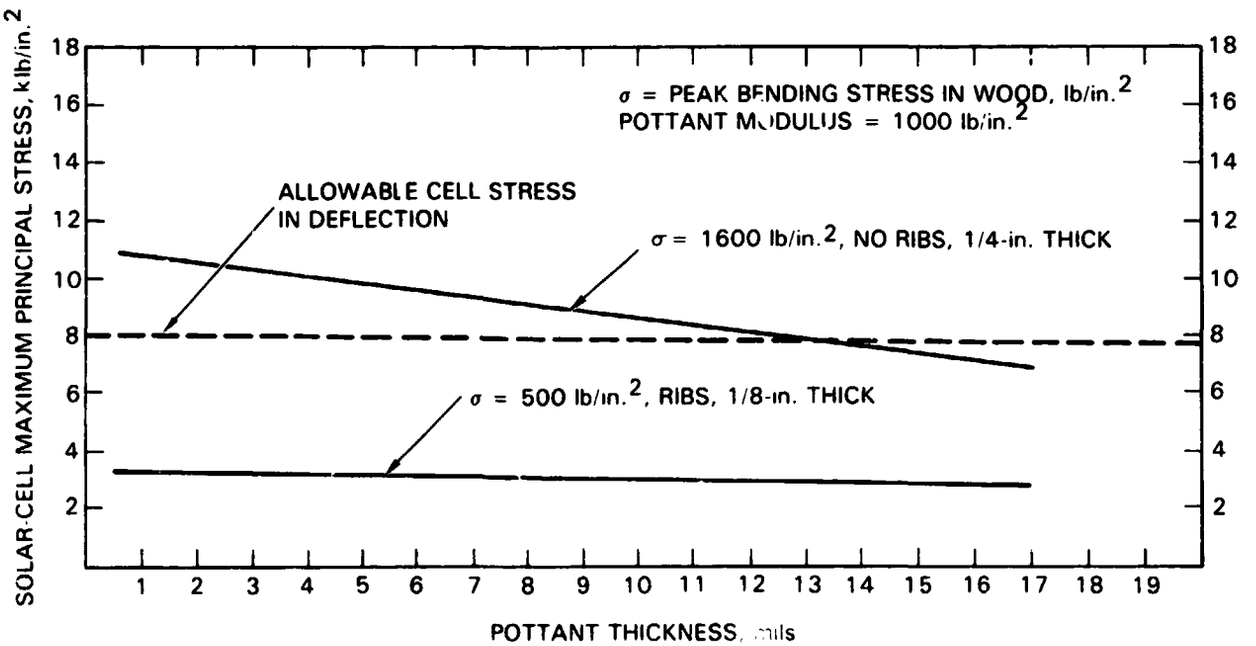

Figure 3-17. Deflection Analysis: Wooden-Substrate Design

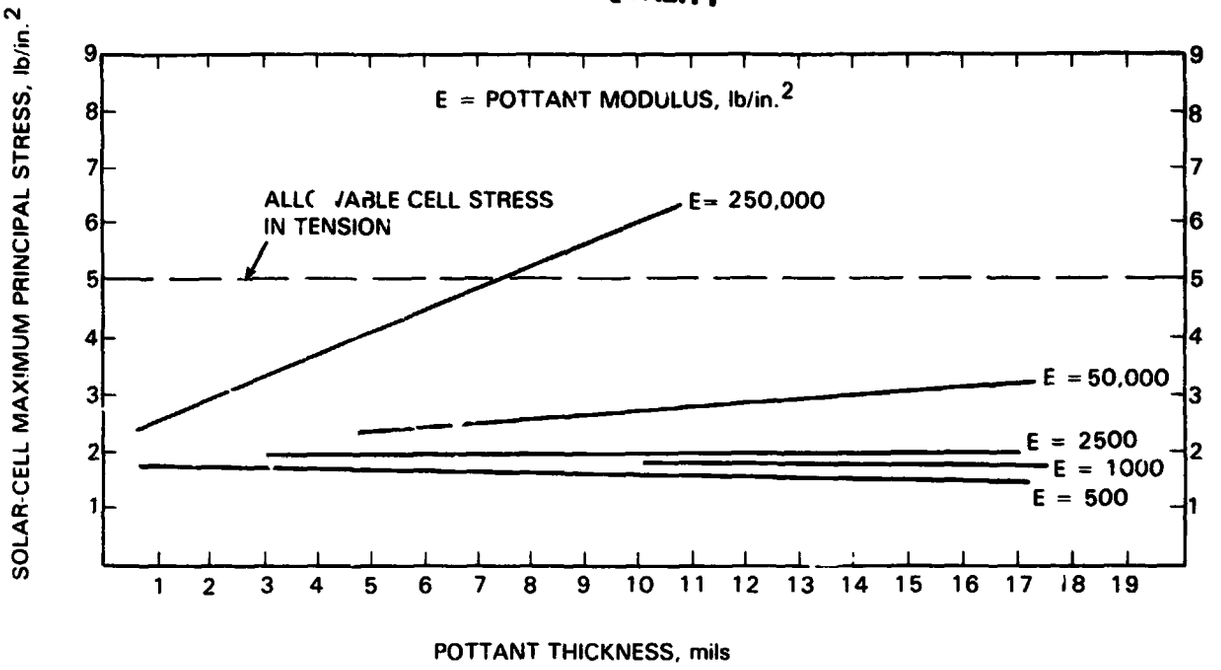

Figure 3-18. Thermal Stress Analysis (ΔT = 100°C): Wooden-Substrate Design

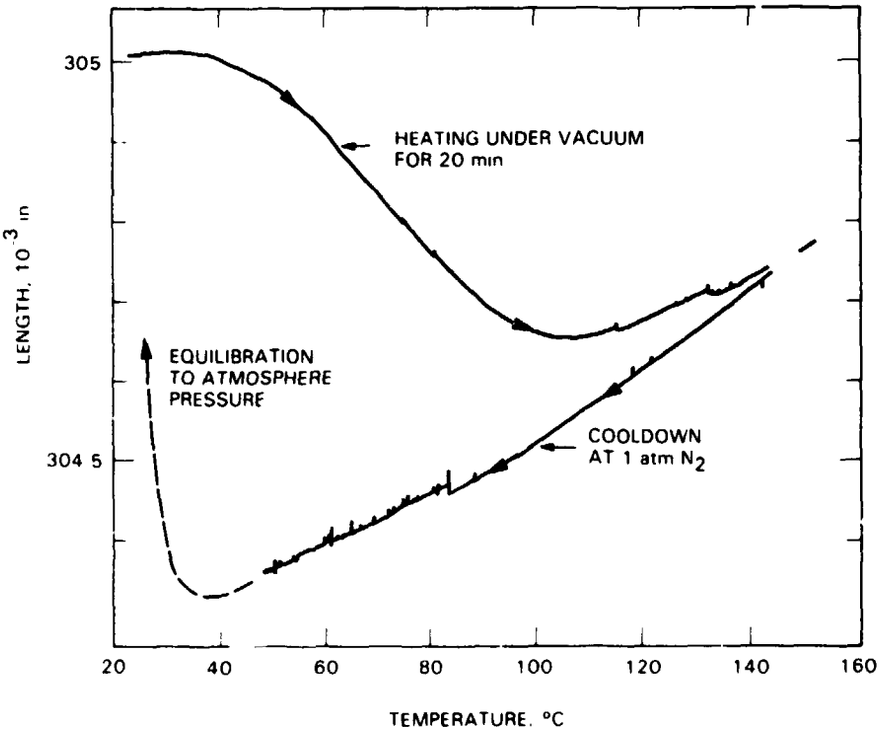

Figure 3-19. Dimensional Change of Hardboard Under Vacuum-Bag-Lamination Processing Condition

Wooden modules fabricated with EVA pottant, and without provisions for preventing wood dry-out during vacuum lamination, are being exposed outdoors as part of the Encapsulation Task minimodule exposure program and several have failed because of broken solar cells.

As part of the Phase I activities, Spectrolab performed a hygroscopic stress analysis of a 4-ft-square wood-substrate module, experiencing expansion from a dry condition at 0% RH to maximum expansion at 100% RH. Mechanical stresses throughout the module were set to zero at 0% RH. The tensile stresses, developed in the solar cells after expansion to 100% RH, are plotted in Figure 3-20 for three levels of pottant modulus and for pottant thicknesses up to 30 mils.

The results indicate a serious fabrication problem. Not even 30 mils of a pottant with a modulus of 1 klb/in.^{2}, nominally EVA, can isolate the solar cells mechanically to achieve a solar-cell stress level less than the allowed cell stress in tension if cells are bonded to a desiccated substrate and allowed to equilibrate at 100% RH. The wooden modules are presently fabricated using a single sheet of EVA laminating film, about 18 mils thick, between the cells and the wooden substrate. After lamination under 1 atm of pressure, the EVA thins to about 10 to 12 mils. Because the outdoor relative humidity has a time-average value of about 60% to 65%, the tensile stresses in the cells were estimated to be about 8.5 klb/in.^{2}, which was obtained by multiplying 0.65 by the tensile-stress value of 13 klb/in.^{2} associated with E = 1000 and a thickness of 11 mils.

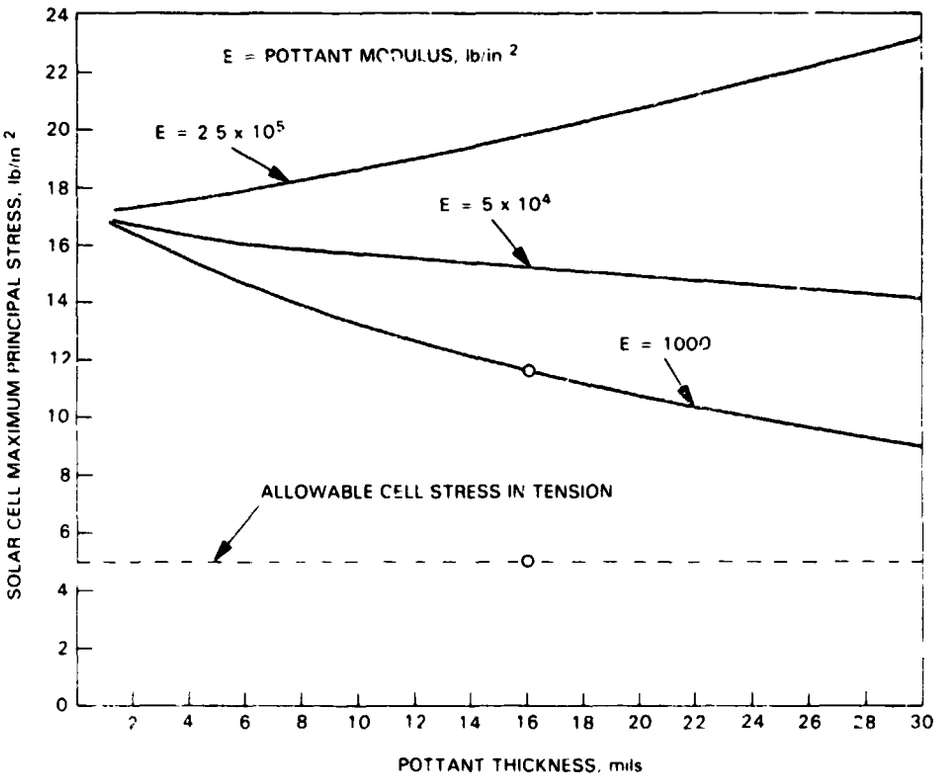

Figure 3-20. Hygroscopic Stress Analysis (ΔRH = 100%): Wooden-Substrate Design

The actual observations of a high incidence of broken cells occurring during outdoor exposure of wooden-substrate modules, and the computer predictions given in Figure 3-20, indicate that the estimated cell stress in tension of 5 klb/in.^{2} may be reasonably near the real value.

The actual occurrences of cell cracking, and the large cell stresses generated by the regain of moisture of desiccated wood, clearly indicate that if wood is to be a viable candidate, it must be adequately packaged before vacuum lamination to prevent desiccation. If this desiccation problem can be solved, wood is definitely a highly attractive substrate candidate for the many reasons presented above. A vigorous experimental program of wood-packaging techniques and approaches, as discussed in Section IV, is being pursued.

d. Module-Edge Support. The 4-ft-square modules, whether fabricated with glass, wood, or mild-steel structural panels, will probably be perimeter-clamped in outdoor framing racks with an open-lattice construction. A 100-mi/h wind, generating 50 lb/ft^2, may result in a force approaching 800 lb over the surface area of a 4-ft square module, acting to push the module out of the perimeter clamps. The mechanical construction of the clamps, and the accumulated surface area of the module covered by the clamps around the module perimeter, must accommodate the 800 lb of force without clamp failure or module failure initiating at its edges. Also, the perimeter clamping must not be so rigid and constraining that the portion of the module perimeter enclosed within the clamp cannot have some freedom to bend out-of-plane when the whole module area bows outward. Such rigid and restricted clamping could result in fracture of the module along a line just outside the edge of the clamps.

Edge-clamping analysis, being done at Spectrolab (see Reference 12), showed that an elastomeric edge gasket is needed, which will be positioned between the framing clamp and the module surface. The design and dimensions of the elastomeric gasket must permit at least two mechanical functions:

(1) Out-of-plane deformation of that portion of the module within the clamped perimeter so that the allowable design stress of the structural panel is not exceeded within and near the perimeter clamp.

(2) Accommodation of the in-plane dimensional growth and shrinkage of the module resulting from daily thermal expansion and contraction.

Initial edge-clamp analysis (see Reference 12) has concentrated on the tempered float-glass superstrate design. Preliminary findings for this design indicate that an elastomeric gasket should: (1) have a channel configuration (illustrated in Figure 3-3), (2) cover a minimum width of 3/8 in. of module perimeter (overlap), and (3) have a minimum thickness of 1/16 in. Gasket analysis for wooden and mild-steel modules are forthcoming.

The gasket is expected to fulfill the mechanical requirements of edge clamping but may not be an effective edge seal, e.g., prevent water intrusion along the interface between itself and the overlapped module surface. To keep water from reaching the physical edge of the module and penetrating into the interior bulk (presenting a potential for metallic corrosion), a gum or paste-like adhesive edge-sealing material, with resistance to water penetration, may fill the channel of the gasket before module installation.

An expanded discussion of material candidates for edge gaskets and seals is given in Section IV and in the Appendix.

e. Summary of Structural Analysis. Findings from the Spectrolab structural analysis are summarized briefly:

(1) Stiffening ribs are desirable on wood and steel panels to reduce panel weight, thickness, and pottant thickness between the cells and the panels.

(2) Ribs will permit the use of 1/8-in.-thick hardboards, for which thermal analysis indicates that wooden-substrate modules will have module operating temperatures comparable to mild-steel-substrate and glass-superstrate modules.

(3) Tempered low-iron, 1/8-in.-thick float glass can be used as a glass superstrate to resist wind loads. The trade-off between use of a 1/8-in.-thick and a 3/16-in.-thick tempered glass is hail resistance.

(4) The pottant material, in terms of its Young's modulus and its thickness between the cells and the structural panel, has considerable structural significance for both the glass-superstrate and mild-steel-substrate designs. There is much less structural significance for a pottant when used in a ribbed wooden-substrate design, if the wood can be properly sealed against humidity-caused expansion and contraction.

(5) An elastomeric edge gasket for the tempered float-glass-superstrate module should be at least 1/16 in. thick, and should have a module overlap of at least 3/8 in.

A method for estimating deflection or thermal-expansion stresses in solar cells for any pottant or unribbed structural panel is described in the Appendix. The approximating method generates simple design guidelines and principles relative to structural considerations, including a capability to assess cost-structure relationships for pottant materials.

4. Electrical Isolation Analysis

The encapsulation materials enclosing the solar cells and their associated electrical conductors and terminals must also function as electrical insulation materials, isolating encapsulated high-voltage points from accidental human contact, and must have sufficient electrical resistance to electrical breakdown or arc-through to external metallic parts in physical contact with the module. Included in this requirement is sufficient electrical insulation between metallic substrates or metallic foils that may be used in back covers and the encapsulated solar cells with their electrical circuitry. The present FSA requirement is that the encapsulation system be capable of insulating against 3000 Vdc.

The electrical insulation of solar cells and their electrical circuitry must be provided by the non-metallic construction materials, such as glass, wood, elastomeric pottants, plastic-film top covers, etc. For these dielectric materials, two physical conditions for electrical insulation can occur:

(1) Flawless: The materials are flaw-free, and their insulation resistance will be controlled primarily by thickness, which can be calculated from knowledge of the bulk materials' dielectric strength, which is typically expressed in units such as V/mil.

(2) Flawed: e.g., bubbles, cracks, or embedded conductive contaminants in the dielectric materials; sharp points in the cell or electrical circuitry generating very high electrical-field intensities, and delaminated interfaces that could result in current-leakage paths (accumulation of water). Some flaws could be inherent in the dielectric materials, but most are recognized as a consequence of poor design, poor workmanship, or inadequate quality control.

The FSA Engineering Area has initiated an experimental program to measure accurately the statistical distribution of dielectric strength of specific plastic films such as Mylar and Tedlar (Reference 15). By using films of constant thickness, large variations were encountered in measured breakdown-voltage values for measurements made at various surface locations on these films. The variations were apparently caused by flaws in the films, such as pinholes and thin spots, which were randomly distributed throughout the film samples.

Large-area film samples were divided into a grid network of small squares; the breakdown voltage in each small square section was measured, and a probability histogram for the level of breakdown voltage was generated. The measured values of breakdown voltage vs the probability of occurrence for both Mylar and Tedlar films of various thicknesses are shown in Figures 3-21 and 3-22.

Data for these two film materials reveal a finite probability of voltage breakdown at levels at and below 3000 Vdc. These data suggest that if breakdown voltage of dielectric materials is generally probabalistic, and in turn is related to a random flaw distribution throughout the materials' bulk volume, then for a module design, a series of two or more dielectric material layers may be used for electrical insulation to reduce greatly the probability of chance flaw alignment. Experimental confirmation of this approach is being pursue

Coupled with this concept is the relationship between dielectric strength V and material thickness t:

$$V = K/\sqrt{t} \qquad K = \text{Constant}$$

which states that the dielectric strength increases with decreasing material thickness. Thus, in a stack-up of thin layers, adequate dielectric strength of each layer can be conceptually achieved, and the probability of flaw-related breakdown significantly reduced because of the small chance of alignment of consecutive flaws in each layer.

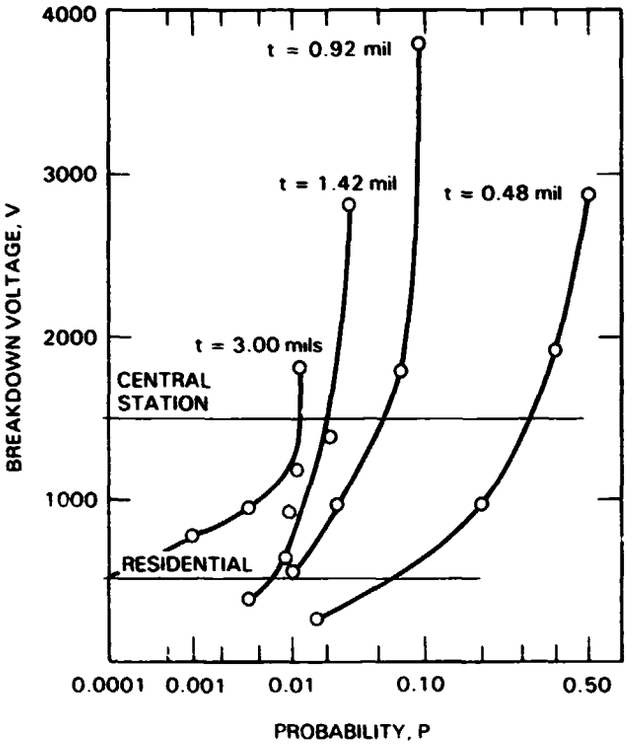

4 X 8 ft MODULE (LAYERS OF MYLAR REQUIRED)

t, mils	NUMBER OF LAYERS	
	CENTRAL STATION	RESIDENTIAL
3.00	4	2
1.42	4	3
0.92	5	3
0.48	>5	5

Figure 3-21. Voltage Breakdown Probability of Mylar (Experimental)

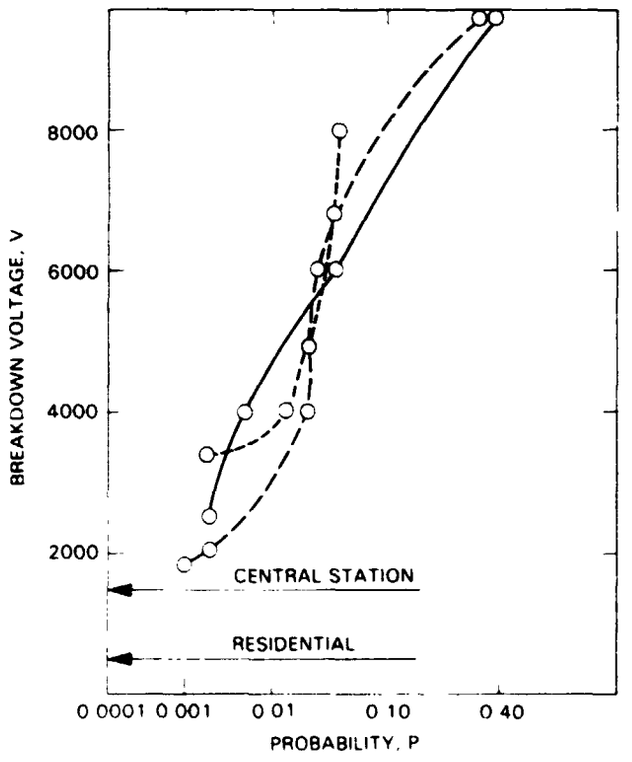

TEDLAR DESIGNATION
----- 200 SG 40 TR, 2 mils
——— 100 SG 30 TR, 1 mil
— — — 100 BG 30 TR, 1 mil

2 LAYERS ARE SUFFICIENT FOR PRESENT AND PROJECTED APPLICATIONS EXPERIMENTS

Figure 3-22. Voltage Breakdown Probability of Tedlar (Experimental)

An example of the inverse relationship between breakdown voltage V and material thickness t is illustrated in Figure 3-23 for polymethyl methacrylate (PMMA). This material is sold commercially under the trade name Lucite by Du Pont, which publishes the following electrical data in its Lucite technical literature:

(1) V = 400 V/mil, t = 125 mils

(2) V = 600 V/mil, t = 63 mils

PMMA is also the acrylic material used by 3M for their X-22416 and X-22417 UV-screening acrylic films. The 3M technical literature for these films provides the following electrical data:

(1) X-22416, V = 4000 V/mil, t = 2 mils

(2) X-22417, V = 3600 V/mil, t = 3 mils

These four data points are plotted on log-log scales in Figure 3-23, where a good straight-line relationship can be observed. The slope of the line is -0.55, yielding the following relationship

$$V = K/t^{0.55}$$

which compares well with the general relationship where the power of t is given as 1/2.

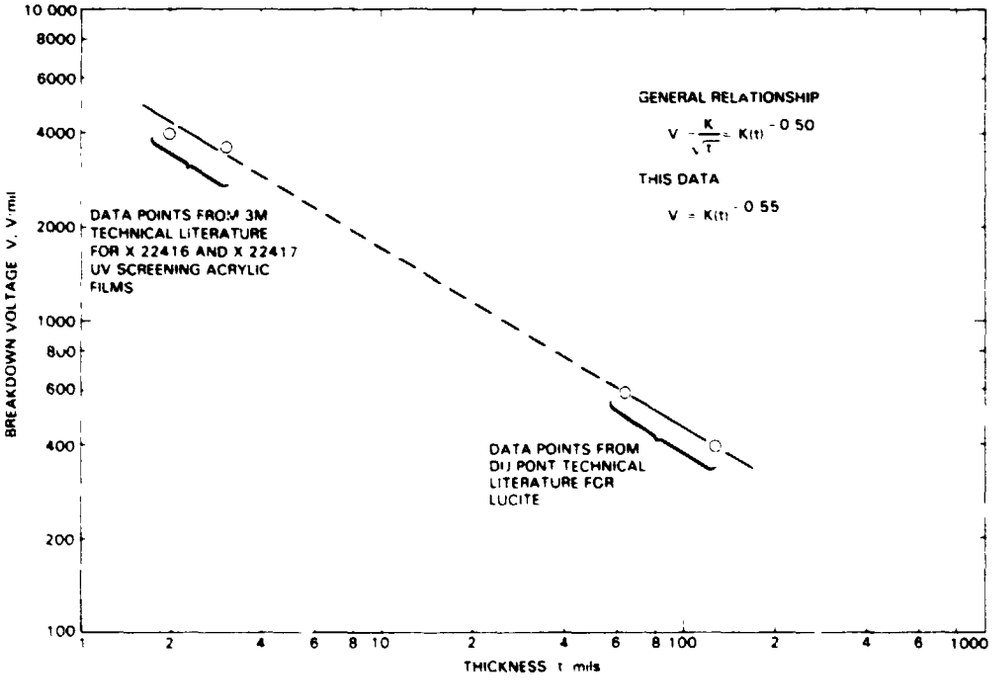

Figure 3-23. Breakdown Voltage of Polymethyl Methacrylate as a Function of Thickness

Returning to module designs, an encapsulated module has become a stack-up of discrete material layers satisfying various system requirements (see Figure 3-3). The concept of multiple layering of insulation materials to reduce the probable chance of flaw-related electrical breakdown is being designed into the modules. Therefore, at this stage of knowledge involving electrical isolation, the emerging information suggests the following two design guidelines for electrical isolation:

(1) Use of a minimum of two dielectric-material layers above the solar cells and the same on the back side of the solar cells.

(2) The minimum thickness of each dielectric layer should be capable of accommodating 3000 Vdc without electrical breakdown, based on the best knowledge of the intrinsic dielectric strength of the material.

These guidelines as related to module designs employing glass, wood, and steel are discussed below; dielectric strength values for a variety of materials are given in Table 3-5.

For a wooden-substrate design, there are dielectric layers of pottant and a plastic-film top cover above the cells, and dielectric layers of pottant and wood on the back side of the cells. If the pottant, for example, is EVA, its experimentally measured dielectric strength is about 620 V/mil, and thus, a minimum of 5 mils of EVA above and below the solar cells is calculated to provide 3000 Vdc electrical breakdown resistance for the pottant dielectric layer. A minimum of 5 mils of EVA can be ensured by using a 5-mil-thick sheet of Craneglas embedded in the pottant layers above and below the cells. Because the Craneglas is about 70% porous, this material is not considered to be a dielectric layer, but only functions to ensure that the dielectric layer of pottant is at its requisite minimum thickness. Because EVA laminating film is presently available in only a single thickness (15 to 20 mils), the practical realities are that the pottant thickness will probably be greater than 5 mils,

Table 3-5. Intrinsic Electrical Isolation, 3000 Vdc

Material	Average Dielectric Strength, V/mil	Minimum Required Material Thickness, mils
Acrylic film	3800	0.8
EVA	620	4.8
Wood	175	17

NOTE: In general, minimum required thicknesses of non-metallic materials for intrinsic electrical isolation are less than thicknesses dictated by structural considerations or present commercial availability.

even with use of the Craneglas. The plastic-film top cover, whether the 2- or 3-mil 3M acrylic film or a minimum 2-mil Tedlar film, meets the requisite 3000-Vdc electrical breakdown requirement. And lastly, on the back side of the solar cells, a 1/8-in. wooden substrate as the second back-side dielectric layer will have the requisite 3000-Vdc electrical-breakdown resistance.

For a mild-steel substrate design, the two dielectric layers of pottant and plastic-film top cover above the solar cells are the same as for the wooden-substrate design. On the back side of the solar cells, however, a single dielectric layer of pottant between the cells and the steel substrate would not satisfy the minimum two-layer requirement. It will be pointed out in Section IV that the corrosion-prevention coatings are required on mild steel with candidate concepts including adhesively attached white-pigmented plastic films or corrosion-preventive white-pigmented organic coatings. The requirement is that the thickness of the organic coating or plastic film be related to its dielectric strength for 3000-Vdc electrical-breakdown resistance. Thus a white-pigmented organic coating or plastic film on the sun-side surface of the mild-steel substrates provides three functions:

(1) The second dielectric layer for electrical isolation.

(2) White background for internal light reflection.

(3) Corrosion protection of the mild steel.

For a glass-superstrate design, the two dielectric layers above the solar cell are the pottant and the tempered float-glass superstrate. The dielectric strength of glass is on the order of 10^7 V/mil (Reference 16), compared with a 3000-Vdc requirement. Nevertheless, the minimum two-dielectric-layer requirement is satisfied; it will be recalled that the structural-deflection analysis of this design indicated that at least 5 mils or more of pottant thickness is required between the glass and the cells. On the back side of the solar cell, there are two back-cover design options being considered. The first option is the use of white-pigmented plastic films, which in combination with the back-side pottant layer satisfies the two-dielectric-layer requirement. The thick-ness of the pottant and the thickness of the plastic film would each be determined by their respective dielectric strength values. The second option involves the use of metal foils for a hermetic module design. For this option, the back cover could be a plastic-film, metal-foil, plastic-film laminate, positioning a plastic film between the metal foil and the pottant and solar cells to provide the second dielectric layer in combination with the pottant. The plastic in the film laminate should be white for internal light reflection, and the outside surface of the laminate should be white for thermal require-ments.

5. Engineering Analysis General Summary

a. Structural. Analysis has shown that:

(1) Tempered low-iron (Fe^{++}), soda-lime glass is recommended for a glass-superstrate design, for reasons of structural properties, optical properties, and cost in large-volume

purchases. A 1/8-in.-thick tempered-glass plate meets the wind requirements for a 4-ft square module, but 3/16 in. may be considered if the trade-off is hail resistance.

(2) Stiffening ribs are desirable on mild-steel and wooden-substrate panels, to reduce weight, thickness, cost, and requirements on pottant thickness to minimize solar-cell tensile stresses from deflection. Ribs on wooden hardboard panels are absolutely necessary to use the minimum commercial thickness of 1/8 in., which is desirable to avoid increasing module operating temperatures.

(3) At least 3/8 in. of the perimeter of a tempered glass-superstrate module must be mechanically clamped in an outdoor mounting rack. An elastomeric gasket between the clamp and the module is required around the edge of the glass module, and must be at least 1/16-in. thick; must extend over the module surface at least 3/8 in. inward from the module edge, and must have high resistance to flow, creep, and compression set.

(4) The magnitude of tensile stresses imposed on solar cells from module deflection or thermal expansion are regulated not only by the mechanical and thermal properties of the structural panel, but also by the Young's modulus and by the thickness of the pottant layer between the cells and the panel. Decreasing pottant modulus and increasing pottant thickness act to lower mechanical stress loads on the solar cells.

b. Electrical Isolation. Analysis has shown that:

(1) At least two dielectric encapsulation layers should be used above the cells and on the back side of the cells to minimize the probability of flaw-related electrical breakdown.

(2) Each of the four dielectric encapsulation layers should be sufficiently thick to withstand 3000 Vdc, with a minimum thickness calculated on the basis of the best available dielectric strength value (V/mil) for the material.

(3) The minimum thickness calculated for each dielectric layer is to be considered the design minimum in a module, but may be made thicker if required structurally. Electrical-isolation requirements establish minimum design thicknesses of the dielectric encapsulation layers for residential and utility applications.

c. Thermal. Analysis has shown that:

(1) The relevant thermal properties of encapsulation materials regulating module operating temperature are thermal conductivity, infrared emissivity of the front and back surface, and solar absorption of the back surface.

(2) In terms of these thermal properties, module operating temperature is primarily regulated by the infrared emissivity of the front and back surface, and secondarily by the thermal conductivity of the encapsulation material layers, except wooden hardboards, if thicker than 1/8 in.

(3) Heat removal from modules is primarily regulated by the rates of heat dissipation from the surfaces by radiation and convection, and less by the rate of heat conduction from the cells to the surface through the various encapsulation layers.

(4) The dominant control on module operating temperature, which can be exercised through selection of encapsulation materials, involves the use of front- and back-cover materials with maximum infrared emissivity (ϵ). Transparent glass and plastic-film front covers have ϵ values ranging between 0.85 to 0.90. Back-cover materials should also have very low solar absorptivity. The two requirements for the back cover are best satisfied using a white organic (non-metallic) material. Values of ϵ for white organic materials can be >0.90.

(5) Module design and field-engineering features that can help lower module operating temperature are the use of fins on the substrates (no horizontal cross fins), which also function as stiffening ribs. The mounting design should provide maximum accessibility of front and back surfaces to circulating air, and minimum exposure to scattered heat-producing radiant energy.

d. Optical. Analysis has shown that:

(1) The spectral-response range of silicon solar cells is 0.4 to 1.1 μm. Incident solar flux on either side (UV, IR) of this wavelength range, which is not reflected at the surface, is essentially absorbed by the module and converted to heat. This is because the transparent front materials are designed to be UV-absorbing, and have inherently strong infrared absorption bands. In addition to this, the silicon solar cells also absorb infrared strongly.

(2) Incident solar flux in the wavelength region of 0.4 to 1.1 μm should be maximally transmitted to the solar cells. The relevant optical properties and features affecting this transmission are Fresnel surface reflection (≈4%), AR coating on the solar cell, absorption bands in the encapsulation materials, and index-of-refraction mismatch at the interfaces.

(3) Front-side transparent encapsulation materials should have virtually flat transmission (no absorption bands) in the

wavelengths from 0.4 to 1.1 μm, and an integrated transmittance $\geq$98%, after correcting for surface reflection losses of about 8%. Low-cost pottant candidates, such as EVA and P-n-BA, have these optical properties. Computer predictions of power output of modules with 10 to 25 mils of EVA indicated no effect of EVA thickness. High-iron (Fe^{+++}) glass does have absorption bands in wavelengths of 0.4 to 1.1 μm.

(4) Antireflective (AR) coatings on silicon solar cells are a necessity. The AR coating should be optically matched with the pottant, but being optically matched with air is acceptable, resulting in only a fractionally small power loss when encapsulated. However, significant power loss occurs for cells without any AR coating.

(5) AR coatings on the module top surface are beneficial, if low cost and durability are enough to achieve favorable cost-benefit advantages. AR coatings on the second surface of glass tend to reduce transmission. Glass superstrates with AR coatings on both sides are not recommended.

(6) Computer analysis of glass-superstrate modules using stippled glass, either stipple-up or stipple-down, found no optical effect beneficial, or detrimental, in normal-incident light. Analysis involving off-normal-incident light has not yet been done.

(7) Matching indexes of refraction of adjacent material layers are desirable, but if not done, back-reflection losses for the combinations of glass, plastic-film front covers, and pottant materials being considered are small because the index-of-refraction differences for these various materials are small.

(8) Craneglas non-woven glass mats can be used above the solar cells without optical loss.

SECTION IV

ENCAPSULATION MATERIALS AND MATERIALS TECHNOLOGY

This section describes the materials being identified or developed for each of the construction element layers illustrated in Figure 3-2 (including selection criteria), and is essentially a status report of encapsulation materials to date of this handbook, updating from the previous publication Encapsulation Materials Status to December 1979 (Reference 17). This section is divided by construction element (for example, pottants) and the materials and relevant technology generally will be described only for those materials listed under the Current Materials column in Table 3-1. For materials listed under the Deleted Materials column, which are not discussed here, see References 17-22.

A. POTTANTS

1. Requirements

Polymeric pottant materials are the encapsulating media for solar cells and their electrical interconnects. There is a significant difference between the thermal-expansion coefficients of polymeric materials and the silicon cells and metallic interconnects; stresses developed from the thousands of daily thermal cycles can result in fractured cells, broken interconnects, or cracks and separations in the pottant material. To avoid these problems, the pottant material must not overstress the cell and interconnects, and must be resistant to fracture. From the results of a theoretical analysis (see Reference 12), experimental efforts (see References 10 and 11), and observations of the materials of choice used for pottants in commercial modules, the pottant must be a low-modulus, elastomeric material.

Also, these materials must be transparent, processible, commercially available, and desirably of low cost. In many cases, the commercially available material is not physically or chemically suitable for immediate encapsulation use and, therefore, must also be amenable to low-cost modification. The pottant material must have either inherent weatherability (retention of transparency and mechanical integrity under weather extremes) or the potential for long life that can be provided by cost-effective protection incorporated into the material or the module design.

In a fabricated module, the pottant provides three critical functions for module life and reliability:

(1) Maximum optical transmission in the silicon solar-cell operating wavelength range of 0.4 to 1.1 μm.

(2) Retention of a required level of electrical insulation to protect against electrical breakdown, arcing, etc., with the associated dangers and hazards of electrical fires, and human safety.

(3) The mechanical properties to maintain spatial containment of the solar cells and interconnects, and to resist mechanical creep. The level of mechanical properties also must not exceed values that would impose undue mechanical stresses on the solar cell.

When exposed to outdoor weathering, polymeric materials can undergo degradation that could affect their optical, mechanical, and electrical insulation properties. Outdoors, polymeric materials can degrade from one or more of the following weathering actions:

(1) UV photooxidation.

(2) UV photolysis.

(3) Thermal oxidation.

(4) Hydrolysis.

For expected temperature levels in operating modules, ≈60°C in a rack-mounted array (and possibly up to 80°C on a rooftop), three generic classes of transparent polymers are generally resistant to the above weathering actions: silicones, fluorocarbons, and PMMA acrylics. Of these three, only silicones, which are expensive, have been available as low-modulus elastomers suitable for pottant application (see Section III).

Therefore, generally all other transparent, low-modulus elastomers are sensitive to some degree to weathering degradation. However, less weatherable and lower-costing materials can be considered for pottant application if the module design can provide the necessary degree of environmental protection. For example, a hermetic design, such as a glass superstrate with a metal-foil back cover and appropriate edge sealing, will essentially isolate the interior pottant from exposure to oxygen and water vapor; the glass itself provides a level of UV shielding. For example, polyvinyl butyral (PVB) would undergo rapid deterioration if directly exposed outdoors to oxygen, water vapor, and UV, but when isolated within the core of a double-glass automotive windshield, PVB lasts virtually forever, except at unsealed windshield edges. If PVB were used in a hermetic module, it could survive and perform satisfactorily as long as the peak temperature of the PVB remained below its pyrolysis threshold.

The situation is different for a substrate module, however, with a weatherable plastic-film front cover. Because all plastic films are permeable to oxygen and water vapor (the only difference is permeation rate), the pottant is exposed to oxygen and water vapor, and also to UV, if the plastic film is non-UV screening. Because isolation of the pottant from oxygen and water vapor is not practically possible in this design option, it becomes a requirement that the pottant be intrinsically resistant to hydrolysis and thermal oxidation, but sensitivity to UV is allowed if the weatherable front-cover plastic film can provide UV shielding.

Therefore, surveys (see References 11, 18, 19, and 20) were done to identify the lowest-costing, transparent, low-modulus elastomers with expected resistance to hydrolysis and thermal oxidation at temperatures up to 80°C, but these materials were allowed to be sensitive to UV deterioration. It was envisioned that if such a set of pottant candidates were selected on the basis

of a less-protecting substrate-module design, they would also be usable in a potentially more-protecting glass-superstrate design. The chemical significance of encapsulation design options for the pottant is shown in Table 4-1.

The historical pottant selections, given in Table 3-1, are divided between pottants still in use and those now deleted. Because the PV industry was fabricating modules by two processes, lamination and casting, the historical list in Table 3-1 encompassed pottant candidates for each of the processes. Part of the early survey efforts concentrated on seeking all-acrylic pottant candidates, but none were found. Accordingly, a developmental program was initiated at JPL to develop an all-acrylic casting liquid, PnBA, and recently the possibility of an all-acrylic laminating pottant was identified.

Therefore, the list of most attractive pottant materials is narrowed to seven candidates, shown in Table 4-2. These pottant materials have been selected for continued development or evaluation, and are divided into two classifications defined by the two methods of module fabrication, lamination and casting. The candidate materials are further specified as to whether they will be developed and evaluated, or evaluated only.

The general plan for the materials' development encompasses two discrete steps:

(1) Evaluation-readiness: An intermediate stage of development where the material can be handled, processed, and fabricated into modules by participating industrial manufacturers. Although fabricability using commercial equipment becomes the key criterion for this level of development, the material will be fully compounded with trial antioxidants, UV stabilizers, other necessary additives, and completed with recommended processing conditions and primers or adhesives.

Table 4-1. Encapsulation Design Options: Chemical Significance

Design	Significance
Glass-Superstrate Designs with Atmospheric Barrier Back Covers (metal foils)	Isolation of organic material interlayers from exposure to atmospheric oxygen and water vapor
	Prevention of venting of volatiles, chemical reaction products from organic interlayers
Substrate Designs with Plastic-Film Front Covers	Permeation access of organic interlayers to atmospheric oxygen and water vapor
	Permeation venting from organic interlayers

Table 4-2. Pottant Candidates

Method	Candidate	Description
Lamination (dry-film materials)	Ethylene vinyl acetate	Base polymer, Elvax 150 supplied by Du Pont; compounding formulation developed by Springborn (A9918)
	Ethylene methyl acrylate	Base polymer from either Gulf or Du Pont, to be selected; compounding formulation to be developed by Springborn
	Acrylic	3M proprietary film material; decision to make material commercially available for encapsulation is pending
Casting (liquid materials)	Poly-n-butyl acrylate	Base monomer, n-butyl acrylate supplied by Rohm and Haas; liquid system concept developed by JPL; industrial-ready version being developed by Springborn
	Acrylic	Alternative to poly-n-butyl acrylate using a different-base monomer to be developed by Richardson Co. (Chicago, IL)
	Aliphatic polyether urethane	Base polymer to be selected by Springborn, followed by compounding to an industrial-ready version
	Silicone 534-044	Marketed by General Electric Co.

(2) Application Readiness: The final stage of development in which the material encompasses improvements of the intermediate-stage material defined by:

(a) Feedback on handling, processing, and fabricability of the intermediate-stage material by participating PV manufacturers

(b) Results of accelerated, abbreviated, and outdoor testing of the material, and modules fabricated with the material.

The following list outlines some of the features of a pottant ready for application evaluation:

(1) Fastest possible fabrication cycle:

  (a) Lowest possible cure temperature.

  (b) Fastest possible cure time.

(2) Self-priming.

(3) Specification of peak-service temperature for 20-yr life in various module designs (superstrate, substrate).

(4) Minimum requirements for stabilization additives, related to (3).

(5) Use of non-woven glass mat as interlayer separator for rolls of lamination films, to prevent film blocking. The glass mat can be optionally used directly as the spacer material in laminated modules.

(6) Optimum viscosity for pumping liquid pottants.

Although pottants will be developed to this stage by the FSA Project, this does not mean that further refinements could or would not occur. At this stage, the technology is transferable to material manufacturers who, in turn, may make additional modifications.

Based on previous pottant experiences, certain specifications and requirements for these materials have emerged, which are shown in Table 4-3. Better thermal stability is the single most important item on the list of desirable properties, which may cause the introduction of new candidate pottant materials for consideration, compared to the present pottant materials. This feature results from an awareness of solar-cell hot-spot heating.

2. Candidates

Pottant development is illustrated in Figure 4-1. Each of the seven pottant candidates in Table 4-2 is described below.

a. Ethylene Vinyl Acetate. EVA is a copolymer of ethylene and vinyl acetate typically sold in pellet form by Du Pont and U.S. Industrial Chemicals, Inc. (USI). The Du Pont name is Elvax; the USI trade name is Vynathane. The cost of EVA typically ranges between $0.55 and $0.65/lb. Springborn Laboratories, Inc. screened all commercially available grades of EVA and reduced the list to four candidates based on maximum transparency: Elvax 150, Elvax 250, Elvax 4320, and Elvax 4355 (see Reference 21). Because EVA is thermoplastic, processing into a module is best accomplished by vacuum-bag lamination with a film of EVA. Based on film extrudability and transparency, the best choice became Elvax 150, at a cost for high-volume purchases of about $0.60/lb. Elvax 250 was an extremely close second choice.

Table 4-3. Evolving Specifications and Requirements for Compounded Pottant Materials

Glass transition temperature	<-40°C
Total hemispherical light transmission through a 20-mil-thick film integrated over the wavelength range from 0.4 to 1.1 μm	>90% of incident
Resistance resistant to hydrolysis	In water at 80°C
Resistant to thermal oxidation (oven aging)	At temperatures <85°C
Mechanical creep Tensile modulus as measured by initial slope of stress-strain curve	None at 90°C <3000 lb/in.^{2} at 25°C
Fabrication compatibililty	Can be fabricated into modules using industrial state-of-the-art lamination or casting equipment
Fabrication temperature	≦150°C for either lamination or liquid pottant systems
Fabrication pressure for lamination pottants	≦1 atm
Chemical inertness	No reaction with embedded copper coupons at 90°C
UV degradation absorption	None at wavelength >0.35 μm
Hazing or clouding	None at 100% RH at 60°C
Humidity swell	To be determined
Minimum thickness on either side of solar cells in fabricated modules	6 mils
Odor, human hazards (toxicity)	None
Additives and stabili ers	To be determined

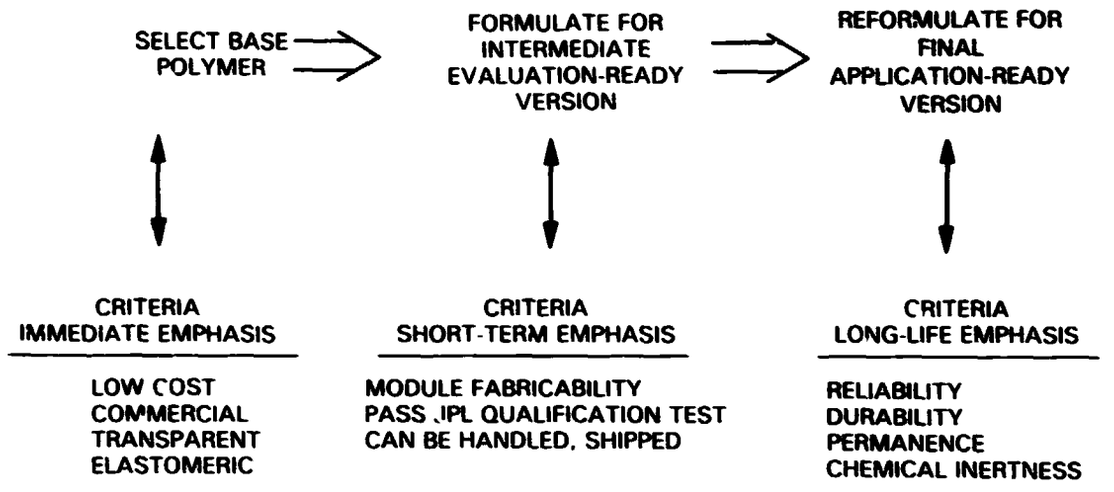

Figure 4-1. Stages of Pottant Development

Elvax 150 softens to a viscous melt above 70°C, and therefore is not suitable for temperature service above 70°C when employed in a fabricated module. Springborn developed a cure system for Elvax 150 that results in a temperature-stable elastomer (see Reference 19). They also compounded Elvax 150 with an antioxidant and UV stabilizers, which improved its weather stability but did not affect its transparency.

In addition to clear EVA, Springborn formulated a white-pigmented EVA film (with ZnO_2 and TiO_2) that can be positioned on the back side of the solar cells in a module lay-up. The pigment provides a light-reflecting background for those module areas not covered by round solar cells, and increases module power output by internal reflection.

Elvax 150 film with two different compounding formulations has been available from Springborn. The first formulation became available in fall 1978, and several module manufacturers evaluated it by fabricating modules using their commercial solar cells. The processing technique in all cases was vacuum-bag lamination. The manufacturers reported certain advantages of EVA when compared to PVB, the laminating film material in common use within the PV module industry. The reported advantages are:

(1) Lower cost.

(2) Better appearance.

(3) Better arity.

(4) Non-yellowing properties.

(5) Eliminates cold storage.

(6) Dimensional stability.

(7) Processing advantages:

(a) Reduces time.

(b) Eliminates pressure autoclave.

(8) Good flow properties and volumetric fill.

Continued experimentation with the EVA formulation resulted in identification of a better antioxidant (Naugard-P) for Elvax 150, which is now used in the second formulation of EVA and considered to be the evaluation-ready version. The formulations for the clear and white-pigmented evaluation-ready EVA films are listed in Table 4-4. These ingredients are compounded into Elvax 150 pellets, followed by extrusion of the compounded pellets at 85°C to form a continuous film. The thickness of the clear film is nominally 18 mils; the white-pigmented film is nominally 14 mils thick. The selected curing system is inactive below 100°C, so that film extruded at 85°C undergoes no curing reaction. The extruded film retains the basic thermoplasticity of the Elvax 150. Therefore, during vacuum-bag lamination, the material will soften and process as a conventional laminating resin. A complete description of the EVA curing properties and of the EVA lamination process is given in Section V, which discusses encapsulation processes.

Table 4-4. Formulation of Evaluation-Ready Ethylene Vinyl Acetate (Springborn Identification Number)

Ingredient	Function	Formulation (parts per hundred parts of rubber)	
		A-9918 Clear	A-9930b .gmented
Elvax 150	Base EVA	100	100
Lupersol 101	Curing agent	1.5	1.5
Naugard-P	Antioxidant	0.2	-
Tinuvin 770	UV stabilizers	0.1	-
Cyasorb UV-531	UV stabilizers	0.3	-
TiO_2	White pigments	-	2.0
ZnO_2	White pigments	-	5.0
Ferro AM-105	UV stabilizer	-	0.5

A primer has been developed by Dow Corning for bonding EVA to glass; its composition is given in Table 4-5. Experimental quantities of this primer are available from Springborn under the designation "A-11861-1, EVA Primer." An advantage of this primer system is that it can optionally be incorporated into EVA as a compounding additive, to generate a self-priming EVA. There will be an additional cost to accomplish this, however, and the cost-benefit-performance trade-offs have not yet been determined.

Clear EVA films with the Springborn Formulation A-9918 (see Table 4-4) are available from two sources: Rowland, Inc., and Springborn. The EVA activities at Rowland are in technical coordination with Du Pont, manufacturers of the ELVAX 150 base polymer. Rowland will market a standard A-9918 EVA film supplied on rolls, which will be nominally 18 mils thick, 27 in. wide, and surface-embossed and textured for non-blocking behavior.

The present minimum order for the standard A-9918 film from Rowland will be 25,000 ft^2, or about 2,275 lb. The price structure quoted in April 1981 is:

Quantity, ft^2	Price Range, $/$ft^2$
> 25,000	0.31 to 0.33
> 50,000	0.30 to 0.32
>100,000	0.25 to 0.27
>250,000	0.23 to 0.25
>500,000	To be negotiated

Table 4-5. Formulation of Glass/EVA Primer Developed by Dow Corning Corp.

Use Options
(1) Self-Priming EVA: Disperse the three-component mixture into EVA pellets before film extrusion (Quantity: 1.0 wt% in EVA film)
(2) Separate Surface-Priming: Dilute the three-component mixture in methanol to 10 wt%, wipe thinly onto surfaces, and allow to air-dry at least 15 min. Diluted primer mixture in methanol available from Springborn under the designation "A-11861-1, EVA Primer"

Component	Composition, parts by weight
Dow Corning Z-6030	90
Benzyl dimethyl amine	10
Lupersol 101 peroxide	1

The address for Rowland is:

Rowland, Inc.
Spruce Brook Industrial Park
Berlin, CT 06037

Springborn will continue to market clear EVA film at quantities less than 25,000 ft^2 (2,275 lb) at a nominal selling price of \$0.35/ft^2. Springborn will also market the white-pigmented EVA film, Formulation A-99308 (see Table 4-4) at a nominal selling price of \$0.40/ft^2. The white-pigmented EVA films are nominally 14 mils thick. The clear and white-pigmented EVA cost quotation from Springborn were effective in April 1981.

Rowland's lowest cost quotation of \$0.23 to \$0.25/ft^2 for 18-mil-thick film comes to about \$0.013/mil of thickness. Cost projections made by Springborn (see Reference 19) indicate that as the annual production of encapsulation-grade EVA approaches 10^6 lb its cost should approach about \$0.95/lb, or about \$0.0048/ft^2/mil of thickness. This cost assumes that the pellets are purchased from Du Pont, then compounded and extruded in a separate manufacturing operation. If encapsulation-grade EVA films were to be produced in a continuous one-company operation from monomer to final product, its cost is estimated at about \$0.76/lb, or about \$0.0038/ft^2/mil of thickness.

The available evaluation-ready EVA has been favorably received by industry. However, its status is still considered to be experimental. To advance EVA toward application-readiness, several developmental tasks remain to be completed:

(1) Faster processing, primarily in the cure schedule, which involves a reduction in cure time and temperature; the minimum cure temperature will be dictated by the requirement that the curing system must not become active during film extrusion.

(2) Optimization of the UV-stabilization additives; the present additives were selected based on literature citation and industrial experience with polymers similar to EVA.

(3) Identification of the peak-service temperature allowed for EVA in a module application, to ensure 20-yr life.

(4) Industrial evaluation of the desirability of having a self-priming EVA, recognizing the possibility of an additional cost component (cost-benefit-performance trade-off).

In addition to the potential of self-priming, other innovations and convenience-features can be contemplated for EVA. One innovation is to extrude the EVA film directly onto the non-woven glass mat-spacer material (see Subsection D below). This composite of spacer and EVA can be wound and unwound, and the porous spacer is directly included in the module assembly as the interfacial air-release material. Both Springborn and Spectrolab have demonstrated that the spacer can be used above the solar cells in an EVA module without optical penalty. Another innovation is to market a laminate of three materials: the porous spacer, EVA, and a UV-screening front-cover plastic film.

A data base of material properties of cured EVA is emerging as the material is increasingly studied. Accumulated data on material properties are shown in Table 4-6. It is recognized that additional properties may be desired by the industry, and recommendations are requested.

The dynamic mechanical properties of uncured and cured EVA were measured at 110 Hz on a Rheovibron-dynamic test machine. Dynamic modulus and loss tangent as a function of temperature are plotted in Figures 4-2 and 4-3, respectively. The softening of uncured EVA to a viscous melt is observed from Figure 4-2 to occur around 75°C to 80°C. After curing, the melting of EVA is prevented (Figure 4-2). The property of EVA (Elvax 150) of softening at 75°C to 80°C is why it is very important to ensure adequate EVA cure, as is detailed in Section V. Without adequate cure, EVA in a module application would creep and flow at temperatures above 75°C to 80°C.

b. Ethylene Methyl Acrylate (EMA). This recently identified material, a copolymer of ethylene and methyl acrylate, has potential as a solar-cell lamination pottant. Plans exist to modify this material to a stage of evaluation-readiness and to provide, with EVA, two potentially useful, low-cost lamination film materials.

There are three suppliers of EMA resins; two are domestic, Du Pont and Gulf Oil Chemicals. The Du Pont EMA resin, designated "VAMAC N-123," cannot be used because of its lack of transparency. The third supplier is foreign.

Table 4-6. Properties of Cured Ethylene Vinyl Acetate (Formulation A-9918)

Properties	Values	Properties	Values
Glass transition temperature	-43°C	Specific heat	2.09 $\frac{W\text{-}s}{g^{\circ}C}$
Density	0.92 g/cm^3 (25°C)	Emissivity (25°C)	0.88 (clear), 0.91 (white)
Coefficient of thermal-expansion	Below Tg (-43°C): 0.9 x 10^{-4}°C^{-1} -43°C to +10°C: 2.0 x 10^{-4}°C^{-1} Above +10°C: 4.0 x 10^{-4}°C^{-1}	Refractive index	1.482
		Tensile strength (25°C)	1900 lb/in.^{2}
Young's modulus (25°C)	900 lb/in.^{2}		
		Elongation at break (25°C)	510%
Thermal conductivity	9 x 10^2 $\frac{W\text{-}mil}{ft^2\text{-}^{\circ}C}$		
Dielectric strength	620 V/mil		

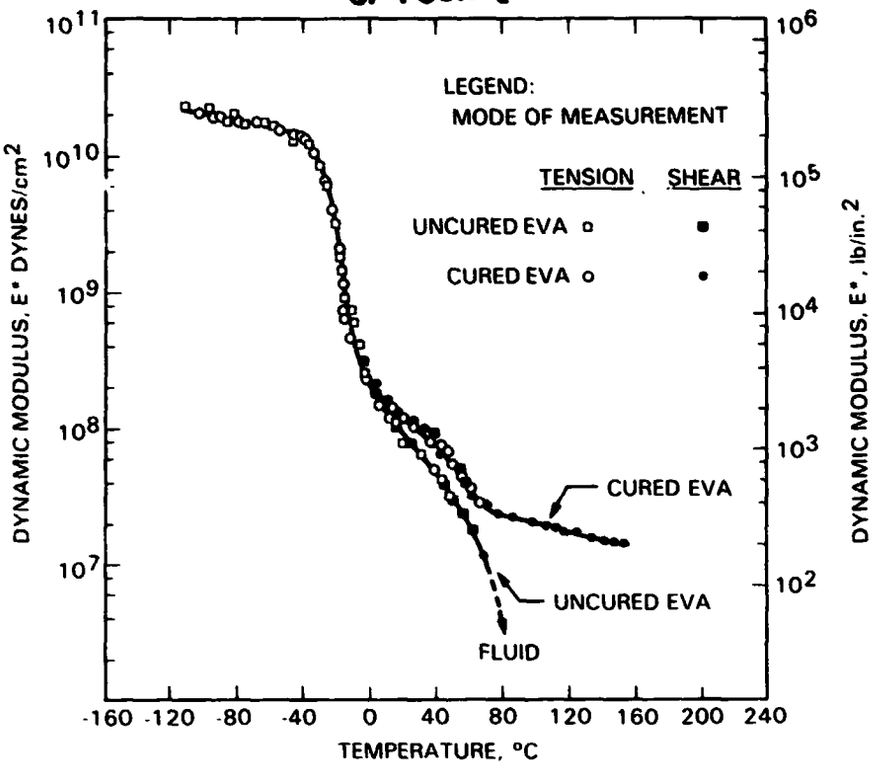

Figure 4-2. Dynamic Modulus (E*) of Encapsulation-Grade Ethylene Vinyl Acetate (A-9918) at a Frequency of 110 Hz

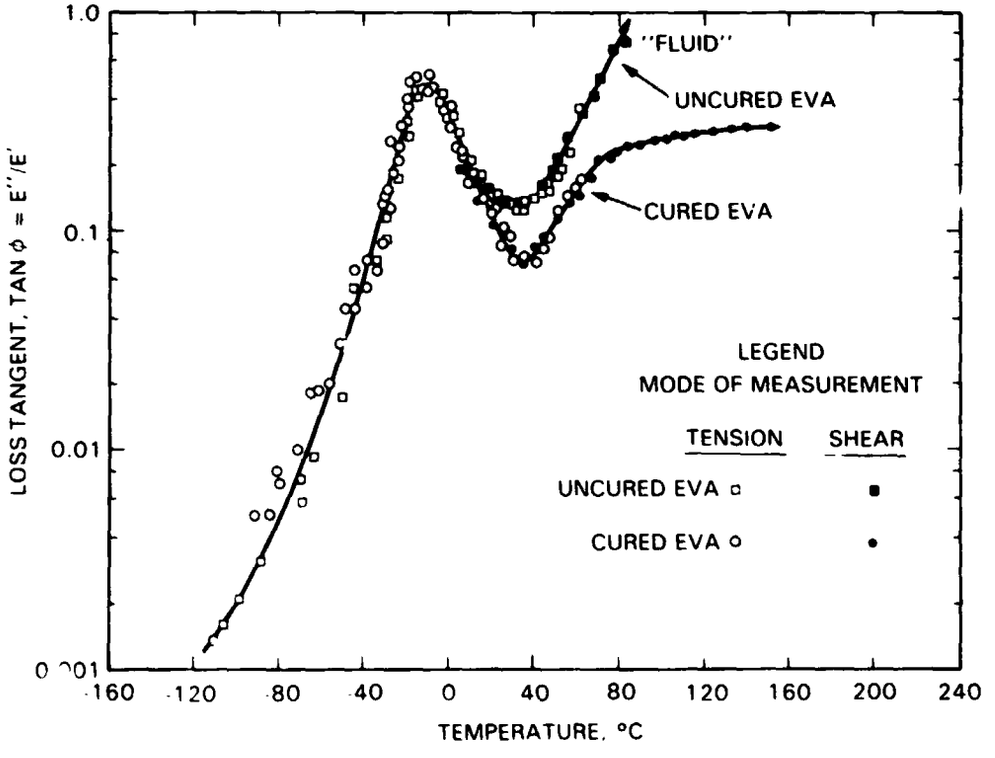

Figure 4-3. Loss Tangent (Tan ϕ) of Encapsulation-Grade Ethylene Vinyl Acetate (A-9918) at a Frequency of 110 Hz

Gulf markets three highly transparent EMA resins that are designated 2205, 2255, and TD-938. Grade 2255 is the same base resin as 2205, except that it contains lubricant and antiblocking additives. Gulf literature for these resins indicate the following features:

(1) Low-extrusion temperatures.

(2) Good heat sealability.

(3) Thermal stability to 315°C (600°F) for short periods of time (manufacturer's claim).

(4) Stress-crack resistance.

(5) Low melt viscosities.

(6) Good adhesion to a variety of substrates.

Springborn evaluated the three Gulf EMA resins experimentally and selected TD-938 based on film transparency, extrudability, and ease of module fabrication by lamination. The TD-938-base resin sells for about $0.60/lb (April 1981). A trial formulation, developed by Springborn, is shown in Table 4-7. The formula number (A-11877) may become the EMA identification number if this trial formulation evolves as the evaluation-ready version.

Modules have been fabricated with this EMA by the vacuum-bag lamination process, and the modules have successfully passed the JPL thermal-cycle qualification test (-40°C to +90°C). Preliminary investigations have also indicated that the Dow Corning primer (see Table 4-5), developed for EVA, is equally effective for bonding EMA to glass.

c. Acrylic Laminating Film. The desirability of an acrylic elastomer suitable for use as an encapsulation pottant has been discussed (see Reference 18). As a class of polymers, acrylics are highly desirable for module application because they are the lowest-costing transparent polymers that are generally resistant to degradation by weathering action. They offer the potential of long outdoor-service life with little or no UV protection required for the top cover.

Surveys for commercial elastomeric acrylic materials, for either lamination or casting fabrication, have not identified a suitable candidate. For a casting resin, a new concept based on n-butyl acrylate chemistry has been developed, starting at the laboratory level, and this material is described in the following section. For a dry-film lamination material, start-up of a laboratory development was also contemplated. Fortunately, during May 1980, the Encapsulation Task learned that the 3M Co., St. Paul, Minnesota, may market elastomeric acrylic films for encapsulation. A product decision by 3M is pending.

d. Poly-n-Butyl Acrylate (PnBA). No commercially available, all-acrylic liquid-casting and curable-elastomeric system could be found. Accordingly, the Encapsulation Task undertook a developmental effort, beginning at the laboratory level.

Table 4-7. Trial Formulation for Ethylene Methyl Acrylate, Formula No. A-11877

Formulation	Parts
EMA TD-938 base resin	100.0
Lupersol 231 (curing agent)	3.0
Cyasorb UV-531 (stabilizer)	0.3
Tinuvin 770	0.1
Naugard-P (antioxidant)	0.2

Observations
Ingredients tumble-blended before extrusion; no separate compounding step required.
No release paper required during roll windup.
Same cure requirements as EVA pottant.

A requirement of encapsulation-grade pottants is retention of elastomeric properties over the temperature range from -40°C to +90°C. This requirement is met by PnBA, which has a glass-transition temperature of -54°C (Reference 23).

PnBA is not commercially available in a form suitable for use as an encapsulation pottant, but the n-butyl acrylate monomer is readily available at a bulk cost of $0.45/lb. As a result of the laboratory developmental program undertaken at JPL, a prototype, 100%-pure PnBA liquid was developed that could be cast as a conventional liquid-casting resin, and that subsequently cured to a tough, temperature-stable elastomer. A module fabricated with the prototype PnBA elastomer successfully passed the JPL thermal-cycle test.

In general, the process for producing the prototype liquid PnBA consisted of first polymerizing a batch of n-butyl acrylate to achieve a high-molecular-weight elastomer, then dissolving the elastomer in an n-butyl acrylate monomer to obtain a solution of acceptable viscosity. A polymerization initiator, Vazo, was also added to the solution. After casting, the liquid was heated for 4 h at 80°C in an oxygen-free environment, which resulted in polymerization of the n-butyl acrylate monomer, and crosslinking, to form a tough, temperature-stable elastomer.

Although the prototype system demonstrated the feasibility and viability of an all-acrylic liquid-casting resin, the prototype system was far from being

a practical material. The existing technology was transferred to Springborn for development to the status of an evaluation-ready pottant and to produce sufficient quantities at the pilot-plant level for industrial evaluation. In parallel, an activity to develop a primer system for PnBA was initiated at Dow Corning.

Experimentation at Springborn has resulted in the development of an evaluation-ready PnBA, described in Table 4-8 (Springborn Identification No. A-13870). The nominal cure time is 20 min at 60°C or 15 min at 70°C, compared with the prototype cure requirements of 4 h at 80°C. Pilot-plant quantities of this evaluation-ready version should become available by Spring 1982. A description of module-processing experiences with PnBA casting liquids is given in Section V. Some mechanical properties of the cured PnBA are also listed in Table 4-8.

The projected high-volume cost for this material is estimated at about $0.85 to $0.90/lb, compared with the commercial selling price of $9 to $11/lb for RTV silicones, which are used in commercial modules as a casting pottant.

e. Aliphatic Polyether Urethane. The commercial liquid-urethane casting systems, which are in common use, are of the aromatic, polyester type. This class of urethanes is unacceptable for encapsulation use because the polyester feature imparts hydrolysis sensitivity and the aromatic feature imparts UV photolysis sensitivity. Urethane liquid systems, based on aliphatic polyether chemistry, are uncommon. Only three companies having these product lines (actually or potentially) have been identified:

(1) H. J. Quinn Co., Malden, Massachusetts.

(2) American Cyanamid Corp., Round Brook, New Jersey.

(3) Development Associates, Inc., North Kingston, Rhode Island.

Only candidate systems from Quinn have been experimentally evaluated; identification and recommendation of specific systems from the others are still pending.

Of the candidate systems available from Quinn, only one approaches the evolving pottant specification and requirements shown in Table 4-3. This is a two-part liquid-casting pottant available from Quinn. The resin, designated Q-626, costs $1.24/lb, and the catalyst, designated Q-621, costs $1.49/lb. The mix ratio is about 3.86 parts resin to 1 part catalyst, which yields a system cost of $1.29/lb. A description of the processing experience with this material is given in Section V.

Some of the required technologies that must be inherent in or developed for urethane systems to enable an acceptable base polymer to acquire the status of evaluation readiness are:

(1) Faster catalyst systems.

(2) Adhesives and primers.

Table 4-8. Evaluation-Ready Poly-n-Butyl Acrylate Casting Syrup

Formulation (Springborn Identification No. A-13870)		
Ingredient	Function	Composition (parts per hundred parts of rubber)
Butyl acrylic, polymer	Base PnBA	35.00
Butyl acrylic, monomer	Viscosity dilutant	60.00
1,6-hexanediol diacrylate	Crosslinker	5.00
Tinuvin-P	Antioxidant	0.25
Tinuvin 770	UV stabilizer	0.05
Alperox-F	Curing agent	0.50

Syrup Properties	Cure Data	Cured Properties at 25°C
Water, white, clear	25°C, no cure within 16 h	Young's modulus: 87 lb/in.^{2}
Viscosity 10,000 centipoise	50°C, no cure within 1 h	100% modulus: 300 lb/in.^{2}
Specific gravity 0.94	60°C, cure in 20 min	Ultimate strength: 293 lb/in.^{2}
	70°C, cure in 15 min	Ultimate elongation: 110%

(3) Antioxidants; thermal stabilizers.

(4) UV stabilizers.

(5) Proof of performance.

f. Silicone Elastomer. The Silicone Products Department of General Electric Co., Waterford, New York, has developed an experimental silicone PV pottant at a present price of about $3.00/lb, or about $0.016/ft^2/mil of thickness. The General Electric designation for this experimental material is 534-044.

The liquid silicone is a room-temperature curing material, requiring a catalyst. After adding the catalyst, the pot life is very short, in the order of 15 to 25 min. In this time the liquid must be deaerated and cast. Full cure occurs in about 4 h at room temperature. To the touch, the cured silicone elastomer is similar to that of Dow Corning's Sylgard 184 and General Electric's RTV/615. Springborn has fabricated a small two-cell glass-superstrate module with this silicone, which passed the JPL thermal-cycle test. Springborn noted that adhesion of this silicone to glass was improved by using a Dow Corning primer, Z-6020. Details of GE's processing experience with this silicone is given in Section V.

There are no cost projections for high-volume use of this material. Although silicone pottant will generally cost more than the other pottant candidates cited above, their use may become attractive in applications where module flammability is a major concern.

B. MODULE FRONT COVERS

1. Requirements

The module front cover is in direct contact with all of the weathering elements: UV, humidity, dew, rain, oxygen, etc.; therefore, the selected materials must be weatherable. Only four classes of transparent materials are known to be weatherable:

(1) Glass.

(2) Fluorocarbons.

(3) Silicones.

(4) PMMA.

In addition to weatherability, the front cover must also function as a UV screen, and possibly as an oxygen barrier, to protect underlying pottants that are sensitive to degradation by UV photooxidation or UV photolysis. The outer surface of the front cover should be easily cleanable and resistant to atmospheric soiling, abrasion-resistant, and antireflective to increase module light transmission. If some or all of these outer-surface characteristics are absent in the front-cover material, additional surfacing materials (to be described in a later section) may be applied. The outer surface may also be chemically modified to achieve a desirable surface characteristic.

2. Candidate Materials

Only four transparent and UV-screening front covers have been identified or developed as promising materials.

a. Glass. Ordinary soda-lime window glass, tempered glass, low-iron glass, etc., can also function as the structural material for glass-superstrate modules without additional mechanical support from a substrate panel.

The UV-absorption characteristics of glass, such as magnitude of absorption and the UV cut-off point, can differ in various glasses; therefore, the selection of a top-cover glass may be keyed to the UV-protection requirements of the underlying pottant. Unlike polymer-film top covers, however, glass is impermeable to oxygen and moisture. The degradation of underlying hydrocarbon pottants (EVA) requires both UV and oxygen for UV photooxidation. Thus, the oxygen-barrier property of glass, rather than UV absorption, may be the feature that prevents pottant degradation, especially if the back cover and edge seal are also oxygen barriers, such as metal foil.

The lowest-costing glass is ordinary soda-lime window glass, estimated by Battelle (see Reference 22) to be about $\$2.58/m^2$ ($\$0.24/ft^2$) for 1/8-in. thickness, when purchased in large volume. At that thickness, all other glasses cost more.

Structural and optical analysis at JPL and Spectrolab (see Reference 12) have identified low-iron, tempered, soda-lime glass as the most cost-effective glass-superstrate candidate. An example of such glass is Sunadex, available from ASG Industries, Inc., costing about \$5.50 to $\$8.50/m^2$, when purchased at the required high-volume level to obtain the lowest selling price.

Structural analysis described in Section III for a 4-ft square glass-superstrate module indicated that a 1/8-in. thickness of such a glass is structurally adequate against mechanical loads, such as 100-mi/h winds. However, increasing the glass thickness to 3/16 in. improves its resistance to damage from hail impact (Figure 4-4), but the glass would cost proportionately more. Any module design using this glass would have to assess the cost-benefit tradeoffs in selecting the thicker or thinner glass with the hail probability history in the geographical area intended for module service.

b. Tedlar. Du Pont markets three 1-mil-thick, clear, Tedlar fluorocarbon UV-screening films. The designation of the three films and their lowest cost for high-volume purchases are:

(1) Tedlar 100 AG 30 UT $\$0.0879/ft^2$.

(2) Tedlar 100 BG 15 UT $\$0.0814/ft^2$.

(3) Tedlar 100 BG 30 UT $\$0.0796/ft^2$.

These designations and cost quotes are extracted from a Tedlar price-list bulletin dated December 1, 1980. Du Pont is considering development of a 2-mil-thick UV-screening Tedlar film.

A past difficulty with Tedlar had been poor adhesion to EVA, both for the clear UV-screening films functioning as front covers, and for white-pigmented Tedlar films functioning as back covers. Du Pont has identified an all-acrylic contact adhesive that can be coated directly onto one surface of Tedlar films. The coated adhesive, a Du Pont product (designated 68040), is dry and non-tacky at ambient conditions; thus, coated Tedlar can be readily unwound from supply rolls. Du Pont experimental testing indicates that when the adhesive is heated during the EVA lamination cycle, strong adhesive bonding develops between EVA and the Tedlar films. The thickness of the adhesive coating investigated by Du Pont ranged between 0.3 to 0.4 mil.

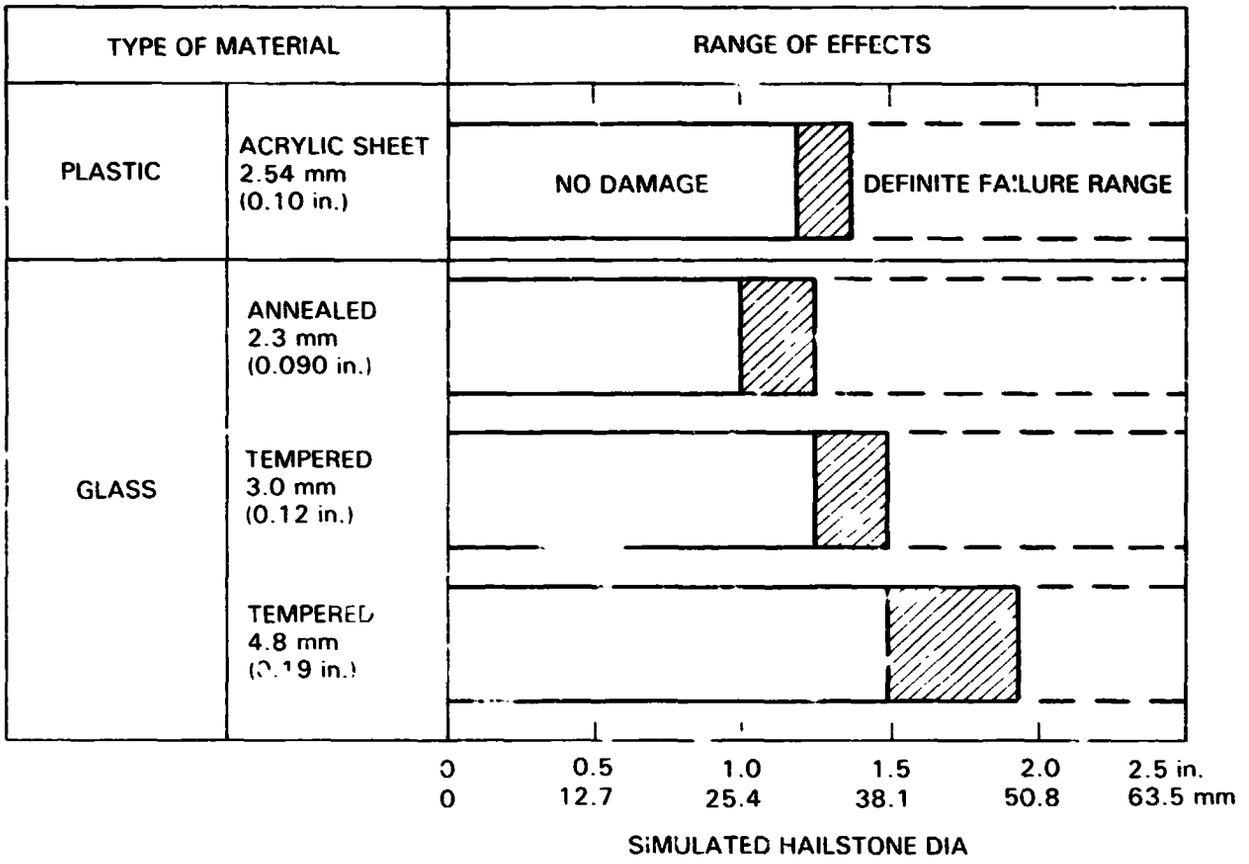

Figure 4-4. Failure Ranges for Glass of Various Thicknesses When Exposed to Simulated Hail

Advantages of Tedlar film are that it is an excellent dielectric, and its surfaces are easily cleaned and generally resistant to retention of atmospheric soiling. Tedlar's soiling characteristics are discussed in the portion on soiling in this section. A discussion of laboratory testing of UV-screening Tedlar films, specifically 100 BG 30 UT, regarding life considerations, is given in Section VI.

c. Acrylic. As of October 1, 1980, 3M began marketing a UV-screening, biaxially-oriented PMMA film. The film product is available in two thicknesses, a 2-mil version, designated X-22416, and a 3-mil version, designated X-22417. In quantities greater than 10 klb, associated with the lowest selling price, the 2-mil film is $\$0.048/ft^2$, and the 3-mil film is $\$0.067/ft^2$. Bulletins describing cost, properties, and features of these film products are available from the 3M Co., under the designation "Acrylar."

PMMA is the most weatherable of all of the acrylic materials, with documented weatherability up to 17 years (Reference 4). A discussion of laboratory testing of these UV-screening PMMA films regarding life considerations is given in Section VI.

Springborn has made small 5- x 8-in. substrate two-cell modules with these films, and is presently fabricating larger-area PV modules. A potential concern with these films is the tendency for thermal shrinkage when heated above 105°C, the glass transition temperature of PMMA. This concern is greater with a free-standing film, but when uniformly pressed and constrained in a module assembly by lamination pressure, the film may be prevented from shrinking. The evidence from the Springborn studies suggests that shrinkage is not a problem. However, Springborn's laminator operates at 1 atm of pressure. Reducing the lamination pressure to less than 1 atm could possibly allow some film shrinkage to occur; however, this has not yet been studied.

Clear Korad 212 acrylic film is no longer recommended for application as a UV-screening front cover. Laboratory testing has shown that the UV-screening property is not permanent, probably limited to less than 2 yr outdoors, and that the clear acrylic film is apparently susceptible to weathering degradation. The clear-film material has been observed to develop surface cracks and crazes in less than 1 yr of natural outdoor exposure; this same behavior has shown up in exposure in accelerated UV weatherometers. (See expanded discussion concerning clear Korad 212 in Section VI.)

The white-pigmented Korad, which acquires weatherability from the pigmentation, may still be considered a viable candidate for back-cover and dielectric-film application. For the latter application in a mild-steel substrate module, or as a back cover for glass-superstrate modules, the film provides a white background behind the solar cells for module-power enhancement.

d. Acrylic-Fluorocarbon Mixtures. These are blends of polyvinylidene fluoride and polymethyl methacrylate, formulated with proprietary UV-screening agents, that are being experimentally developed by several film manufacturing companies. One material is designated Fluorex-A, 1.8-mil thick, and available in experimental quantities for evaluation from Rexham Co.

3. Evolving Material Specifications

Based on experiences with front covers, a list of cover-material specifications can be generated, which is given in Table 4-9. The rationale for some of them is briefly:

(1) Glass Transition Temperature Tg >90°C: The JPL thermal-cycle qualification test exposes modules to a low temperature of -40°C, and a high of +90°C. It is desirable to have the front-cover plastic-film remain at its maximum hardness (to resist softening) at 90°C. Therefore, the requirements of Tg are >90°C for the front cover.

(2) Non-Clouding at 100% RH at 60°C: The module will operate typically near 50°C during daytime, and when exposed simultaneously to a high relative humidity; it is not desirable to have the front cover become opaque from absorbed water (hygroscopic absorption).

Table 4-9. Evolving Specifications and Requirements for Outer Covers

Description	Requirements and Specifications
Glass transition temperature	Tg >90°C
Non-hazing or cloudy	At 100% RH at 60°C
UV screening:	
For oxygen and/or water permeable outer covers	Total absorption 0.36 μm
For oxygen and/or water impermeable outer covers	Total absorption 0.31 μm
Thickness	>1 mil
Total hemispherical light transmission (integrated over the wavelength ranges from 0.4 μm to 1.1 μm)	92%
UV-screening agent:	
Sacrifice	None
Physical loss	None in water at 60°C
Weather-resistant bonding to pottants	No delamination allowed
Mechanical durability and weatherability on modules	Yes
Wrinkling	None
Crazing or cracking	None
Resistant to fracture and fatigue failure	Yes
Resistant to solvent stress cracking	Yes
Hail-resistant	For glass only
Compatible with module fabrication	By lamination, casting, or both

(3) UV-Screening, ≈100% For Wavelengths ≤0.36 μm: This requirement is for plastic films, not glass. The present front-cover candidates meet this, and it is not desirable to retrench.

(4) UV-Screening Agents: The key additive that makes UV-screening front covers work, even if the carrier film is intrinsically weatherable. It should be permanently retained within the carrier film, and also should not be sacrificed to do its job.

(5) Transparent: Film should have maximum light transparency in the wavelengths of solar-cell sensitivity (0.4 - 1.1 μm).

4. Chemically Attachable Ultraviolet Screening Agents

A major premise for the durability of low-cost, UV-sensitive pottants is that protection will be ensured by UV filtering through the glass-superstrate, or by UV filtering through UV-screening plastic-film front covers, and that any harmful UV that does pass through the filters will be absorbed harmlessly within the pottant itself with uniformly dispersed UV screening agents. Loss of UV protection for the pottant by either chemical consumption of the screening agents or by physical loss from bleeding, migration, rain-water leaching, etc., could limit module longevity.

Fortunately, commercial UV screening agents in widespread use, and those used in the pottants and front-cover plastic films, are not susceptible to chemical consumption. They are not chemically destroyed when absorbing UV radiation; they convert UV photon energy into heat. Thus, these agents perform their UV-screening function when they are retained in the film and/or the pottant.

UV screening agents can be divided into two classes: those that are only physically dispersed throughout the bulk volume of a carrier medium, and those that are dispersed throughout the bulk volume of the carrier medium and also are chemically bound to the carrier. Those that are only physically dispersed can be classified on the basis of their molecular weight or on the basis of whether they are small molecules or polymer molecules.

Small-molecule UV screening agents are the most susceptible to physical loss by migration, bleeding, evaporation, leaching, etc. Efforts to diminish these physical-loss tendencies by making the molecules bigger, but not polymeric, increases the problem of uniform dispersal compatibility because the UV screening agents tend to agglomerate into tiny discrete globules. If this occurs in a pottant, no protection is afforded. Thus, there is an inverse relationship between uniform dispersal and molecule size.

Although the physical-loss tendencies for small-molecule UV screening agents are recognized, it is important to recognize that a pottant will be sandwiched between front- and back-covering materials, thereby introducing some partial or total barrier resistance to physical loss of the UV screening agents. No physical loss is expected for a glass-superstrate module with a metal-foil back cover. However, a loss possibility exists for a design with other than a metal-foil back cover and for a substrate design with a plastic-film front cover.

At this stage in developing encapsulation technology for specific additives, it cannot be stated with any certainty that deleterious losses would occur over the 20-yr desired lifetime of terrestrial modules.

Thus, supporting activity to develop and evaluate permanent UV screening by chemical attachment has become an activity of the FSA Encapsulation Task. Table 4-10 summarizes three monomeric chemically attachable UV screening agents of present interest. Permasorb MA is available in limited quantities from National Starch and Chemicals Corp.; vinyl Tinuvin is just barely out of the laboratory, with small quantities being produced at Springborn, and the 2-hydroxy-3-allyl-4,4'-dimethoxybenzophenone is still at the laboratory developmental level. Very preliminary work suggests that vinyl Tinuvin will chemically attach to EVA without difficulty, but not as readily to PnBA. For PnBA, it seems that Permasorb MA may be a better choice.

A final approach is to produce polymeric UV absorbers, copolymerizing the monomeric UV screening agent (see Table 4-9) with a polymeric material that is compatible with the intended carrier medium. Efforts are still at the laboratory level. Physically dispersed polymeric UV screening agents would be significantly more resistant to physical-loss mechanisms than small-molecule UV screening agents.

C. SUBSTRATES

1. Requirements

Structural panel materials that have been surveyed for potential application as module substrates include glass, metals, plastics, inorganics, paper products, and wood products. Included under inorganic products were bricks, tiles, ceramic slabs, resin-bonded sand, and glass-fiber-reinforced concrete. Details of these surveys and extensive master lists of materials have been previously published (see References 10, 11, 18, and 20).

Table 4-10. Chemically Attachable Ultraviolet Screening Agents

Agent	Stage of Development	Researchers
Permasorb MA	Limited availability	National Starch and Chemical Corp.
Vinyl Tinuvin	Laboratory-scale production	Asahi Chemicals, University of Massachusetts and Springborn
2-hydroxy-3-allyl-4,4'-dimethoxybenzophenone	Experimental	JPL

If a 1986 module may be at least 4 ft square, and if it may be mounted in an open-lattice frame by perimeter attachment, then the substrate must support the mechanical loads over the module area, such as wind, hail, snow, etc. Accordingly, the lowest-costing structurally adequate material candidates become:

(1) Mild steel.

(2) Wood (hardboard panels).

(3) Glass-fiber-reinforced concrete.

2. Candidate Materials

a. Mild Steel. This is the least expensive commercially available metallic panel material, based on structural capacity for module application. An advantage of mild steel is that it can be shaped easily to a flat panel with integral stiffening ribs on the back side. The stiffening ribs would reduce the panel thickness required, compared with a panel without ribs carrying the same area load. Optimization of a ribbed-substrate design is being done as part of the FSA Spectrolab design analysis activity.

Mild steel is available in hot-rolled and cold-rolled form, and as a substrate panel the differences are a slight cost differential, the range of standard thicknesses, and surface finishes. Cold-rolled mild steel is commercially available in a standard thickness range from 0.0142 to 0.229 in.; hot-rolled mild steel typically begins at a thickness of 0.061 in. (other thicknesses for either kind can be obtained by special request, but at a higher cost). Generally, the surface-finish quality of cold-rolled is better than hot-rolled. Cost data for cold-rolled mild steel and a quotation for 0.061-in.-thick hot-rolled mild steel are included in Table 4-11. Based on the general quality of surface finishes and the range of readily available thicknesses, it seems advisable to use cold-rolled mild steel.

A disadvantage of mild steel is its corrosion sensitivity. There is evidence (References 25 to 29) that metallic corrosion may be arrested when the metal is wholly enclosed within a polymeric conformal coating, chemically bonded to the metallic surface. The chemical bonding between the metal surface and the polymer coating is accomplished with chemical-coupling agents, e.g., silanes. Reference 28 points out that organic-coated metals have remained uncorroded after 19 yr of direct exposure to salt water. Following this approach, Figure 4-5 illustrates three conceptual packaging techniques for mild steel that can be described by the materials to be used:

(1) Organic coating with primers.

(2) Plastic films.

(3) Aluminum and stainless-steel foils.

Table 4-11. 1979 Cost Quotations for Mild Steel

Type	Thickness, in.	Cost	
		$/ft^2	$/lb
Cold-rolled	0.0142	0.137	0.2400
	0.0280	0.236	0.2075
	0.0630	0.533	0.2075
	0.0810	0.589	0.1785
	0.2290	1.570	0.1785
Hot-rolled	0.0610	0.460	0.1850

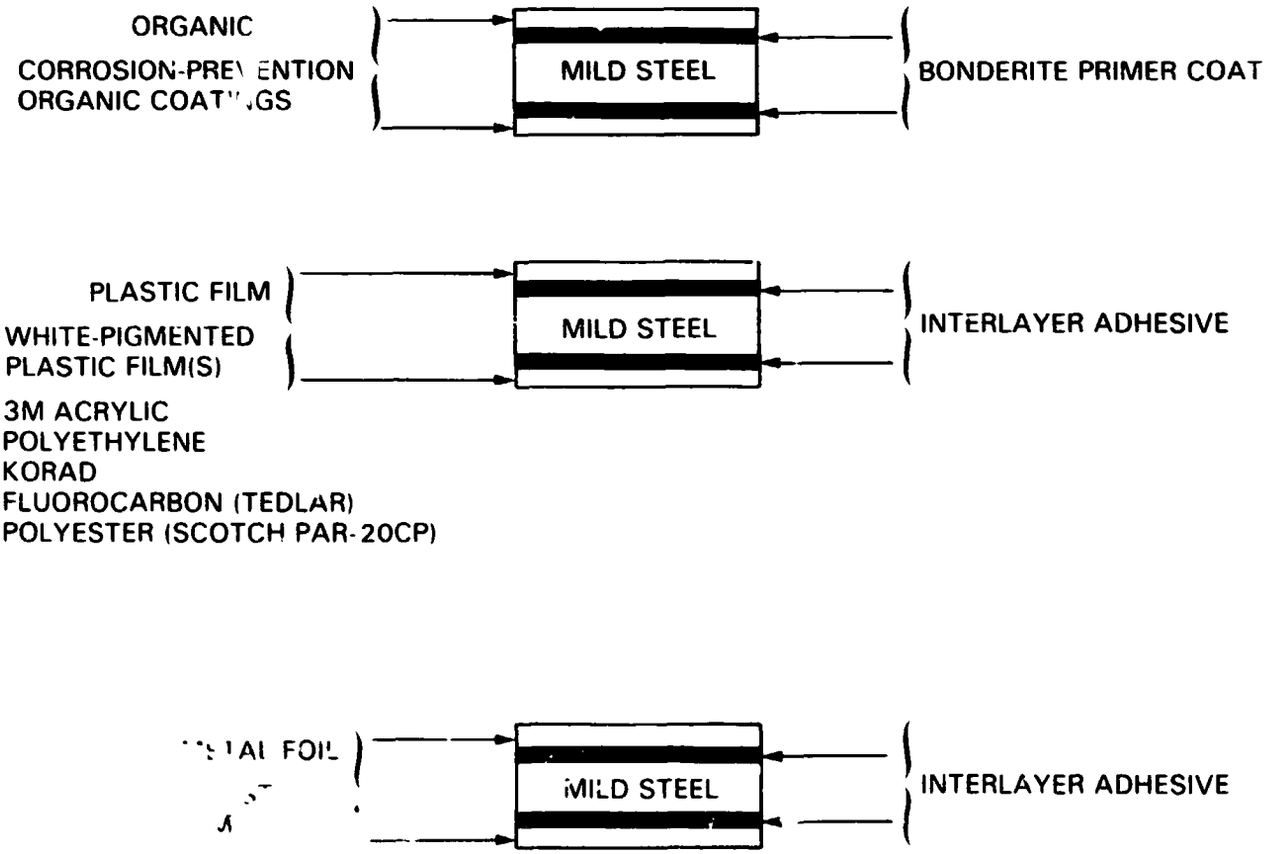

Figure 4-5. Mild-Steel Packaging Concepts

Alternatives to mild steel are galvanized (zinc-coated) and enameled steel. In general, galvanized steel will cost about 20% more than mild steel. Steel sheet, which can be enameled, costs about 15% more than mild steel, and there are additional costs for the enamel and the enameling process. Detailed cost analyses of enameled steel products for PV modules have not been completed.

The organic coatings and primers (commercially available corrosion-protection coatings, recommended by an industrial consultant) are shown in Table 4-12, with their costs and remarks on expected lifetimes. This approach has greater potential of lower cost than those of galvanized or enameled-steel coatings.

The plastic films would be adhesively bonded to the mild steel, with the initial proposal that the adhesive material will be based on pressure-sensitive acrylics. Candidate adhesive systems are being identified, but specific brand-name identifications are not yet available.

Another option may be the use of hot-melt adhesives. The plastic film, which would function as the back covers, would be white, and some possible candidates are white-pigmented Tedlar (Du Pont), white-pigmented 3M acrylic film, white-pigmented polyethylene, and white-pigmented polyester films marketed by 3M under the trade name Scotchpar 20-CP-White. The white-pigmented 3M acrylic film will be a version of X-22416 or X-22417, which is being developed experimentally at this time by 3M. Springborn will identify a white-pigmented polyethylene that is weatherable, and will also recommend the appropriate interlayer adhesive(s). The plastic film on the top, or sunlit, side of the mild steel is proposed to be a white-pigmented Korad acrylic film (XCEL Corp.). Korad was selected because it will readily undergo chemical bonding with EVA, which would be in contact with this film, and the whiting would provide the white background desired for internal light reflection to enhance solar-cell output. The white-pigmented Korad could also be used as the back cover over the steel.

The aluminum and stainless-steel foils may be adhesively bonded to the mild-steel panel, providing hermetic isolation of the mild steel. The stainless-steel foils would provide matched thermal-expansion properties; with the aluminum foils, the adhesive interlayer would have to provide strain-relief between the two dissimilar expanding metals.

Mild-steel panels, which have been wholly enclosed in clear EVA that has been chemically coupled to the metal surfaces with silane coupling agents recommended by Dow Corning, are being tested at Springborn (Reference 30; see also Table 4-5). After several thousands of hours of exposure to corrosive environments, such as salt spray, there is no visual evidence of metallic corrosion. On the other hand, unprotected metallic controls corrode rapidly.

Additionally, metallic strips were partially coated, with half of the strip wholly enclosed and the other half exposed. The uncoated-half corroded rapidly, and there is visual evidence that surface corrosion is proceeding slowly under the edge of the EVA coating.

The conclusion is that mild-steel substrates, no matter how they are shaped, would have to be wholly enclosed (top side, back side, and edges) within a continuous and unbroken corrosion-protection coating.

Table 4-12. Commercial Corrosion-Prevention Coatings for Mild Steel

Coatings, Supplier, Endurance to Date	Cost, Both Sides $/ft^2
Polyvinylidene fluoride (primer + enamel) PPG Industries; 10 yr outdoor	0.112
Silicone-Polyester Dexter-Midland; prototypes to 20 yr	0.054
Polyester Dexter-Midland; 5 to 10 yr outdoors	0.040
Acrylic Coating PPG Industries; 5 yr outdoors	0.040
Polyester (compliance coat) Dexter-Midland; 5 yr outdoors	0.040
Acrylic Emulsion Coating Dexter-Midland; 5 yr (extrapolated)	0.052
Polyester Powder Coating Dexter-Midland	0.056
"Bonderite" Primer-Treated Conversion (to be applied before coating)	0.002

Springborn and Solar Power Corp. have fabricated 11- x 16-in. PV modules with flat sheets of mild steel as the substrate and EVA pottant. The white-pigmented EVA is being used as the conformal coating to wholly enclose the mild steel, which is achieved during vacuum-bag lamination. Modules of this design are now mounted outdoors in marine, desert, and urban environments.

b. Wood. Wood is the least-expensive structural material identified to date that could be used as a substrate panel for a perimeter-clamped, 4-ft-square module. Structural wood products are divided into two classifications: prime lumber and reconstituted wood products. The reconstituted wood products for large-area wood panels, such as particle boards, plywood, fiberboards, etc., are useful as module substrates.

Of all of the varieties of reconstituted wood panels, only two kinds are considered to be viable candidates: strandboards and hardboards. The latter are fiberboards with densities greater than 50 lb/ft^3. Both of these wood products are moldable and can be shaped as flat panels with integral stiffening ribs. With rib stiffening, the thickness of the hardboard need be only 1/8 in. Optimization of a panel rib design is being studied at Spectrolab.

Hardboard panels are readily available: Masonite Corp. markets several 1/8-in.-thick panels with modulus values on the order of 800 klb/in.^{2} to 10^6 lb/in^2. The price of these panels is about \$0.12/ft^2. The specific hardboard being experimentally evaluated as a module substrate panel is Super-Dorlux.

U.S. Gypsum also markets a comparable hardboard panel, designated Duron, which is available in a 1/8-in. thickness, costing \$0.12 to \$0.13/ft^2, essentially the same as the Masonite hardboards.

Strandboard panels are being developed by Potlatch Corp., which will shortly begin commercial production. Strandboard panels with modulus values about 800 klb/in.^{2} are being manufactured for evaluation at pilot-plant production levels. The projected price of strandboard panels is about \$0.16/ft^2 for 3/8-in. thickness, which will probably be the thinnest such panel to be marketed by Potlatch.

The thermal analysis report in Section III indicates that the operating temperature of modules with a glass superstrate, mild-steel substrate, and 1/8-in.-thick wood-panel substrate will be within 1°C of each other. The use of wood panels thicker than 1/8-in. would increase the module operating temperature because of restricted bulk-thermal conduction to the back surface. Therefore, for array applications where module cooling can occur from the front and back surfaces, the thinner, 1/8-in.-thick ribbed hardboards may be preferable. But for rooftop applications where module cooling may be restricted to occur principally from the front, and negligibly from the back, thicker wood panels, such as strandboards, may be preferable, with the panel also becoming part of the rooftop structure.

In an outdoor weathering environment, wood products generally deteriorate from one or more of the following actions:

(1) UV photooxidation of the lignin.

(2) Structural breakdown from extremes of hygroscopic expansion and contraction.

(3) Water rot.

For long service life outdoors as a substrate panel, the wood product must be protected from UV and hygroscopic-expansion extremes. UV protection seems to be relatively easy to provide. By design, the front surface of the wood panel is positioned behind a UV-screening front cover (and pottant and solar cells), and the back surface needs only to be coated with an opaque surfacing material.

The real problem with wood panel is its hygroscopic behavior. For example, available data indicate that the thermal-expansion coefficient of hardboard is about 7×10^{-6} in./in./°C, and that its hygroscopic-expansion coefficient is about 5×10^{-5} in./in./% RH. Thus, a 1%-RH fluctuation causes about the same expansion and contraction as a temperature change of 7°C.

When hardboards with these kinds of thermal and hygroscopic-expansion and contraction properties are cycled during module fabrication in a vacuum-bag

lamination up to 150°C, the hardboard will experience a net contraction from water dryout, and later, when returned to a humid environment, the wood will expand. Assuming that the encapsulated solar cells are at zero or near-zero mechanical stress at the end of the lamination cycle, gradual regaining of atmospheric moisture by the wood panel to equilibrium with outdoor relative humidities imposes significant tensile strains (stress) on the solar cells, leading to cell cracking or interconnect failure. (This behavior is described in Section III.)

Hardboards must be packaged before lamination to prevent or limit wood dryout during vacuum lamination. The same packaging must prevent or limit the hygroscopic response of the hardboard from outdoor relative-humidity fluctuations during service. With sufficient thickness of a polymeric conformal coating or plastic film, the hygroscopic response fluctuations of a wood panel can be damped to the point where the wood's absorbed-water content is in virtual equilibrium with the annual average relative humidity of its locale. In effect, hygroscopic expansion and contraction of the wood panel is arrested. The optimum thickness of wood coating to achieve required time constant has not yet been determined.

About 85% of the United States has an annual average relative humidity of about 55% to 65% RH (according to the U.S. Weather Bureau). This suggests that wood panels should probably be equilibrated to near 60% RH before being fabricated into modules.

Assuming that equilibration to 60% RH (or whatever may be optimum) is accomplished before lamination, then pre-lamination packaging must seal the wood against significant water loss. It would also be desirable if the packaging approaches served useful module functions later during outdoor service. With these objectives in mind, packaging concepts for hardboards have been suggested that are similar to those proposed for mild steel and can also be described by the intended protective materials:

(1) Organic coatings.

(2) Plastic films.

(3) Metal foils.

The three packaging concepts are illustrated in Figure 4-6. The viable candidates for the organic coatings are melamine formaldehydes. Surveys for applicable melamine-formaldehyde coatings will be done shortly. The plastic films and metal foils being considered are the same ones being considered for mild steel, but the interlayer adhesives could be different. This will be assessed by Springborn.

Although organic coatings and plastic films used on wood are not impermeable to moisture, the intention is to limit moisture loss significantly during the lamination process.

As with mild steel, the wood-packaging concept can be hybridized to have a metal-foil back cover and a plastic-film or organic-coated top-side cover.

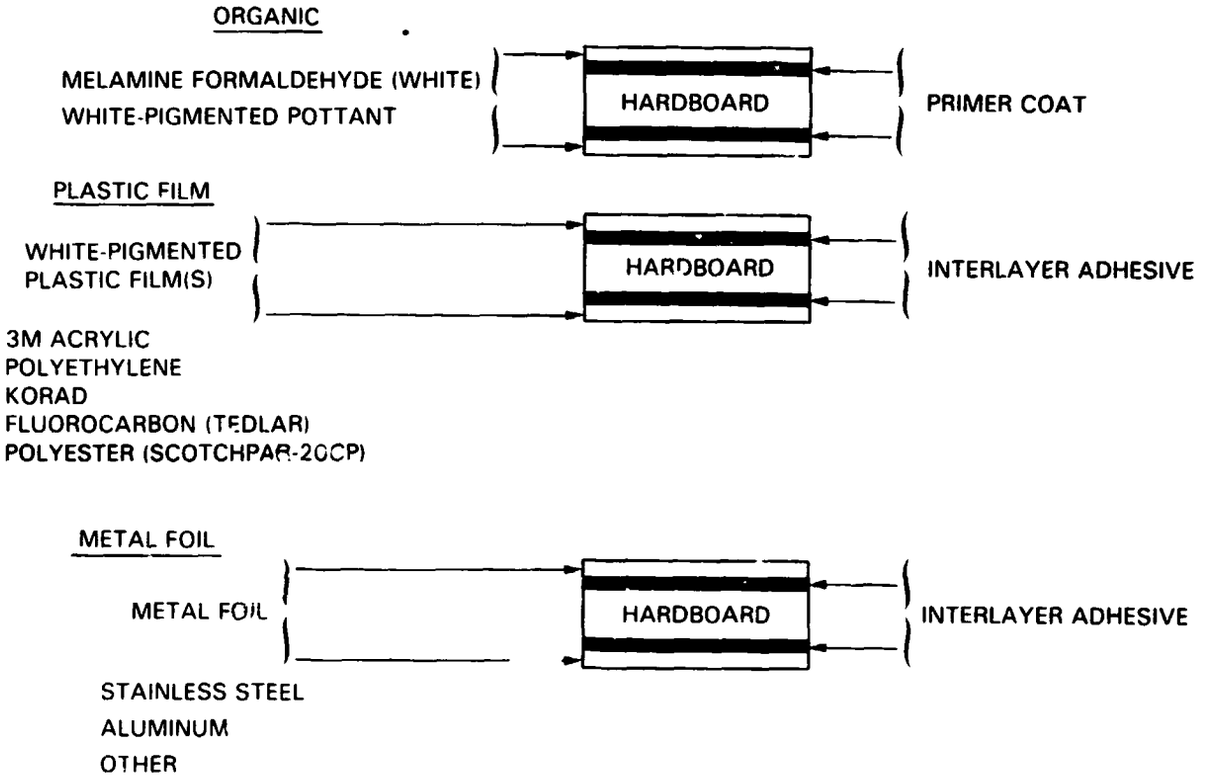

Figure 4-6. Hardboard Packaging Concepts

Test samples of wood and mild steel with all of the various packaging combinations, and edge-sealed with an appropriate edge-sealing tape, are scheduled for outdoor weathering exposure. Additionally, mild-steel test samples with edge-sealing tape will be subjected to accelerated-corrosion testing. Springborn will also investigate the module fabricability of wood and mild-steel panels with various combinations of the proposed packaging techniques, and will recommend the most promising combinations for further consideration.

Separately, JPL will investigate the rate and equilibrium behavior of the thermal and hygroscopic properties of hardboard.

Springborn and Solar Power Corp. have fabricated 11- x 16-in. EVA modules with Super-Dorlux hardboard-substrate panels. The hardboard panels are wholly enclosed within a continuous, conformal coating of white-pigmented EVA. Modules of this design are being exposed outdoors in marine, desert, and urban environments.

c. Glass-Reinforced Concrete (GRC). GRC-substrate panels have been developed by Tracor MBA, San Ramon, California (Reference 31). The 4- x 8-ft panels are 1/4 in. thick, and have integral reinforcing ribs on their back

sides. The projected cost of a panel is $0.62/ft^2, but this cost is partially offset by the fact that its inherent mechanical rigidity reduces the cost of rack materials required for outdoor mounting. Total-cost analyses indicate that GRC may be cost-effective if it is part of the solar-array field-mounting structure and serves as a module substrate.

Tracor MBA has manufactured a 4- x 8-ft demonstration module with this substrate material, using EVA as the encapsulation pottant and clear, UV-screening Korad 212 as the top cover. The demonstration module is mounted directly on 6- x 6-in. pressure-treated wood posts, simulating an array field structure.

D. POROUS SPACER

Fabrication of large-area modules by vacuum-bag lamination will require the use of air-release spacer materials at various interfaces in the pre-laminated module-assembly stack-up. This requirement becomes more important for lamination pottants that tend to block or stick on contact with other surfaces. If air is interfacially trapped during lay-ups because of film blocking, it will be virtually impossible to exhaust this air from the interface in a vacuum-bag laminator, and air bubbles will be retained in the finished module. Air exhaustion, even with non-blocking pottants, tends to become more difficult as the module area increases.

The air-release porous spacer material can serve additional useful functions. Substrate modules using metallic substrates, or glass-superstrate modules using metallic foils as back covers, must be fabricated in such a way that the electrical-insulation thickness between the solar-cell circuitry and metallic surfaces is maintained during fabrication. This can be accomplished by positioning an incompressible and non-conductive spacer between the solar cells and the metallic surface, which then prevents physical contact between the cells or interconnects and any metallic surface. The dielectric strength of the pottant, and the voltage difference to be insulated against, will result in a specification of absolute minimum thickness of pottant to ensure electrical isolation, avoidance of electrical breakdown, and subsequent arcing through the pottant. By selecting the thickness of the porous spacer used between the cells and metallic surfaces to be equal to or thicker than the absolute minimum requirement, reliable fabrication of a module with the required pottant insulation thickness is ensured as the spacer material becomes embedded completely in the pottant. Structural analysis at Spectrolab (see Reference 12) clearly demonstrates that stress coupling between the solar cells and the structural panel involves the tensile modulus of the pottant and the thickness of the pottant separation between the cells and the structural panel. Therefore, based on mechanical considerations, there will be requirements on minimum pottant thickness to limit the tensile stress developed in solar cells.

In summary, the interfacial spacer must at least be:

(1) Electrically non-conductive.

(2) Mechanically non-compressible.

(3) Porous for in-plane air flow.

(4) Inexpensive.

(5) Transparent after processing (when above cells).

Several candidate spacer materials were investigated (see Reference 19), and the best materials satisfying these four criteria are non-woven glass mats manufactured by the Crane Co., Dalton, Massachusetts. The materials are sold under the trade name Craneglas, and are distributed by Electrolock, Inc., Chagrin Falls, Ohio. The designation and cost of these materials are listed in Table 4-13. One result of the Spectrolab encapsulation design and analysis activity is the finding that a minimum thickness of 5 mils of EVA is sufficient for both electrical insulation and mechanical-stress decoupling. Therefore the specific mat being used in experimental modules fabricated with EVA is the Craneglas Type 230, 5 mils thick, costing $\$0.0078/ft^2$.

The level of voltage achieved before electrical breakdown of EVA-encapsulated modules with this 5-mil spacer material has been investigated experimentally. Test modules were constructed with the following materials (top to bottom):

(1) Soda-lime window glass.

(2) 20-mil clear EVA film.

(3) Cell string.

(4) 5-mil non-woven glass mat.

(5) 14-mil white-pigmented EVA.

(6) 1-mil aluminum foil.

Table 4-13. Non-Woven Glass Mats for Electrical and Mechanical Spacer Application (Craneglas)

Type	Thickness, mils				
	3	5	7	9	12
	Cost, $\$/ft^2$				
200	0.0132	0.0176	0.022	0.028	0.037
210	-	-	0.0156	-	-
230	0.0066	0.0078	0.0097	0.0136	0.0181

Under lamination pressure, the thickness of the non-woven glass mat would limit the minimum thickness of pottant between cells and the aluminum foil to the required 5 mils. However, cross-sectional measurements made on those modules indicate a pottant thickness about 10 mils. The electrical breakdown voltage of several test modules was measured at 5.8 kV, $\pm$0.2 kV.

The non-woven glass mats will provide another useful function if used on the back side of wood-substrate modules. As mentioned earlier, the hygroscopic response of wood panels can be arrested with sufficient thickness of the conformal polymer coating. Some wood-substrate modules, fabricated by vacuum-bag lamination, include in the lay-up a 14-mil white-pigmented EVA film on the back side of the wood panel. Under lamination pressure, this film thins to an uncontrolled thickness. By including a non-woven mat on the back side, the thickness of the back-side EVA film will always be at least the thickness of the mat. The 5-mil-thick mat is being used now; however, future experimentation will identify the optimum required thickness and how thin the pigmented EVA film may be (for cost savings).

Optical-transmission measurements, as explained in Section III, have adequately demonstrated that the Craneglas spacer material can be used above the active surface of the solar cells (on the sun side) without loss of electrical performance or optical transmission. In fact, some preliminary evidence suggests performance enhancement, which is thought to be caused by internal light scattering and reflections involving the spacer.

E. BACK COVERS

Back covers are evolving from the specific need to protect the back side of a low-cost module. There are three back-side materials considered attractive for low-cost modules: wood and mild steel for the substrate designs, and the laminating pottant for glass-superstrate designs. Wood and mild steel require back covers for reasons stated earlier, such as UV isolation and humidity-fluctuation barriers for wood, and corrosion protection for mild steel. The back-cover candidates for wood and mild steel were described in the substrate section, and are summarized in Figures 4-5 and 4-6.

For glass-superstrate designs, the pottants, which are polymeric materials, may need added protection from humidity or from back-scattered UV, or may need durable back covers for protection during storage, shipment, and mechanical action, such as blowing sand. The need for a hermetic metal-foil back cover in the glass-superstrate design may be determined by the moisture sensitivity of different low-cost cell-metallization materials.

An additional requirement that has evolved for back-cover materials is that they be non-metallic and white, as indicated in the section on thermal analysis in Section III. This analysis showed that the module operating temperature is significantly regulated by the infrared (IR) emissivity of the back surface. To lower module operating temperature, the highest possible IR emissivity is desired. To minimize absorption of reflected and scattered light reaching the back surface, the back surface should have the minimum possible solar absorptivity. The condition of high IR emissivity and low solar absorptivity is met by having a non-metallic, white surface.

C-2

Back covers proposed for glass superstrate modules are:

(1) White-pigmented pottants.

(2) White-pigmented plastic films.

(3) Metal foils with white back surfaces.

White-pigmented pottants can be prepared by appropriate compounding with whiting agents, such as zinc oxide or titanium oxide, as has already been done with EVA. The plastic films and metal foils can be the same ones described earlier for wood and mild steel. Generally, back covers for glass-superstrate designs are:

(1) White-pigmented pottants (Springborn).

(2) Scotchpar CP-White polyester films (3M):

(a) 1-mil standard $\approx$ \$0.02/ft^2

(b) 2-mil standard $\approx$ \$0.04/ft^2

(c) 2-mil hi-filled $\approx$ \$0.05/ft^2

(3) White-pigmented versions of X-22416 and X-22417 UV-screening acrylic films, being developed by 3M.

(4) Metal foils.

(5) Plastic film, metal-foil laminates.

(6) Clear Mylar, \$0.014/ft^2/mil.

(7) White Tedlar:

(a) 150 BL 30 WH, 1.5 mil, $\approx$\$0.075/ft^2.

(b) 200 BS 30 WH, 2.0 mil, $\approx$\$0.142/ft^2.

Aluminum is the most appealing metal-foil candidate because of cost, availability, and weatherability. However, other metal foils, such as steel, will be investigated. The minimum thickness of aluminum foil that can be classified pinhole free is 1 mil, at a high-volume cost of \$0.019/ft^2. The use of aluminum foil requires an electrically nonconductive film layer between itself and the solar cells to maintain positive voltage isolation. It is recommended that the aluminum foil be pre-coated or laminated with a nonconductive material, such as Mylar, obviating an additional spacer material.

Laminates of aluminum or steel foil and polymer films are commercially available, as are polymer films that have been coated with vapor-deposited aluminum. Commercial products and their suppliers are shown in Tables 4-14 and 4-15. The prices quoted in the tables are for routine low-volume sales. Cost projections for high-volume sales have not been made, but as an initial guideline, the cost of 92-gauge Mylar (0.00092 in.) for high-volume sales is

Table 4-14. Aluminum Foil-Polymer Laminates[a]

Supplier	Product	Price, $/ft^2
Acme Backing	Polyester/aluminum/polyester	
	0.5 mil PET/1-mil aluminum/0.5 mil PET	0.10
3M Co.	No. 431 aluminum-foil tape with acrylic adhesive	0.35
	No. 425 aluminum-foil tape with acrylic adhesive	0.35
Spaulding	0.007 Tedlar (PVF)/0.001 aluminum:	
	regular	0.16
	adhesive	0.40
	0.001 aluminum/0.001 Mylar:	
	regular	0.19
	adhesive	0.44
	0.001 aluminum/0.001 fiber:	
	regular	0.22
	adhesive	0.47
Surgicot	SPF-2273	
	0.066 nylon/ream polyethylene	0.08
	0.00035 aluminum-foil/ream polyethylene	
	0.002 polyethylene film	

[a]PVF = Polyvinyl fluoride.

$0.014/ft^2. Mylar is a polyethylene terephthalate (PET) product, and as noted earlier, 1-mil aluminum foil is $0.019/ft^2. The combined cost is therefore $0.033/ft^2, which can be proportioned appropriately for comparison with aluminum-PET described in the tables. The combined cost of the aluminum foil and the 5-mil non-woven glass mat is the lowest identified: $0.027/ft^2.

If the back surface of a glass-superstrate design is a white-pigmented layer of the pottant, it can be expected that the pigment filler will increase

Table 4-15. Polymer Films with Vapor-Deposited Aluminum

Supplier	Product	Price, $/ft^2
Coating Products	Metallized Mylar:	
	0.05-mil	0.02
	1-mil	0.03
	2-mil	0.06
	1/2-mil Mylar/white polyvinyl chloride (PVC):	
	4-mil PVC	0.09
	8-mil PVC	0.11
	12-mil PVC	0.14
	Mylar/60-lb paper:	
	1-mil Mylar/paper	0.06
	2-mil Mylar/paper	0.10
	3-mil Mylar/paper	0.13
	0.5-mil Mylar/aluminum deposit/adhesive:	
	5-mil Mylar	0.26
	0.5-mil Mylar/aluminum deposit/adhesive:	
	1-mil Mylar	0.22
Hilcor Plastics	Metallized Mylar:	
	2-mil	0.08
King Seeley	Metallized Mylar:	
	0.5-mil	0.02
	1.0-mil	0.03
	2.0-mil	0.06
ICI	Melinex polyester 0.5-mil:	
	clear	0.07
	metallized	0.10

Table 4-15. (Cont'd)

Supplier	Product	Price, $/ft^2
3M Co.	No. 852 metallized polyester (adhesive)	0.68
Milprint	Metallized polypropylene:	
	0.9-mil	0.02
	Metallized-oriented nylon:	
	0.9-mil	0.02
	Metallized high-density:	
	polyethylene	0.01
Mobil Chemical Co.	Oriented polypropylene	
	Metallized on side with a heat-sealing resin on the other side	
	Metallized Bicor:	
	0.7-mil	0.01
	0.9-mil	0.01
National Metallizing (A. Saxon Corp.)	Metallized-polyester laminated to polyethylene	0.02
St. Regis	Metallized polyester:	
	0.5-mil	0.01
Vacumet	Metallized polyester:	
	1-mil	0.03
	2-mil	0.06

the mechanical toughness and durability of the pottant, and if properly selected, also enhance UV protection. Examples of experimental modules with a back cover of a pigmented layer of the laminating pottant are:

(1) Glass.

(2) 20-mil clear EVA film.

(3) Cell string.

(4) 5-mil non-woven glass mat.

(5) 14-mil white-pigmented EVA film.

The back surface is mechanically tough and durable, and the glass mat isolates the solar cells electrically from the back surface. From the front, the white pigmentation provides a light-reflecting background that increases module power output.

F. EDGE SEALS AND GASKETS

The edge of an encapsulated module must also be sealed to prevent intrusion of water and other harmful environmental substances, and must be gasketed with a material that will cushion and isolate the edge against damaging stresses set up by perimeter clamping of a module in an outdoor mounting frame. The terminology, edge seal and gasket, connotes the dual requirement of atmospheric isolation and mechanical-stress cushioning, respectively, but does not necessarily imply that two or more discrete materia are required.

Table 4-16 documents a first effort at defining requirements for edge seals and gaskets for module application, which became guidelines for material surveys that still continue.

Generic classes of materials being surveyed for edge-seal gaskets are shown in Table 4-17. For gaskets, the four candidate materials are ethylene propylene rubber (EPDM), EVA, neoprene, and silicone. The prime candidate of the four is EPDM. For seals, the prime material candidate is butyl, from among the following tacky-filler materials:

(1) Butyls.

(2) Polysulfides.

(3) Polyurethanes.

(4) Silicones.

(5) Hypalons.

(6) Neoprenes.

(7) Polyamides.

(8) Acrylics.

Table 4-16. Evolving Specifications and Requirements for Edge Seals and Gaskets[a]

Item	Description	Requirements and Specifications
Edge seal	Weather-stable, permanent adhesive material incommon contact with gasket and module edges	Non-staining Tg $<-40^{o}C$ Liquid-water barrier Low water-vapor transmission Chemically inert Non-debonding Accommodates module expansion, contraction Resistance to mechanical fracture Restricted flow, creep, spread Low cost
Gasket[b]	Elastomeric, one-piece, seamless stripping with channel filled with edge-seal material	Tg $<-40^{o}C$ Weather-stable Unplasticized Extrudable Accommodates module expansion, contraction Low-compression set at $90^{o}C$ Low cost Chemically inert

[a]Separate edge-seal and gasket concepts may have to be developed for laminated and cast module designs.
[b]Alternative design is a gasket-primer combination.

A critical property that is needed for elastomeric gasket materials is compression-set-recovery (CSR), which is a measure of the recovery of the material to its initial thickness after a compressive load is relieved. A corollary is that elastomers with good CSR should resist flow-out, creep, or decay from the internal stress of the elastomer. This internal stress, acting to restore the gasket to its initial thickness, is what maintains a tight fit. Table 4-18 summarizes the average cost per pound of the four gasket candidate materials, and the generally observed range of CSR for this family of materials. The CSR behavior for all four is essentially the same. Because there is a variety of EPDM formulations with various fillers and additives, there is a need to identify those specific EPDM gasket formulations that will be best suited for outdoor module applications.

Table 4-17. Edge-Gasket Materials Survey: Elastomeric Molding

Candidates	Non-Candidates
Ethylene Propylene (EPDM)	Natural rubber
Ethylene Vinyl Acetate (EVA)	Styrene butadiene
Neoprene	Butyl, halogenated butyl rubbers
Silicone	Nitrile, butadiene
	Polysulfide
	Hypalon
	Fluoroelastomers

A preliminary cost analysis can be made using a figure of $0.58/lb for gasket-grade EPDM. Structural analysis at Spectrolab (see Reference 12) indicates that an edge gasket for a 4-ft-square glass-superstrate module should be at least 1/16 in. thick, and have a surface coverage of 3/8 in. inward from the module edge. Allowing the module to be 1/4 in. thick, the cross section of the gasket can be represented as essentially a rectangle 1/16 in. wide x 1 in. long. Because a module that is 4 ft square has a surface area of 16 ft^2 and a perimeter of 16 ft, cost expressed on the basis of 1 ft is also cost/ft^2 of module area. Using the indicated cross-sectional area for the gasket, a material density of 1 g/cc, and a cost of $0.58/lb, the estimated cost of EPDM material is $0.016/ft.

EPDM compound advantages are:

(1) Best compression set-cost ratio.

(2) Low cost.

(3) Easy extrusion, complex profiles.

(4) Demonstrated weatherability.

(5) History of successful use in related application (automotive windshields).

Table 4-19 . an extensive summary of sealant compounds being identified from seal surveys, with approximate cost/foot. In general, the nominal cost of commercial sealants will vary from $0.016/ft to $0.042/ft of module edge. If the estimated material cost of the sealant is added to the cost estimates for an EPDM gasket, an aggregate edge-seal-and-gasket-system cost for materials is estimated at $0.032/ft to $0.058/ft. Increasing the estimate by a factor of

Table 4-18. Gasket Compounds

Compounded Elastomer	Cost, $/lb	Compression-Set-Recovery, %	Cost/Set-Recovery Index,[a] $/%
Silicone	2.53	65 - 90	2.81 - 3.89
EVA	0.85	65 - 80	1.06 - 1.31
Neoprene	0.87	75 - 85	1.02 - 1.16
EPDM	0.58	70 - 90	0.64 - 0.83

[a]For comparative purposes only.

three to allow for inaccuracies, thicker material usage, manufacturing and installation costs, etc., still yields an estimate of $0.10/ft to $0.18/ft, which is within the cost allocation of $0.11/ft to $0.26/ft for edge seals and gaskets.

G. PRIMERS AND ADHESIVES

Modules must perform reliably for 20 yr, resisting delamination and separation of any of the encapsulant materials. Delamination of encapsulant materials can create voids for accumulation of water and potential corrosive failure. Delamination of silicone elastomers from substrate surfaces was a common occurrence with Block I modules, but the incidences of silicone delamination with Block II and Block III modules decreased when adhesion promoters (recommended by the silicone manufacturers) were used. An investigation of silicone delamination from unprimed surfaces identified the failure mechanism, which is reported in References 32 and 33.

It would be desirable to have all of the interfaces in encapsulation materials and between encapsulation materials and solar cells held together by environmentally stable primary chemical bonds (Reference 34). Some materials bond to each other chemically during the module fabrication process, but the majority of interfaces will probably require the use of a chemical-coupling primer or adhesive.

Chemical bonding materials are divided into three classifications: coupling agents, primers, and adhesives. The distinctions among these classes are not based on chemical differences but on the thickness of the chemical bonding material between adjacent adherents.

Therefore, based on these distinctions, a chemical-bonding material is referred to as a coupling agent if its thickness is of the order of that of a

Table 4-19. Solar Module Sealants[a]

Class	Approximate Cost, $/lb	Approximate Cost, $/ft and ft^2
Silicone	3.50	4.2
Polyamides	2.60	2.5
Polysulfides	2.25	2.3
Polyurethane	2.25	2.3
Acrylics	1.70	2.0
Butyls:		
Tape compounds	3.67	3.6
Hot melt (non-cure)	2.00	2.0
Hot Melt	1.62	1.6

[a]4- x 4-ft module (1/8-in. bead of sealant); cost/foot equals cost/ft^2 for this module size.

monomolecular layer. A chemical-bonding material with a thickness of about 0.1 to 10.0 μm will be referred to as a primer. An adhesive is generally a gap-filling material thicker than 10.0 μm.

Thickness is generally mandated by the physical states of the adherends, specifically, the capability of one adherend to coat the interfacial surface conforming to the other. For example, liquid resins spread readily over the surfaces of woven glass cloths, so only a monomolecular layer of a chemical-bonding material need be on the surface of the glass cloth when manufacturing glass-reinforced polymer composites. Thus, in the composites industry, the chemical-bonding material is referred to as a coupling agent.

On the other hand, solid adherends, such as brass and steel or two pieces of wood, do not have surfaces that will conform to each other on contact. Therefore, the gap between the solid adherends is filled with a conformal, gap-filling adhesive. Primer is a thin adhesive applied to a solid surface that is to be bonded to a conformal adherent, such as paint, laminating film, etc.

Whether functioning in a thin layer as a primer, or a thicker one as an adhesive, the chemical-bonding material must have adequate mechanical film properties, such as rigidity, tensile strength, and toughness, to carry the mechanical load when the bonded system is stressed. This is not a requirement for application as a coupling agent.

Generally, coupling agents are low molecular-weight fluids; the molecules contain two distinct reactive chemical groups (bifunctional), one for each adherend. Many bifunctional materials can function dually as coupling agents and primers, but some are restricted to functioning as coupling agents only because of inferior film properties, such as brittleness.

Primers and adhesives are generally film-forming polym mat ls. Primers are usually sold as solvent solutions to facilitate ositing thin film; adhesives are usually sold in bulk to achieve thickness. Primers are generally bifunctional as are coupling agents, but adhesives are not. Adhesive materials are used in combination with coupling agents or primers, or the coupling agents or primer are physically blended into the adhesive material. Under the latter conditions, the primer or coupling agent diffuses to the interface between the adherends and the adhesive to promote chemical bonding.

Coupling agents and primers may be applied to surfaces with a variety of techniques; the selection is best determined by the nature of the parts to be bonded. These materials can be brushed-on, sprayed-on, or wiped-on with a cloth. Alternatively, the parts can be dip-coated. If one of the parts is an organic polymer, such as EVA, a coupling agent could be physically dispersed throughout the polymer. Then, during processing (such as vacuum-bag lamination) the coupling agent would diffuse to all interfaces in contact with the EVA.

Physically, the strength of an adhesive bond is measured under dry conditions, but for outdoor applications, the real assessment of an adhesive bond lies in the measurement of bond strength under wet conditions. When wet, the simple criteria of bond quality are that the bonded parts do not readily or easily separate, and that there be some measurable bond strength greater than zero. Generally, wet-bond strength will be lower than dry-bond strength, which is not a concern as long as the wet bond strength is sufficient to hold the parts together against the stress encountered in service. Of course, the objective is that both wet and dry failures be cohesive.

To evaluate the durability of a chemically bonded interface, replicates of the bonded system are immersed in water at room temperature, and periodically the peel strength of a wet sample is measured. An excellent example of chemical bonding stability in water is seen in glass-fiber-reinforced boats, where the glass fiber is chemically coupled with silane to the laminating resin.

Experience indicates that under wet conditions, or exposure to moist atmospheres at high temperatures and humidities, the strength of the bonded interface generally decays logarithmically at a rate influenced by stress, temperature, and relative humidity. But the strength of the bonded interface recovers reversibly as environmental conditions become drier, and bond-strength decay begins again as moist conditions return. Fortunately, the bond strength does not seem to undergo cumulative damage with each cycle of exposure to moisture, because outdoor weather cycles from wet to moist to dry conditions and back again.

There is also accumulating evidence that proper selection of chemical-bonding agents or adhesion promoters can also prevent metallic corrosion (see References 26 to 29) on mild-steel substrates and on copper as a solar-cell metallization material.

A recent FSA report (see Reference 30) describes the fundamentals of chemical-bonding technology in more detail and the specific principles and practices that would apply to terrestrial solar-cell modules.

Emphasis has been placed on developing a primer system for EVA pottant, the first of the elastomeric pottants to reach an advanced stage of development. The primer system for EVA and glass (shown in Table 4-5) can be used optionally as either a wipe-on primer or as a compounding additive to generate a self-priming EVA.

This high-performance primer for EVA was developed at Dow Corning, and is similar in composition to previously recommended primers; it has, however, been modified with a small quantity of peroxide. The concep employed in this formulation is that the addition of the peroxide will cause a localized generation of active free radicals during the heating and curing stage, and consequently will give a higher crosslink density at the polymer-substrate interface. The primer has been assigned a Springborn primer number: A-11861-1.

This new formulation has longer shelf life, turning a light pink after storing at room temperature for 1 month, as contrasted with the opaque, dark red that resulted from decomposition encountered with previous formulations.

The new primer was tested by priming clean soda-lime glass slides with a thin layer of the primer (wiped on with moistened pad) and air drying for 15 min. The fully formulated EVA compound (A-9918) was then compression-molded and cured to the surface. The resulting specimen was tested for peel strength by ASTM D-903. The results (shown in Table 4-20) were excellent, showing an average peel strength of 39.6 lb/in. of width, and a small scattering of data points. Duplicate specimens were placed in boiling water for 2 h evaluated by the same process. The average strength was 27 lb/in. of width, still excellent adhesion. A quantity of the primer formulation was prepared without the alcohol diluent and blended into the standard A-9918 EVA formulation at 1 part per hundred of compound to test the self-priming effect. The resulting resin was then compression-molded to a clean glass slide, as before, and tested for peel strength by the same method. The average strength was 35.4 lb/in. of width (see Table 4-20), with a variation of ±4 lb. The bond strength of the self-priming EVA after room-temperature water immersion for 2 weeks increased from the initial value of 35.4 to 41.9 lb/in. of width.

As shown in Table 4-20, the new formulation not only gives excellent and durable bonds to regular soda-lime (microscope slides) and low-iron glass (Sunadex), but also is effective with aluminum and mild steel. Aluminum, primed with A-11861, gave an average dry-bond peel strength of 41.0 lb/in. of width and the adhesion to mild steel was even higher, with an average dry strength of 56.0 lb/in. of width. This is the highest bond strength found between EVA and any other material. The wet-bond strength is excellent to mild steel and poor to aluminum. Dry-bond strengths to Tedlar were very low, however, indicating that a different approach is necessary with this material.

This new EVA primer is the most effective formulation tested for glass, aluminum, and mild steel; preliminary testing indicates that this primer is equally as effective with EMA. Du Pont has identified an adhesive system for bonding clear and white-pigmented Tedlar to EVA. The adhesive is a Du Pont product designated 68040, and is an acrylic contact adhesive. As supplied by

Table 4-20. Adhesive Bond-Strength Evaluation with A-9918 EVA and Primer A-1186-1[a]

Test Specimens[b]	Dry	Water Immersion, 2 wk	Boiling Water, 2 h
	lb/in.		
Glass, EVA[c]	39.6	37.9	27.1
Glass, EVA + primer blend	35.4	41.9	Glass broke
Mild Steel, EVA	56.0	42.6	50.7
Aluminum, EVA	41.0	2.3	2.6
Tedlar, EVA	4.5	NT[d]	NT
Sunadex, EVA	34.8	NT	32.3

[a]Average bond strength by ASTM D903 or ASTM D1876.
[b]Glass samples are microscope slides; Sunadex is a low-iron, tempered, soda-lime glass.
[c]Primer wiped on glass with moistened cloth pad.
[d]NT = Not tested.

Du Pont, the acrylic adhesive system is a solution in toluene, which is spread onto the Tedlar surface and then allowed to dry. The resultant adhesive coating is dry and non-tacky, and the coated Tedlar film can be wound and unwound. Experimental work with this adhesive system has employed a coating thickness of 0.3 to 0.4 mil, which has yielded acceptable performance. The contact adhesive develops its bonding qualities at the high temperature of the EVA lamination cycle. A PV manufacturer may coat Tedlar optionally with the adhesive as part of its manufacturing operation, or arrange to have the coating put on by an independent coating vendor.

The acrylic adhesive system 68040 is not recommended for bonding Tedlar to wood or mild steel. Du Pont will eventually recommend proper interlayer adhesive systems for bonding Tedlar to wood and mild steel. Further, the acrylic adhesive system, 68040, has not yet been evaluated for its bonding qualities with EMA and PnBA.

H. SURFACING MATERIALS AND MODIFICATIONS

The top surface of a module is where the action begins. Incident light enters the module, or is partially blocked by surface accumulations of soiling, or is reduced by back-scattering losses from an abraded or roughened surface. The top surface should be resistant to permanent retention of atmospheric soiling, easily and readily cleanable, resistant to abrasion and roughening, and if possible, antireflective (to increase the transmission of incident light). One or more of these surface requirements may be inherent in the top-covering materials, but if not, additional surfacing materials or surface modifications may be needed. This area is under investigation.

Module soiling during field testing has produced significant power losses (to 40%) in a few weeks of exposure. However, the FSA Project is not aware of any significant surface abrasion that has occurred to modules in the field. Efforts to develop or to qualify commercial abrasion-resistant surfacing materials for modules should be scaled to the seriousness of material-abrasion occurrences. If natural abrasion is not a problem, attention can then be focused on non-abrading cleaning strategies.

Sand-blasted surfaces of an annealed-glass-superstrate module have experienced only a 10% decrease in module power output. Abraded surfaces, whether natural or as a result of cleaning, may have more significance to enhanced soil retention.

Based on observations of the details of the accumulation of soiling matter on module surfaces, and from soiling studies done at JPL (References 36 and 37), there is now reasonable evidence that soil may accumulate on surfaces in three distinct soil layers. These three soil layers, shown in Figure 4-7, can be designated and defined for descriptive purposes as:

(1) Layer A: A primary-surface layer of soil that is resistant to removal by rain or maintenance washing, and can only be removed by abrasive scrubbing.

(2) Layer B: A secondary-surface layer of soil that is resistant to removal by rain, but can be removed readily by maintenance washing or adhesive tape.

(3) Layer C: A top-surface layer of dirt that can be removed readily by rain; the quantity of Layer C soil fluctuates with rain patterns.

The field observations suggest that if Layer A forms, it will do so directly on the material surface, and then Layer A will be overcoated by Layer B, which in turn will be overcoated by Layer C.

Lastly, if Layer B does not form, then only Layer C will reside on the material surface. The field observations have not indicated in any way that Layer C will reside directly on Layer A without the intermediary of a Layer B. In other words, the soiling possibilities seem to be:

(1) A + B + C.

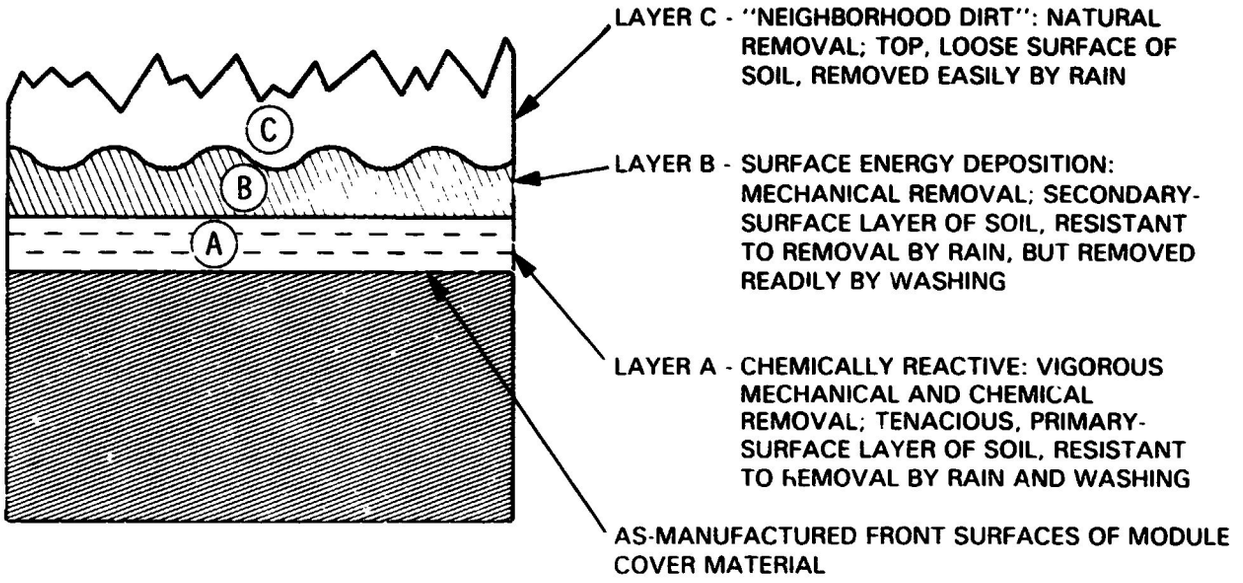

Figure 4-7. Three Soil Layers

(2) B + C.

(3) C only.

The JPL study (see Reference 37) monitored the natural soiling behavior of seven different transparent materials at 11 climatically different locations. The seven materials include three different glasses; Korad acrylic film; Tedlar fluorocarbon film; a semihard silicone surfacing material, and a soft silicone elastomer (RTV-615). Soiling accumulation was monitored by measurement of the short-circuit current from a standard solar cell positioned behind the transparent but soiled materials. The short-circuit current decreased with increased quantities of soil on the surfaces of the transparent material. Test results are reported as a percentage, using the equation:

$$\% \text{ loss from soiling} = \frac{I_c - I_s}{I_c} \times 100$$

where I_c is the short-circuit current measured with the clean, transparent material over the cell; I_s is the short-circuit current measured with the soiled transparent material over the cell.

The test materials have been outdoors for over 1 yr, unwashed, and with soiling measurements made on these materials at intervals of 2 to 3 months.

With the exception at some sites of the soft silicone elastomer (RTV-615), the time dependence of the outdoor soiling behavior of the materials generally follows the pattern schematically illustrated in Figure 4-8. The oscillating solid line traces the time-dependent magnitude and behavior of the surface soiling, which increases during dry periods and decreases during rainy periods.

Accepting the soil-layering concept, the curve of Figure 4-8 should reflect the existence of rain-resistant and rain-removable soil layers. The dotted line connecting the minimums, therefore, is associated with the light obscuration caused by the development of the rain-resistant layers, either Layers A and B, or just Layer B, and the solid oscillating line riding on the dotted line, therefore, is associated with the light obscuration caused by the rain-controlled Layer C. A characteristic of Figure 4-8 is that the dotted line approaches an asymptote after about 30 to 60 days.

An exercise can be done in the asymptotic region of the available JPL soiling data (see Reference 37), where the minimums of the curves are allocated as the light obscuration associated with the rain-resistant layers (A + B, or B only), and the difference between this minimum and the maximum peak is allocated as the maximum light obscuration associated with Layer C. This latter calculation is arbitrary, as there are other intermediate highs in the soiling data. Thus, the calculated value to be allocated to Layer C represents the maximum quantity of Layer C soil to have been present on the surface during the outdoor exposure period.

Light obscuration values, as described and extracted from the JPL soiling data (see Reference 37) for seven different sites, are shown in Table 4-21. The available data do not permit decoupling of the minimum into separate values for A and B; therefore, the minimum is considered the sum of A and B, as indicated in the column heading of Table 4-21.

As expected, the data indicate that the largest quantity of rain-resistant soil (Column A + B) is found on the soft silicone, followed next by the semihard silicone, and lastly, by the remaining five harder materials. Although the numbers for these latter five materials are small, there is an indicated ranking.

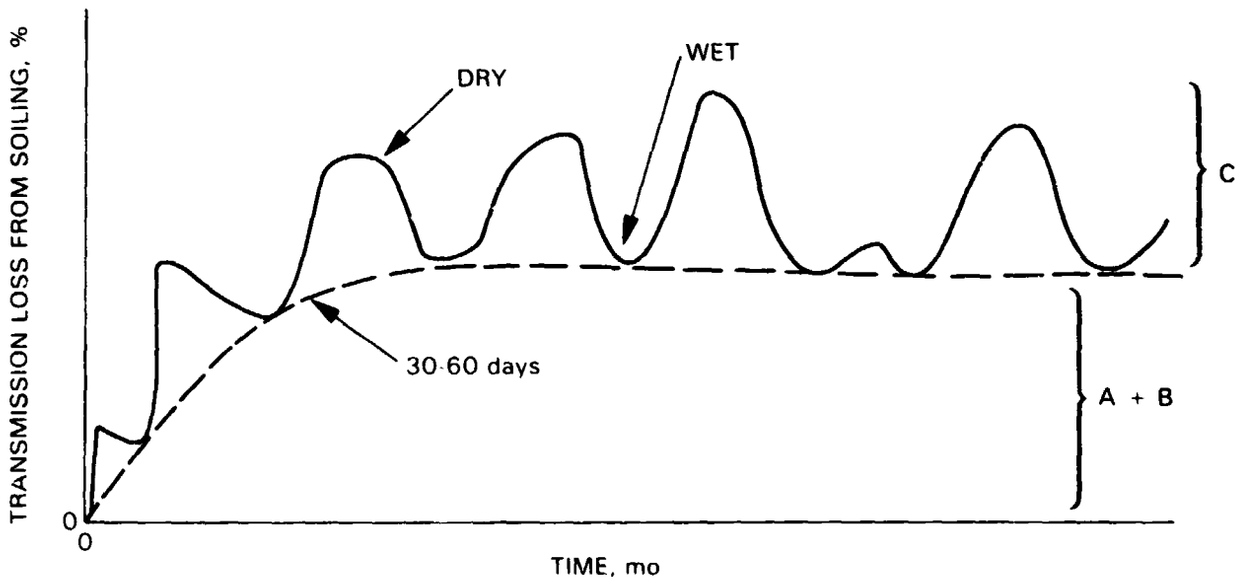

Figure 4-8. JPL Soiling Data (Data from Reference 37)

Table 4-21. JPL Soiling Data: Reductions in Short-Circuit Current from Soiling Layers, %[a]

Site	Torrance		Pt. Vicente		Goldstone		Table Mountain		Pasadena[b]		JPL 34° Site[c]		JPL 45° Site[c]	
Materials	A + B	C	A + B	C	A + B	C	A + B	C	A + B	C	A + B	C	A + B	C
	% of Reduction													
Soft silicone RTV 615	20	10	?	?	?	?	?	?	25	8	24	6	24	7
Semihard silicone, Q1-2577	14	8	5	2	6	2	1	3	17	15	16	12	15	8
Acrylic film, Korad 212	3	8	0	8	1	2	2	1	5	14	3	13	3	11
Fluorocarbon film, Tedlar	1	8	0	5	0		0	2	3	13	1	16	2	12
Soda-lime glass	2	6	1	4	2	2	0	2	3	9	4	12	3	9
Alumino-silicate glass	1	12	1	5	0	2	0	2	2	12	2	13	2	11
Borosilicate glass	0	7	0	5	0	2	0	2	1	11	1	15	1	13
Average for Layer C	8.2		4.8		2		2		12.3		13.5		10.6	

[a]See Reference 37.
[b]Pasadena station of South Coast Air Quality Management District.
[c]34° and 45° tilt angle.

Comparing the plastic films, the fluorocarbon (Tedlar) is slightly better than the acrylic (Korad). Comparing the glasses, the ranking (in improving order) is soda-lime, alumino-silicate, and borosilicate. JPL soiling data indicate, for some combinations of sites and materials, that neither Layers A nor B have formed (the minimums of the soiling curves are zero). The data suggest that the formation of the rain-resistant soil layers are both material- and site-dependent, but that material dependency dominates.

Layer C behavior is interesting; there is a strong indication in the data that the magnitude of Layer C soiling is site-dependent and material-independent. This is understandable; given the development of Layer B, it is on this surface, rather than the natural-material surface, that Layer C resides. Thus, the development of Layer B leads to material independence. For those materials that do not form a Layer B, their natural surface must have properties similar to Layer B.

The site-dependency for Layer C relates to the atmospheric concentration of soiling materials, type, and rain cycles. The average of the six or seven values of light obscuration by Layer C is also included in Table 4-21. If the average value for Layer C is treated as a measure of the soilability of an environment, then (of the sites listed in Table 4-21) JPL and Pasadena are the dirtiest, and Goldstone and Table Mountain are the cleanest.

The two JPL sites designated as 34° and 45° tilt angles are at the same location, differing only in tilt angle. The tilt-angle dependence implied for Layer C is a reduction in Layer C accumulation with increasing tilt toward the vertical. There appears to be no tilt-angle effect on the formation of the rain-resistant soil layers.

Theoretical and practical considerations (see Reference 37) enable definition of surface requirements and properties that would resist the formation of the rain-resistant surface Layers A and B. These minimum requirements are that the surface must be:

(1) Hard.

(2) Smooth.

(3) Hydrophobic.

(4) Of low surface energy.

(5) Chemically clean of sticky materials (surface and bulk).

(6) Chemically clean of water-soluble salts.

Given the validity of these surface characteristics, it is possible to initiate selection and consideration of candidate antisoiling coatings or surface treatments, and eight candidate concepts are shown in Table 4-22. Experimental work is just beginning.

Table 4-22. Candidate Antisoiling Coatings or Surface Treatments

Coating or Surface Treatment	Manufacturer
Fluorinated silane, L-1668	3M
FC-721 and FC-723, fluorinated acrylic polymer	3M
Perfluorodecanoic acid with chemical-coupling primer	Various
Glass resin 650	Owens
WL-81 acrylic	Rohm and Haas
Santicizer 141 surfactant with chemical-coupling Primer Q3-6060	Monsanto
Primer Q3-6060	Dow Corning
SHC-1000 antiabrasion coating	General Electric
Magnesium fluoride AR coating (deposited on glass by ion-plating)	Illinois Tool Works

From the perspective of developing maintenance-cleaning strategies and techniques, the soiling studies suggest that for hard surfaces, light obscuration by rain-resistant Layers A and B is low, typically much less than 4%. The real problem is the three layers that develop on soft and semihard surfaces, and Layer C on hard surfaces. Because soft and semihard surfaces are being replaced industrially with hard surfaces, the future requirements for establishing maintenance-cleaning methods should be related to Layer C behavior on hard surfaces.

It is suggested that cleaning techniques for hard surfaces should not be designed for Layers A and B, which generate the least light obscuration but that would require the most demanding cleaning approaches, such as extremely high-pressure water. Rather, cleaning strategies should be developed for Layer C behavior, suggesting low-pressure water spray (rain simulation) during dry cycles.

The economics of field-cleaning techniques, explored initially on the soiling behavior of soft and semihard surfaces, may be dramatically different for cleaning strategies and techniques based on Layer C for hard surfaces.

The theoretical considerations of soiling also enable the definition of the characteristics of low-soiling environments:

(1) Low-to-zero airborne organic vapors.

(2) Frequent rains, or general dryness (low dew, low RH).

(3) Few dew cycles or occurrences of high RH between heavy rain periods.

To generate AR front surfaces, work was done at Motorola, Inc., Phoenix, to achieve AR surfaces on glasses by chemical-etching techniques. Transmission of 98% has been demonstrated. Automated mass-production procedures and scale-up development is needed.

Another approach to applying an AR coating is by using ion plating (see Reference 38). This process for depositing thin surface films is capable of regulating the morphology of the deposited phase, which has an influence on the level of light reflection. Potentially, hard-surfaced materials with soiling and abrasion resistance, coupled with the preferred morphology for AR properties, could be deposited. The process can deposit materials on glass and non-glass surfaces. This work is just beginning.

SECTION V

ENCAPSULATION PROCESSES

Solar-module encapsulation, as in any assembly operation, consists of several fabrication steps, some done concurrently and some done consecutively. The cost of the total process will be partly related to: (1) complexity and time consumed in the individual fabrication steps, (2) the number of fabrication steps involved, and (3) the engineering details of the equipment required for each step.

The module fabrication scheme will probably be built around the processing requirements of the chosen polymeric pottant, which will affect the total process complexity, sequence, and cost. This decision may lead to excluding certain pottant candidates because their associated polymeric-process requirement may not be suitable for rapid, automated module fabrication. Therefore, module-fabrication operations and polymeric-pottant processing requirements that involve a minimum number of easily performed fabrication steps are most desirable.

Five processes that have been investigated or are being used for encapsulation are:

(1) Vacuum lamination.

(2) Liquid casting.

(3) Spraying.

(4) Direct extrusion of a melt.

(5) Electrostatic bonding (ESB).

These five processes are not considered all-inclusive or final. The suitability of the five processes for automation will have to be established, and this may lead to deleting one or more of the processes or may necessitate exploring new and different process operations.

This section describes encapsulation processes and experiences resulting from module encapsulation done by the FSA Encapsulation Task. The two encapsulation processes, lamination and casting, are used commercially. The other three processes, spraying, direct extrusion of pottant, and ESB, have been investigated experimentally within the Encapsulation Task, and are not known to be used in commercial operations. The one exception is spraying, not as a pottant process but as a commercial process to deposit a front-cover layer of a transparent semihard silicone resin on soft silicone pottants (substrate module design).

Cost analysis of the lamination and casting process have been performed (Reference 39) for a hypothetical automated process producing large quantities of modules. The encapsulation process costs, excluding encapsulated materials are estimated at $\$0.44/ft^2$ of module area for lamination, and $\$0.32/ft^2$ of module area for casting. Cost analyses for spraying and direct extrusion have not been done.

A. LAMINATION

A major effort of the Encapsulation Task has been concerned with EVA lamination. EVA, unlike PVB laminating film, requires temperature processing to cause softening of the EVA for flow and volumetric fill, and subsequent cure; PVB, which does not cure and requires temperature processing only for softening and volumetric fill. Thus, time-temperature process sequences for EVA are determined by the cure requirements, which if followed, also ensure flow and volumetric fill.

This section details the cure properties of the EVA material, the EVA lamination process, and the techniques for measuring EVA cure.

1. Ethylene Vinyl Acetate Cure Studies

The EVA copolymer (Elvax 150, Du Pont) is cured with an aliphatic peroxide curing agent. This curing agent thermally decomposes at elevated temperature to generate cure-active chemical species. The specific curing agent, Lupersol 101, was selected because there is:

(1) Neglible decomposition at 85°C to 90°C, the temperature range at which the EVA is extruded to a film.

(2) Generation of chemically inert decomposition residues.

(3) No UV-sensitivity for itself and the EVA.

Laboratory experiments with this curing agent have established a time-temperature relationship for achieving acceptable and repeatable cure of EVA. The cure curve is shown in Figure 5-1. The EVA was brought almost instantly to the specified temperature, then the level of cure (gel content) was monitored as a function of cure time and at a constant temperature. The criterion for acceptable cure was the achievement of mechanical-creep resistance of the cured EVA at 90°C, which corresponded to gel content in excess of 65%. Under these laboratory conditions, about 20 min at 150°C are required to achieve acceptable cure, and the cure times increase by a factor of nearly three for every 12°C decrease in cure temperature.

Laboratory experiments also indicated that the EVA copolymer cannot be acceptably cured below 120°C, even though the curing reaction (peroxide decomposition) is proceeding (at an extremely slow rate). Users of EVA material, formulated with Lupersol 101, are cautioned that maintaining the molten EVA for excessive lengths of time in the temperature range between 85°C and 120°C may result in depletion of the curing agent to a level where cure of the EVA cannot be achieved when the EVA is later heated to higher temperatures. This area of EVA-cure technology has not been thoroughly studied.

The cure-active chemical species generated by the thermal decomposition of the peroxide are inhibited from forming gas bubbles in the curing EVA by lamination pressure. Laboratory experiments have adequately shown that 1 atm of lamination pressure at 150°C will prevent the thermally decomposing peroxide from forming gas bubbles. Use of lamination pressures at less than 1 atm at 150°C may lead to insufficient containment pressure, resulting in trapped gas

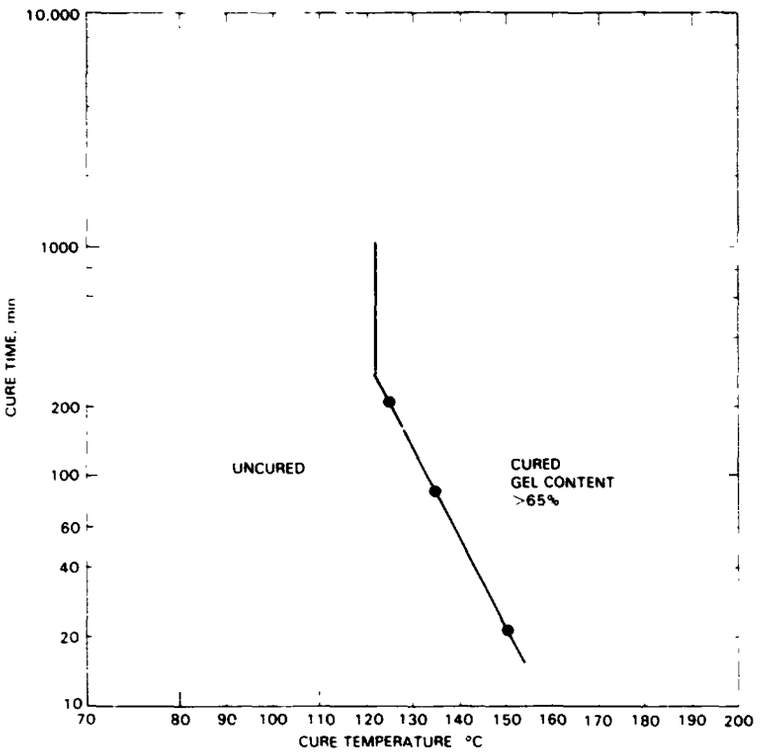

Figure 5-1. Laboratory-Measured Cure Conditions for Ethylene Vinyl Acetate (Formulation No. A-9918)

bubbles in the cured EVA. For low pressure (<1 atm) lamination, this may be corrected by trial-and-error lowering of the peak cure temperature, but will also result in progressively longer cure times for the EVA.

2. Ethylene Vinyl Acetate Lamination Process

A successful and predictable module-fabrication process for EVA pottant has been achieved through a double vacuum-bag technique. To implement this technique, a special piece of equipment was built. The apparatus, schematically shown in Figure 5-2 and pictured in Figure 5-3, consists of a double-sectioned aluminum picture frame, enclosed on the top and bottom with aluminum plates. A flexible polymer diaphragm separates the upper and lower cavities. Each chamber has its own vacuum gauges and valves for its individual evacuation. The top-cover plate is permanently attached and sealed to the top cavity with bolts and silicone rubber gasket. The lower plate is removable and seals to the bottom of the lower frame piece with a silicone rubber O-ring gasket. The diaphragm material used is a high-temperature nylon film, 0.003 in. thick, and is flexible but not elastic. Conceivably, other types of films would work well in this application.

The module assembly is positioned below the flexible diaphragm in the lower cavity. The top surface of the module assembly is flush with the top edge of the lower cavity, by stacking a necessary number of thin metal plates in the

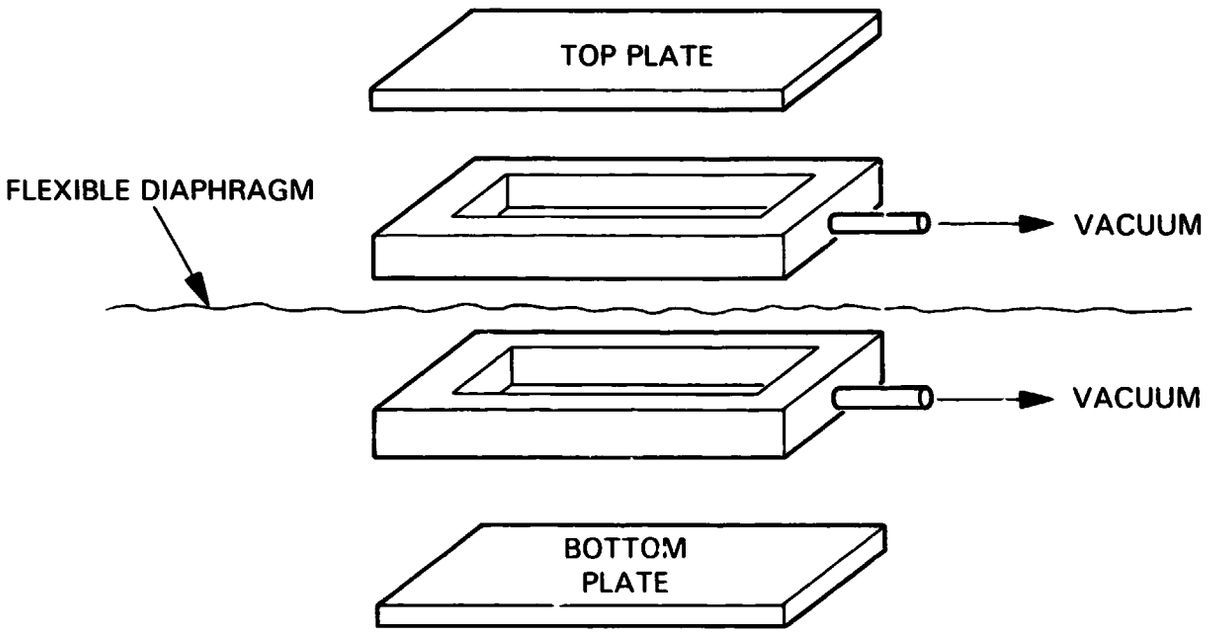

Figure 5-2. Laboratory-Scale Double Vacuum-Bag Fixture

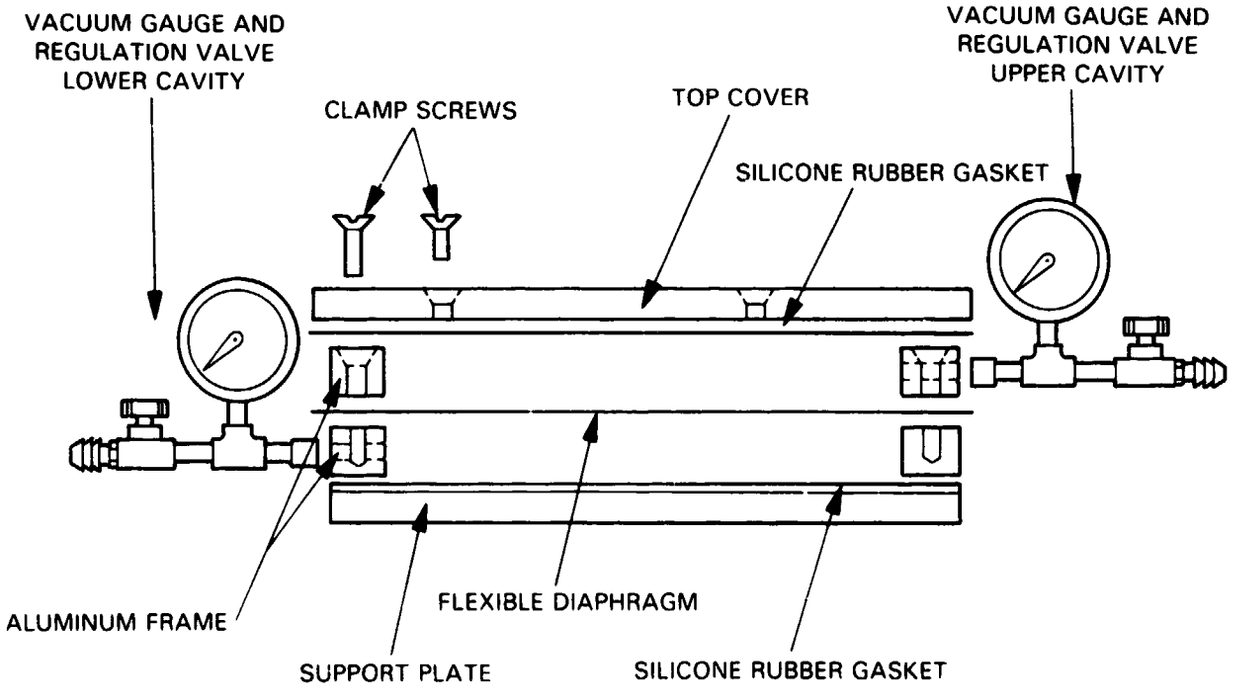

Figure 5-3. Laboratory-Scale Double Vacuum-Bag Assembly

bottom of the lower cavity. The double vacuum-bag design enables initial exposure of the module assembly to a vacuum without simultaneous compression of the diaphragm, thus greatly enhancing air exhaustion from the module assembly. To ensure thorough air exhaustion, especially from large-area modules, the use of air-release scrim sheets, such as Craneglas, should be incorporated as integral parts of the module assembly. Experimentation has demonstrated that a 5-mil-thick Craneglas mat can be positioned above the active surface of the solar cells without optical obstruction (see Section III).

Diaphragm compression of the module assembly can be done at any stage of the lamination cycle by pressurizing the upper cavity. Compression should be initiated or achieved before the temperature of the EVA reaches 120°C.

In practice, the module components are preassembled into a sandwich before the encapsulation step. The basic assembly of materials required for vacuum-bag processing of substrate and superstrate modules are shown in Table 5-1.

Table 5-1. Basic Assembly of Materials Required for Vacuum-Bag Processing of Substrate and Superstrate Modules[a]

Superstrate[b]		Substrate[b]	
Material	Function	Material	Function
White plastic film	Back cover	Clear plastic film	UV-screening front cover
Clear EVA	Transparent pottant	Clear EVA	Transparent pottant
Craneglas	Air release mat		
Solar cells with interconnects (face down)		Solar cells with interconnects (face up)	
Clear EVA	Transparent pottant	Craneglas	Air release mat
Craneglas	Air release mat	White EVA	Transparent pottant
Glass, primed[c]	Superstrate	Substrate	Substrate

[a]From top to bottom, as fabricated.
[b]Two basic designs that have been fabricated with success. The clear EVA is 0.018 in. thick. The load-bearing member, either superstrate or substrate, always faces the bottom of the assembly.
[c]The EVA primer is discussed in Section IV.

Once the basic module components for either design have been assembled, a 10-mil-thick fluorinated ethylene propylene (FEP) release film or an equivalent should be included above and below the assembly. The release films should be cut to match the area of the module. These outer FEP film layers are then taped together over the edges of the module assembly with masking tape to contain the EVA when it softens during the heating cycles. The wrap-around of masking tape is attached to the FEP film layers, rather than to surfaces of the module. Although the edges are taped firmly, entrapped air seems to diffuse easily. Some type of innovation in equipment design will probably eliminate the need for this wrap-around approach.

A useful fabrication aid is to include two 5-mil-thick (or thicker) metal plates (steel or aluminum), one on either side, of the taped module assembly. These plates distribute the lamination pressure uniformly over the module area, and result in uniformly thick modules, with smooth, wrinkle-free back- or front-cover surfaces.

The completed module assembly with taped edges is then placed in the lower cavity of the laminator and a microthermocouple is taped onto the FEP release film at the module center. The thermocouple permits convenient monitoring of the module temperature during the lamination cycle. The flexible diaphragm and upper-cavity fixtures are then positioned.

Both the upper and lower cavity are then evacuated, at least 5 min elapse before heating, to exhaust the air from within the module assembly. During continuous vacuum in both the upper and lower cavity the entire vacuum-bag fixture is loaded between the preheated (150°C) platens of a hydraulic press (Figure 5-4) which serve as the heat source. The ram pressure is just sufficient to close the press and provide good heat transfer to the vacuum-bag fixture. The pressure from the platen should rest only on the frame of the fixture and should not contribute any pressure to the surface of the module.

The time-temperature heating pattern of the module assembly after loading the vacuum-bag fixture into the preheated hydraulic press is shown in Figure 5-5. Experimentation with this heating process has demonstrated that a dwell time of 10 min at 150°C results in an acceptable EVA cure, which is less than the 20 min determined in the laboratory testing. The reduced dwell time reflects the degree of partial curing that occurs during the heat-up time to 150°C (faster or slower heating rates may require adjustment of the dwell time at the peak cure temperature). Samples of EVA taken from modules laminated by this process and associated time-temperature heating patterns exhibit acceptable cure with gel contents over 75%.

In this process, pressurization of the upper cavity to 1 atm of pressure is initiated when the module assembly temperature reaches 120°C. A slow pressurization to 1 atm is accomplished by partial opening of the valve on the upper-cavity chamber to regulate the time of pressure rise to about 8 to 10 min. This pressurization scheme is not mandatory or necessarily optimum, and users of EVA material may explore alternative pressurization techniques. The double-vacuum-bag fixture provides a capability to limit pressurization in the upper cavity to less than 1 atm. However, low-pressure (<1 atm) lamination has not yet been experimentally investigated to determine the effect of pressure in inhibiting gas-bubble formation due to peroxide decomposition.

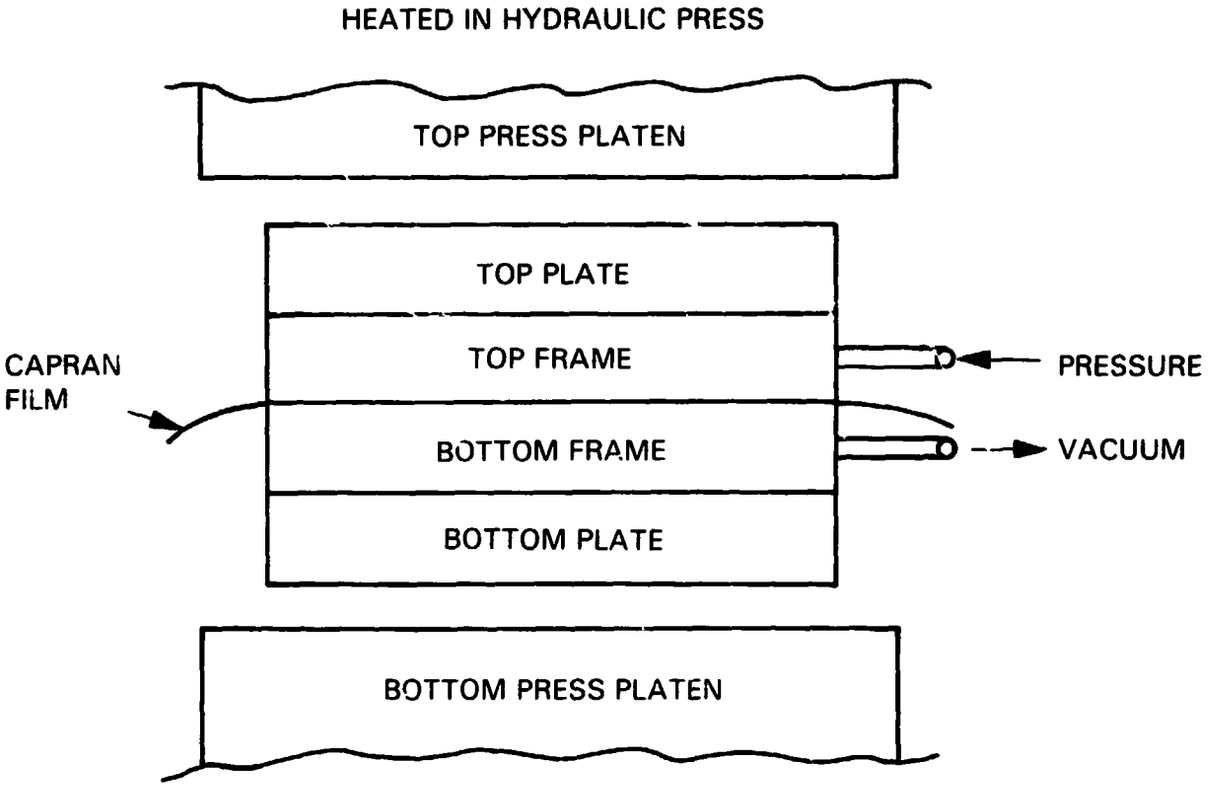

Figure 5-4. Laboratory-Scale Vacuum-Bag Fixture Positioned in Heated Hydraulic Press

After the 10-min dwell at 150°C, the laminator can be removed from the heating press and permitted to cool in still air. When a temperature of about 40°C is reached, the vacuum in the lower cavity may be released, and the completed module may be removed from the laminator. A time-temperature profile of this cooling process is also shown in Figure 5-5.

Modules prepared by the preceding process have been fully cured, and are bubble-free and of good appearance. No evidence of cell damage has been noticed.

The use of Primer No. A-11861 results in excellent adhesion between the EVA pottant, glass, and many other surfaces.

The rate of temperature rise that the module assembly experiences during lamination may be an important factor. EVA heated to the cure temperature too slowly may not cure properly because of depletion of the curing agent before the minimum EVA cure temperature of 120°C to 125°C is reached. The average EVA heating rate in this process is about 4°C/min. Investigations have not been done on slowing the heating rate. Failure of the EVA to achieve an acceptable cure using the time-temperature cure relationship given in Figure 5-1 may be related to slow EVA heating rates. Users should also be aware that open exposure of EVA material to air at high cure temperatures may inhibit the cure.

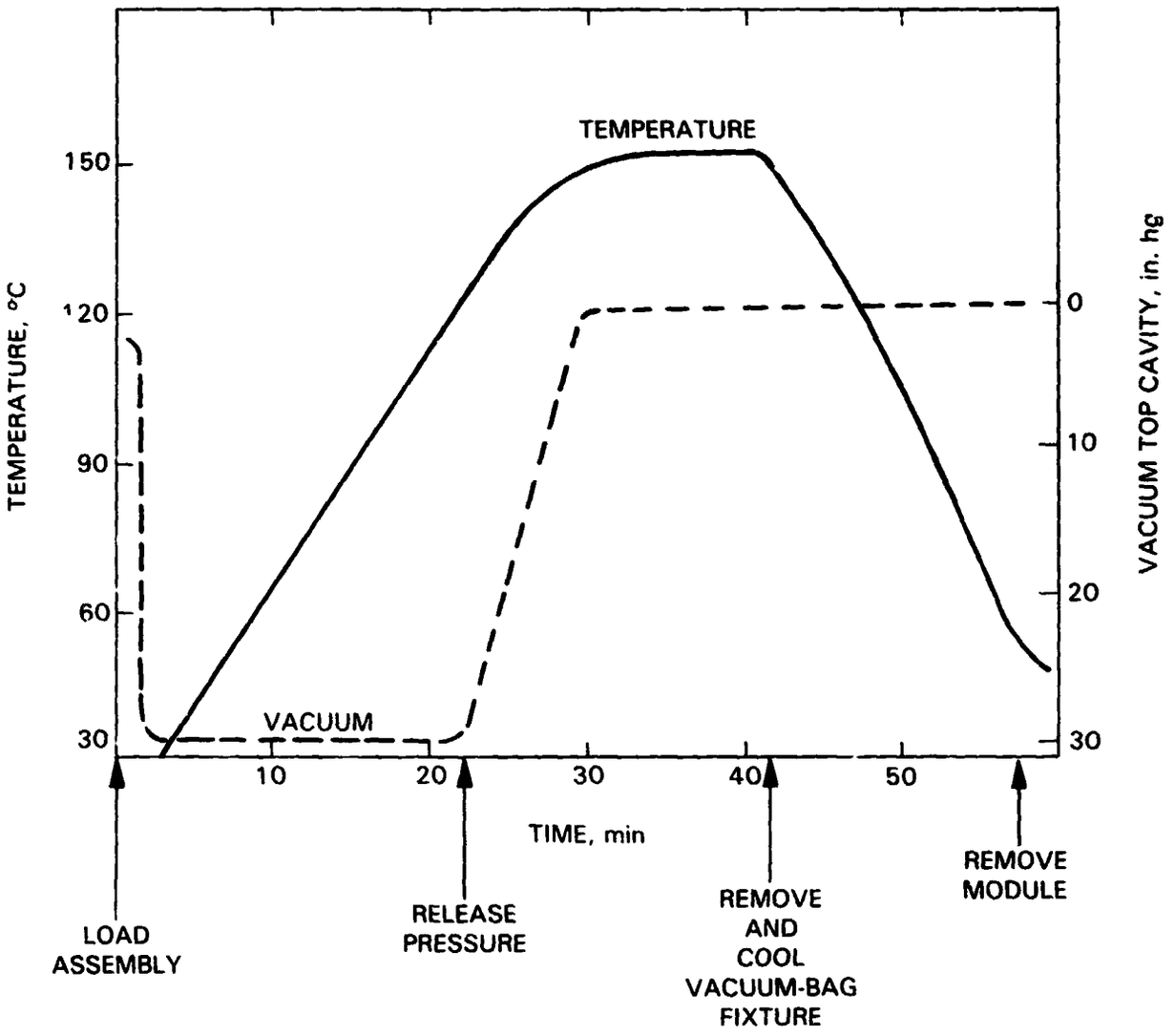

STEPS:

1. LOAD PREASSEMBLED MODULE INTO VACUUM-BAG FIXTURE AND PUMP BOTH CAVITIES DOWN TO 30 in. hg FOR AT LEAST 5 min.
2. LOAD INTO PREHEATED PLATEN PRESS TO HEAT MODULE AT APPROXIMATE RATE OF 4°C/min; BOTH CAVITIES ARE KEPT UNDER FULL VACUUM.
3. AT A TEMPERATURE OF 120°C, THE PRESSURE OF THE UPPER CAVITY IS GRADUALLY RELEASED AND PERMITTED TO COME TO ROOM PRESSURE OVER AN 8- TO 10-min PERIOD.
4. THE ASSEMBLY IS KEPT IN THE PRESS FOR 10 min AFTER REACHING A TEMPERATURE OF 150°C THEN REMOVED WITH THE LOWER CAVITY STILL UNDER EVACUATION.
5. THE MODULE IS REMOVED FROM THE VACUUM BAG AFTER COOLING FOR ABOUT 10 min.

Figure 5-5. EVA Module Lamination: Time-Temperature-Pressure Cycle

3. Determination of EVA Cure Level by Gel Content

The degree of cure of the resin may be determined in the following simple laboratory procedure:

(1) Remove a small piece of cured resin (1 to 2 g) and weigh on an analytical balance, to three decimal places.

(2) Place the specimen in 100 ml of toluene and heat to 60°C for 3 h.

(3) Pour the mixture through a piece of weighed filter paper to catch the gel fraction and permit to drain completely.

(4) Dry the filter paper and gel fraction at 60°C for 3 to 4 h (no odor of toluene solvent should remain).

(5) Weigh to three decimal places and subtract the weight of the filter paper.

(6) The gel content is calculated as:

$$\% \text{ gel} = \frac{\text{weight of polymer residue from toluene}}{\text{weight of original specimen}} \times 100$$

(7) EVA with gel content over 65% may be regarded as acceptably cured. The described lamination process results in gel content consistently from 75% to 80%.

4. Ethylene Vinyl Acetate Process Summary

The process described above evolved from laboratory efforts to achieve EVA module fabrication by a fast, reproducible process that did not damage solar cells or incorporate bubbles, voids, or other defects that could be nuclei for module failure or problems. During the development of the EVA lamination process, two problems of significance (trapped bubbles and failure of the EVA to cure) were encountered which necessitated detailed studies of EVA cure technology and an understanding of the origin and elimination of trapped bubbles (i.e., trapped air and peroxide decompositon).

Lessons learned from the historical development indicated that an EVA lamination method needs to:

(1) Prevent exposure of the EVA to oxygen of the air during heating, which chemically acts to inhibit cure.

(2) Hold the module components physically in place. (Between 70°C and 120°C, the EVA is in a fluid state.)

(3) Apply uniform pressure of 1 atm over the surface area of the module during processing.

(4) Ensure rapid temperature rise of the EVA to its cure temperature of 150°C, to minimize lower-temperature loss of the peroxide curing agent through thermal decomposition.

(5) Maintain constant vacuum for air and gas removal.

(6) Use of air-release spacers (e.g., Craneglas) in the module assembly to facilitate total air removal from module interfaces.

The practical double vacuum-bag lamination process to accomplish the six needs may be summarized as a sequence of the following steps:

(1) Assemble module construction materials, including the 10-mil FEP release films and seal the edges firmly with masking tape.

(2) Place the pre-assembled module between the diaphragm picture frame and lower-support plate.

(3) Evacuate the entire assembly (top and bottom chambers) through the side connections for at least 5 min, with vacuum applied.

(4) Place the vacuum bag between the heated platens of a hydraulic press or any other heat source capable of making intimate contact; the temperature should be set at 150°C.

(5) Follow as closely as possible the time-temperature-pressure curve as shown in Figure 5-5:

   (a) Heating rate should be about 4°C/min.

   (b) Top cavity should be returned to ambient pressure starting when the module temperature reaches about 120°C; regulate the rate of pressure increase so that 8 to 10 min are required to achieve atmospheric pressure in the upper cavity; continue heating to 150°C without interruption.

   (c) Cure temperature should be 150°C for at least 10 min.

(6) Cool to room temperature, release vacuum, remove the module assembly, peel off the masking tape, and lift away the FEP films (edges of the fabricated module can be cleaned up, if necessary, with a sharp blade).

The advantages with this encapsulation method are briefly:

(1) Rapid fabrication, about 1-h cycle.

(2) Bubble- and void-free.

(3) Ease of materials handling.

(4) Good cure of the resin.

(5) Good adhesion (with the primers already used).

(6) No cell shifting.

(7) Minimal loss of encapsulant during fusion.

(8) No cell or interconnect damage.

(9) Potential for automation.

Modules 11 x 15 in., fabricated by this process, have successfully passed the JPL thermal-cycle qualification test described in Reference 40.

As laminated module sizes approach 1- x 4-ft, 2- x 4-ft, and 4- x 4-ft, concerns about the lamination process for large-area modules have been expressed:

(1) Handling and shifting of large-area prefabricated cell strings to position the interconnected assembly in the module lay-up stack. This is as yet unresolved.

(2) Air removal from large-area modules. This may not be a problem, using double vacuum-bag lamination with sufficient Craneglas spacers at various interfaces.

(3) Provisions for external connectors and leads. This concern is apparently being solved, by using AMP connectors for example, that are being designed specially for compatibility with the lamination process.

(4) Cell shifting. This has been resolved, in some cases, by bridging the cells with Scotch-brand Magic Tape; it may be permanently resolved by interconnecting cells mechanically with electrically conducting cross-ties for series-parallel wiring.

B. CASTING

Investigation of casting as an encapsulation process has been limited in scope by the Encapsulation Task, not because less importance is attached to it compared with lamination, but because the advanced castable pottant being developed by the Encapsulation Task, PnBA, is not yet at a stage of development where extensive module fabrication activities are warranted. A prototype PnBA liquid system, however, has been evaluated independently by a PV manufacturer in a glass-superstrate module as a substitute for curable liquid silicones. The viscosity of the prototype curable-PnBA liquid system was adjusted to match the liquid silicone approximately, and then was used directly in the commercial casting equipment. No handling and casting-related problems were encountered, and the prototype PnBA liquid system was judged to be readily interchangeable in the casting-process line. The problems encountered with the initial PnBA formulation were gassing additives and slow cure, which are being resolved in the present material development program.

The other liquid pottant with which the Encapsulation Task has limited casting experience is an aliphatic polyether urethane. Specifically, this is a two-part liquid casting pottant available from H. J. Quinn in Malden, Massachusetts. The resin, designated as Q-626, costs $1.24/lb, and the catalyst, designated Q-621, costs $1.49/lb. The mix ratio is about 3.86 parts resin to 1 part catalyst, which yields a system cost of $1.29/lb (1980$).

Both the resin and the curing agent are viscous fluids of about the consistency of heavy motor oil. The curing agent is chemically a diisocyanate, which is chemically very reactive with water, generating CO_2. Therefore, it is necessary that this diisocyanate curing agent avoid contact with moist air; it is also necessary that the surfaces of all module components that will come in contact with the mixed-liquid system be dry to avoid gas generation and trapped bubbles. Attempts to use this material in direct contact with wooden substrates were unsuccessful because wood is hygroscopic and difficult to free of all absorbed water by drying. There has been partial success with glass-superstrate and metal-substrate modules, which are easier to dry. The casting efforts with this system were done by assembling the various components of the module in a metal mold with non-stick surfaces and adjustable walls that could be snugly pressed around the module edge, therefore providing liquid containment until after the urethane is cured. The casting fixture could be moved into a chamber with a dry gas atmosphere before pouring in the liquid urethane.

Casting activities with the urethane were suspended pending development of better approaches to ensuring proper desiccation of module components, provisions for removing CO_2 gas bubbles if formed (this may dictate need for vacuum operation), and possibly identifying a different urethane system that would generate less, or no, CO_2 in the presence of moisture.

C. SPRAYING

This encapsulation process has been limited to liquid silicones where thin coverage was desired to reduce the cost of material usage in the module; GE and Dow Corning have used this process.

The Silicone Products Department of GE, Waterford, New York, has developed an experimental silicone PV pottant at a present price of about $3/lb, or about $0.016/ft^2/mil of thickness (1980$). The GE designation for this experimental material is GE-534-044.

General Electric developed a method of fabricating minimodules with GE-534-044, using liquid-application systems such as automatic-mixing equipment and airless spraying. The automatic-mixing equipment combines catalyst and base resin in precise proportions with practically instant mixing and without the necessity of deaerating, so that short-pot-life materials can be easily used in an automated setup. Also, airless spraying enables the application of thin, uniform layers of catalyzed resin without the inclusion of air.

Dow Corning identified a commercial silicone resin, Q1-2577, that can be spray coated (see Reference 21) as a conformal coating pottant. Modules up to 11 x 16 in. that have been spray coated with Q1-2577 passed the JPL thermal-cycle test. After spray coating, the modules can be air-dried at room temperature for 24 h, or the air-drying can be accelerated to a few hours at 75°C.

Whiting pigment, TiO_2, can be easily dispersed in Q1-2577 and can be spray-coated as a thin layer on substrate panels to provide a light-reflecting white background on module areas not covered by round solar cells. The pigmented Q1-2577 has also been used as a back cover for glass-superstrate modules.

One Dow Corning innovation to reduce silicone material use (and cost) involved the machining of circular recesses into wood substrates to a depth and diameter slightly larger than the solar cells to be encapsulated. Notches were machined between the circular recesses to accommodate the interconnects. The recessed and notched wood substrate was then spray-coated with the white-pigmented Q1-2577, and while still wet (uncured), the interconnected cell string was gently positioned in the recesses and notches. Then the connections to electrical terminals were passed through holes drilled in the wood to the back surface. The module was put into a vacuum chamber at room temperature to exhaust the air from the back sides of the cells and interconnects. Slight pressure on the cells and interconnects caused an outward spread of the white-pigmented silicone liquid from the back surfaces. There was sufficient outward flow to fill and slightly overflow the annular spaces between the cell perimeters, inside walls of the recesses, and all spaces in the notches around the interconnects. An overcoat of clear Q1-2577 was sprayed on the entire top surface of the module and cells, and the silicone was cured for a few hours at 75°C.

This module design passed the JPL thermal-cycle test, and one module, installed on an outdoor weathering rack at JPL, is still functional after 2 yr.

Possible concerns that have been expressed about the spray process include:

(1) Cleanliness.

(2) Incomplete coverage: shadowing and filling.

(3) Thin coverage:

  (a) Exposed electrical conductor.

  (b) Stepped cell edges:

    1) Mechanical damage.

    2) Cracking and fracturing of coating (thermal expansion).

(4) Material waste from spray losses: health (toxic fumes).

D. DIRECT EXTRUSION

Very limited investigations of this process have been done, and only EVA was used. Using a substrate design as an illustration, the envisioned concept would have substrate panels on a belt, moving underneath a continuous film extruder that deposits a layer of uncured pottant directly on the substrate. The panel with a layer of pottant would then move to the next assembly station, where an interconnected cell string would be positioned on top of the pottant

layer, followed by electrical connections of the terminals. This partially assembled module would then move again underneath a continuous film extruder that would deposit another layer of uncured pottant, followed by automated overlaying of the plastic-film front cover. The module unit would then enter an automated vacuum laminator to heat, fuse, and cure the pottant.

Craneglas air-release spacers, which would be used at various module interfaces, and the plastic-film top cover would feed into the assembly line from supply rolls, be automatically cut to size, and deposited as film layers at appropriate stations in the assembly line.

Glass-superstrate modules could also be fabricated with this process, except that the interconnected solar-cell string would be handled face down, instead of face up as in substrate designs.

Attempts at direct extrusion of EVA with wood and glass panels were made with an 8-in.-wide laboratory-scale film extruder. Although the approach worked in principle, the EVA melt had a tendency to deposit onto the panels with trapped air bubbles, both in the bulk and at the panel-EVA interface. The trapped air was difficult to remove during the vacuum-lamination cycle.

Through experience, deposition of bubble-free layers of EVA became possible. Some of the parameters that had to be regulated and controlled to accomplish this included synchronization and speed of film extrusion, panel movement, melt fluidity, drop height, and angle of contact of the melt onto the panel.

No further work has been done with this encapsulation process.

E. ELECTROSTATIC BONDING

Electrostatic bonding (ESB) is a method of attaching glass sheets to metals or dielectrics without using an additional adhesive. It can be used, for example, to attach silicon solar cells to a glass superstrate, or to attach one sheet of glass to another with a dielectric-film interlayer. In the bonding process, the glass is heated to a temperature high enough to allow ion mobility, but lower than the softening point of the glass, typically 350°C to 650°C. At this temperature, high voltage is applied across the glass and the object to be bonded. Rearrangement of ions within the glass causes a permanent chemical bond to be formed across the interface. The resulting seal is completely hermetic, and will generally be as strong as the materials being bonded.

Because of the thermal processing involved, the glass used must generally be a near match in thermal-expansion coefficient to the object to be bonded. For silicon solar cells, Pyrex (Corning type 7740) or Tempax (Schott Glass 8330) is acceptable up to a process temperature of about 400°C, and Corning type 7070, Schott type 8248 or Owens-Illinois type ES-1 is acceptable up to 650°C.

For adhesion to cells with significant surface metallization, it is necessary to deform the glass around the metal contacts. In this case, process temperatures near the high end of the range are needed, and in some cases external pressure must be applied to increase the amount of deformation.

Module designs using ESB have several advantages:

(1) The ESB seal is an integral bond between glass and silicon, thus is fully hermetic.

(2) There is no pottant between cells and glass cover to be subject to degradation.

(3) Cells are attached to a thermal-expansion-matched glass.

The present process has several requirements:

(1) Thermal expansion of the glass must match that of the silicon.

(2) Glass deformation when bonding solar cells with raised front metallization, and thus, temperatures above 500°C are required. Cells must be able to withstand at least 5 min of exposure to this temperature without significant thermal degradation.

Figure 5-6 shows a module configuration that takes advantage of the fully integral bonding possible using ESB. The cells are completely sealed in glass, front and back. Figure 5-7 shows the modules' output terminals. A thin metal foil is sealed to the front and back glass, allowing no moisture penetration with the interconnects. In cases where extreme environments may be encountered, this module design may be preferred.

Figure 5-8 shows a hybrid module with ESB front lamination and conventional back. This design retains many of the advantages of the fully integral module, at lower cost: no pottant between glass front and cells, expansion-matched superstrate, and hermetic protection of cell-front metallization.

ESB also may be used to trap a metal mesh preform between the cell and the glass superstrate. This preform can then serve as the front-cell contact, eliminating the cell-metallization step. Figure 5-9 shows a module using a preformed mesh as the cell-contact method.

For cells with no metallization on the front surface, such as interdigitated back contact (IBC) or tandem-junction cells (TJC), a lower processing temperature can be used, allowing the use of glass with a less critical thermal-expansion match to silicon. Such glass is presently available in large sheets. ESB integral front bonding of up to eighteen 3-in.-round silicon wafers to a 16- x 18-in. sheet of glass has been demonstrated.

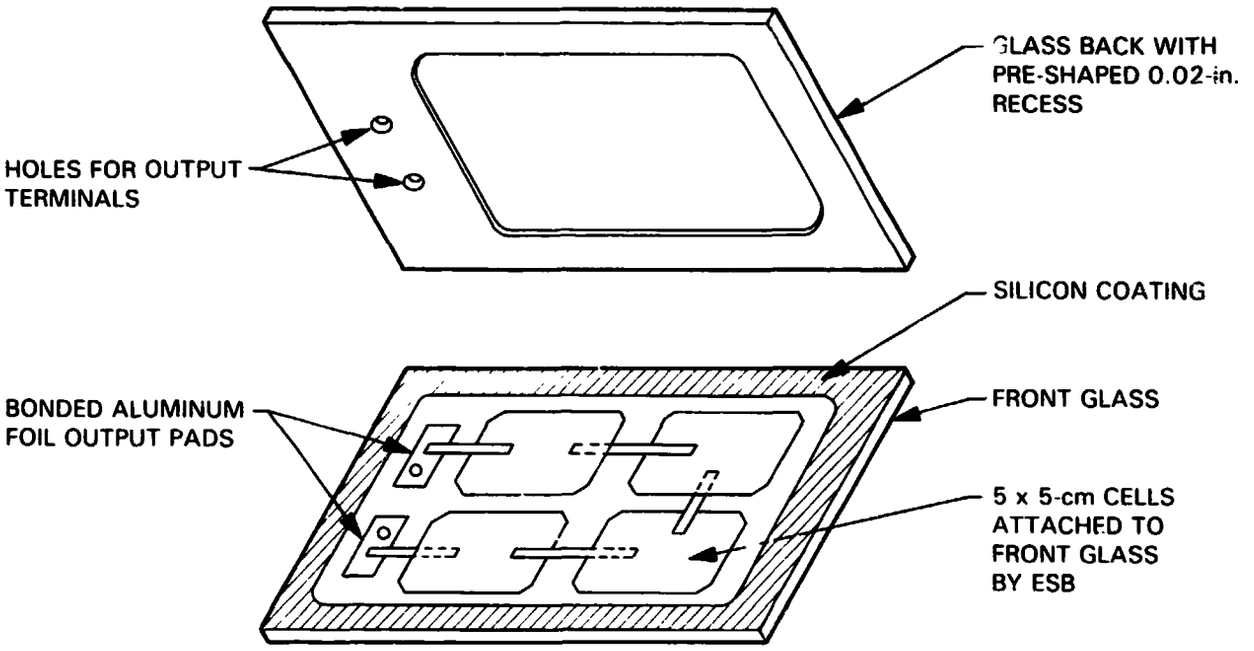

Figure 5-6. Fully Integral Electrostatic-Bonding Module Configuration

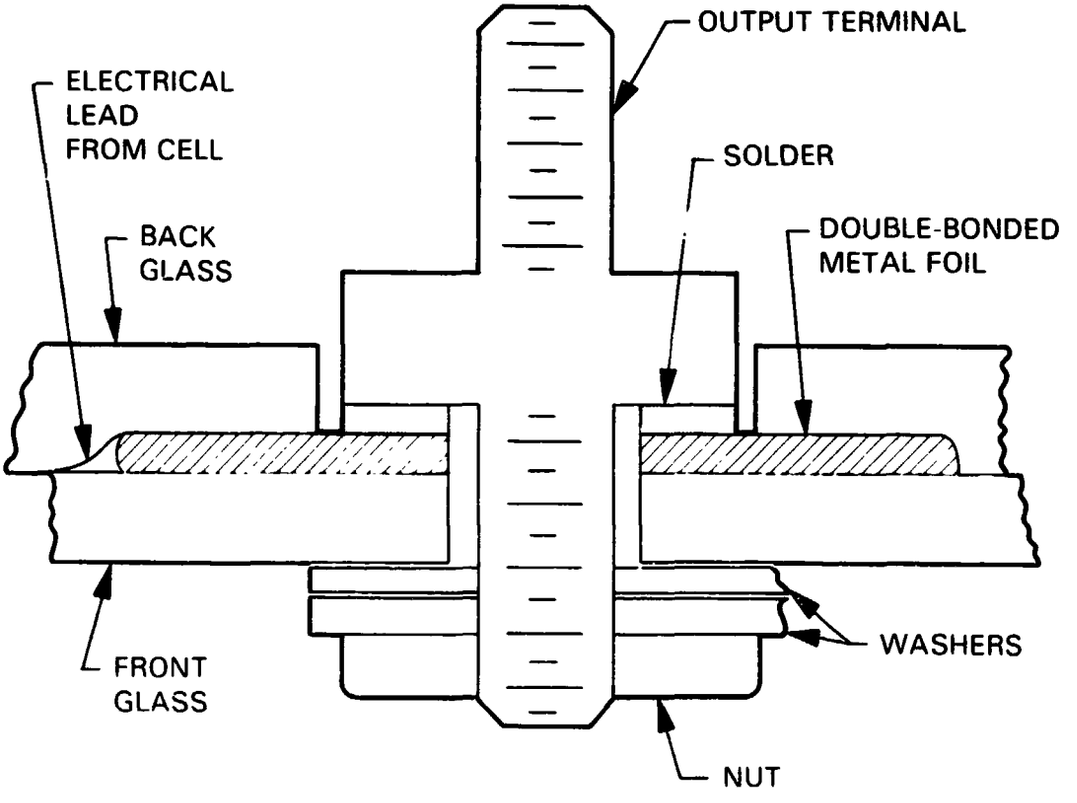

Figure 5-7. Integral Module Output Terminal Design

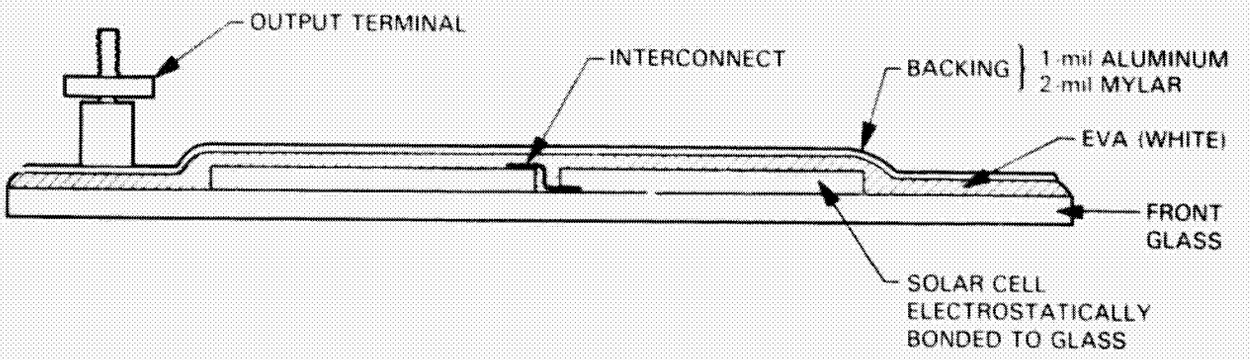

F ,ure 5-8. Cross-Sectional View of Integral Front-Conventional Back Module Assembly

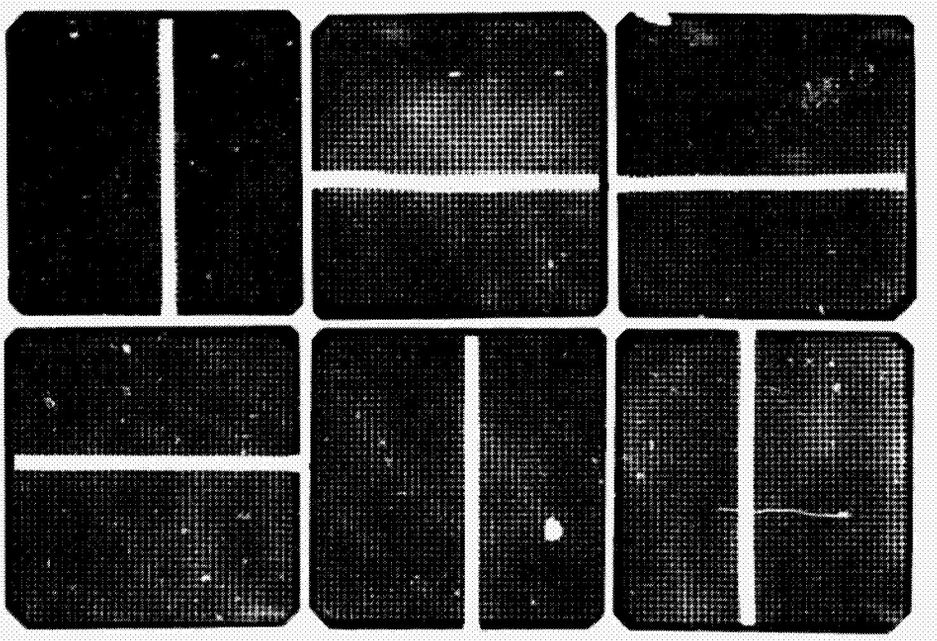

Figure 5-9. Six-Cell ESB Module with Pre-Formed Contact, Bonded to Antireflective-Coated Glass

SECTION VI

MODULE DURABILITY AND LIFE TESTING

A. DEFINITION OF MODULE DURABILITY

Experience with failures of encapsulated solar modules and with most other types of hardware leads to expectation of the existence of a bathtub curve of failure rate vs time. The bathtub curve is the superposition of three curves or failure rates (Figure 6-1), consisting first of those early failures because of various flaws acquired in the manufacturing process but not inherent in the hardware design. These failures (infant mortality) should decrease with time as the faulty units are identified and eliminated. The level portion of the failure-rate curve describes the random failure rate during the useful life of the component and is characterized by its reliability rating or mean time between failures (MTBF).

As time continues, failure rates would be expected to increase because of wear-out and material-aging effects. Failure modes for encapsulated solar cells in this long-term regime could include degradation of the physical properties (optical, electrical, and mechanical) of the encapsulant, and corrosion, fatigue, delaminations, loss in transmittance, and abrasion of the module cover. Fatigue failures may be caused by combinations of thermal cycling, moisture cycling, and

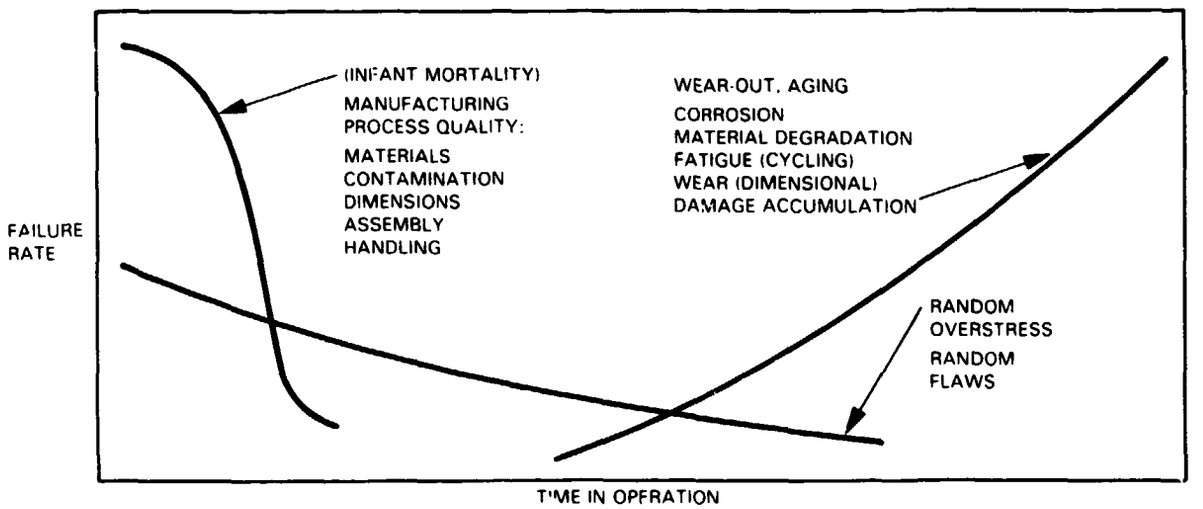

Figure 6-1. Three Types of Failure Experiences Expected in Assessing Module Durability

mechanical (wind) flexing, and may result in cell cracking, electrical interconnect failures, propagation of delaminations, or cracks through the encapsulant itself.

Module failures can be defined by three consequences of degradation: non-operative modules, unsafe modules, or modules that suffer power-output loss of 25% or more. Discrete element failures observed within a module (e.g., delamination or cell crack) may or may not constitute a module failure, depending on the module's design-fault tolerance.

A significant goal of the FSA Project since its beginning has been a module service life of 20 yr. In evolving the terminology for relating the FSA objective of a 20-yr life to the actual durability characteristics of a specific module design, two terms are proposed for describing module durability in a quantitative manner: life potential and probability of failure. As defined below, these terms would bracket the expected durability characteristics of PV modules.

1. Life Potential

A life potential of 20 yr or more, assigned to a material or to a module, should indicate (as a result of literature surveys, testing, and property measurement) that the material properties or module performance would not decrease to unacceptable values during 20 yr of use or exposure. The corollary to this definition is that the useful life beyond 20 yr could be indefinite and not be specifically predictable. Many candidate module materials fall into this category, such as glass, concrete, aluminum, stainless steel, etc.

The recommended module design approach to the achievement of a 20-yr-life potential is to:

(1) Select materials that have inherent long-term stability under known loads and stresses.

(2) Select material combinations and configurations of which the material responses to the environment either are non-degrading or result in acceptable degradation rates over a 20-yr period or more.

(3) Ensure adequate design margins by performing an analytical or experimental analysis of the module response to normal loads and possible extreme loads, based on initial material properties and on predicted changes in material properties after environmental aging.

This approach allows the analysis of wear-out and the calculation of design margins to be separated from reliability considerations and the statistical analysis of the probability of failure.

2. Probability of Failure

The probability of failure for a qualified module (within a specific period) would be the sum of all module-failure probabilities because of discrete

failure modes identified by analysis or test experience. The probability of module failure would include the statistical experience of infant mortality (electrical insulation flaws, etc.), derived from the standards of acceptance that testing imposed. The probability of failure would also include the failure rate, derived from the probability of random overstress failures from statistically predicted extreme winds, large hailstones, etc. The probability of failure from module wear-out or damage accumulation would be derived from the calculated or experimentally determined rate of module power loss from material degradation. This value would include the effects of surface soiling, delamination, cell cracks, yellowing, electrical insulation failure, fatigue damage, and corrosion effects.

Instead of calculating or assigning an integrated single probability of failure from all causes, a more useful approach may be to use the individual failure probabilities and performance loss rates to calculate the effect of specific failure modes and performance losses on life-cycle energy cost. Then the trade-off between the cost of corrective action and the effect on energy cost could be evaluated.

B. FAILURE PROBABILITY ANALYSIS

Many elements of a module-failure probability and life-assessment analysis have already been developed within the FSA Project and are being validated and refined. The potential service life of a module is a complex function of the characteristics of the solar cells, the interconnect circuitry, the encapsulant materials, their configuration and interfaces with the solar-cell assembly, and the solar-array structure. The FSA Engineering Area has vigorously investigated these elements of failure probability dealing with solar-cell-assembly characteristics (i.e., interconnect fatigue, cell fracture, hot-spot cell heating, electrical safety, etc.), and also the durability characteristics of the solar-array structure and related module structural responses (i.e., wind, hail, mounting, maintenance, etc.).

The FSA Engineering Area and the Encapsulation Task are investigating several specific failure and degradation modes and have developed design analysis methods and design criteria that may be applied to ensure that new module designs will pass the appropriate qualification tests and withstand expected field-exposure conditions. The following reports and design guidelines are available for use in evaluating PV module designs:

(1) JPL Internal Document No. 5101-161, Block V Solar Cell Module Design and Test Specification for Intermediate Load Applications, 1981.

(2) JPL Internal Document No. 5101-170, Flat-Plate Photovoltaic Module and Array Circuit Design Optimization Workshop Proceedings, May 19-20, 1980.

(3) JPL Internal Document No. 5101-148, Proposed Method for Determining the Thickness of Glass in Solar Collector Panels.

(4) JPL Internal Document No. 5101-131, Photovoltaic Module Soiling Studies, May 1978-October 1980.

(5) JPL Internal Document No. 5101-62, Photovoltaic Solar Panel Resistance to Simulated Hail, 1978.

(6) JPL Internal Document No. 5101-21, Revision B, Rejection Criteria for JPL/LSA Modules, 1977.

Other FSA contractor reports and JPL reports will be available to provide analysis methods and design guidelines in the areas of interconnect fatigue, soiling control, cell resistance to fracture, electrical isolation criteria, and photothermal stability of polymers.

The efforts of the FSA Encapsulation Task have been focused on measuring and modeling the long-term aging effects of the module environment (e.g., temperature, UV, humidity, oxidation, etc.) on the physical-chemical degradation of candidate polymeric encapsulation materials and on interface-bonding integrity.

An FSA Project-sponsored program with Spectrolab, Inc., has provided a module-design analysis approach for calculating the effects of encapsulant material physical properties and configuration on module performance and design margins for optical, thermal, structural, and electrical isolation design requirements.

One premise of a potential life assessment is: If predictable encapsulant material property changes because of aging are used in the module design analysis method discussed above to calculate the reduction in module performance or module design margins, an assessment of the module-life potential can be inferred. Therefore, specific property changes to be monitored during aging include spectral transmission, refractive index, thermal conductivity, expansion coefficient, dielectric properties, shrinkage, elastic modulus, creep, elongation, permeability, and hygroscopic response. Other properties measured, such as molecular weight and long-wavelength absorbance, reveal chemical changes in the polymers that are clues or precursors to related physical property changes.

C. MODULE DURABILITY EXPERIENCE

Module durability experience discussed in this section comes from two main sources: module qualification testing at JPL, and field-testing experience acquired at JPL and from other agency application experiments. Detailed reports on module durability experience have been published (References 41, 42, and 43) and a formalized system of problem-failure reports (PFRs) has been established at JPL to document and follow module failure experience.

General progress in increasing module durability may be tracked by reviewing the performance of modules in the different FSA block procurements since 1975 from various vendors in conformance with FSA module design specifications, referred to as Block I, II, III, IV, and V. Block I and II modules were delivered during 1976 and 1977 and some have accumulated field exposures over 4 yr (Figure 6-2).

The majority of these early PV modules used silicone rubber (RTV 615 and Sylgard 184) as the pottant material (Table 6-1). The top-surface cover materials used have been glass, silicone plastic (R4-3117) or the bare

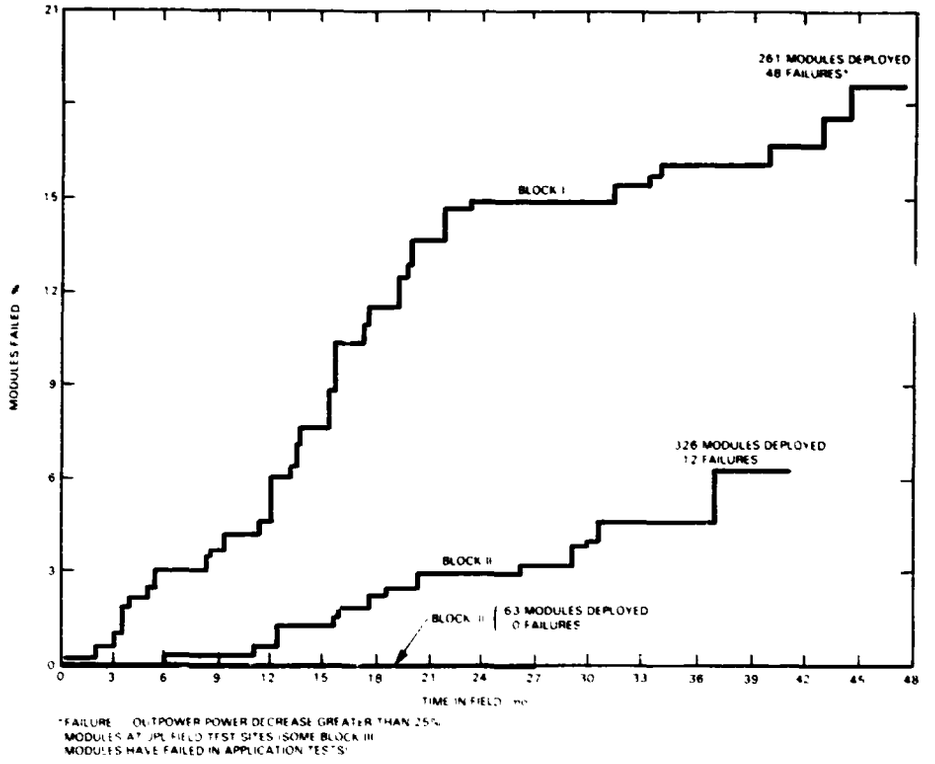

Figure 6-2. Module Durability

silicone rubber. An alternative Block II module design that has been under evaluation used PVB as the pottant between a glass superstrate and Mylar back cover.

Substrate panels for these early modules have included aluminum sheet and extrusions, epoxy and glass fiber (G-10 board), polyester and glass fiber, and stainless steel. Modules using PMMA (Plexiglas) have been tested and nearly all have encountered thermal-expansion stress failure during qualification tests.

An additional source of field testing data for modules designed for more severe exposure conditions is available in U.S. Coast Guard Report No. CG-D-10-81, November 1980 (Reference 44). In this test program, about 400 solar PV modules from nine manufacturers were tested over a 2-yr period, 1978-1980, at marine-environment sites in Connecticut and Florida. These module designs included superstrate and substrate designs, and modules with top and bottom panels of rigid material (e.g., glass or metal). Two pottant materials, silicone rubber and PVB, were evaluated. The detailed results of these tests provide useful insights into the durability of various module design configurations and a comparison of field-test results and a pressure-immersion-temperature (PIT) test. Briefly, the report conclusions relative to achieving module durability in a marine environment were:

(1) The terminals were the most vulnerable area of the panel to the effects of the marine environment.

Table 6-1. Typical Module Encapsulant Systems and Temperature Response: Nominal Operating Cell Temperature (NOCT)

No.	Module	Cover Material	Encapsulant	Electrical Isolator	Substrate: Material	Substrate: Geometry	Front Intercell Area Color	NOCT, °C	No. of Tests	Air Void	Thermally Significant: Metal Substrate	Thermally Significant: Fins	Thermally Significant: Non-Metal Substrate: Opaque	Thermally Significant: Non-Metal Substrate: Transparent	Comment
	Block I														
1	Spectrolab	Glass	Sylgard	Dextiles paper	Aluminum	I-Beam	Aluminum	35.2	13		X	X			Lowest NOCT
2	Sensor Tech	Sylgard	Sylgard	Sylgard	Aluminum	Finned	Aluminum	39.0	6		X	X			
3	Solarex	Sylgard	Sylgard	Not required	G-10 board	Sheet	Green	47.5	10				X		
4	Solar Power	Sylgard	Sylgard	Not required	G-10 board	Sheet	Green	48.8	5				X		
5	M-7	Plexiglas	Air	Not required	Plexiglas	Sheet	Transparent	59.0	5	X				X	Highest NOCT
	Block II and Mini														
6	Block II (Spectrolab)	Glass	PVB	Not required	Polyester	Sheet	Transparent	41.1	9					X	
7	Mini (Spectrolab)	Glass	PVB	Not required	Polyester	Sheet	Transparent	43.1	5					X	
8	Block II (Sensor Tech)	RTV 615	RTV 615	PVC/glass fiber	Aluminum	Pan	Aluminum	42.9	8		X				
9	Mini (Sensor Tech)	RTV 615	RTV 615	PVC/glass fiber	Aluminum	Pan	Aluminum	44.4	13		X				
10	Block II (Solarex)	RTV	RTV	Not required	Polyester	Sheet	Tan	47.1	8				X		
11	Mini (Solarex)	RTV	RTV	Not required	Polyester	Sheet	Tan	46.2	12				X		
12	Block II (Solar Power)	Silicone coating	RTV	Not required	Polyester	Molded	White	46.0	2				X		
13	Mini (Solar Power)	Silicone coating	RTV	Not required	Polyester	Molded	White	44.9	12				X		
	R&D														
14	EDS (Xerox)	Glass	RTV 615	Circuit board	Aluminum	Extruded	Blue	46.3	7	X	X				
15	Lockheed	Glass	Sylgard	Not required	Silicone coating	Sheet	Transparent	42.4	13					X	
16	Motorola	Glass	Silicone gel	Polyimid/glass	Stainless	Pan	Orange	53.3	10		X				Local void beneath cell suspected
17	Sensor Tech	RTV 615	RTV 615	RTV 615	Aluminum	Pan	Aluminum	44.5	15		X				
18	OCLI	Glass	RTV	Mylar	Aluminum	Sheet	Aluminum	45.5	5		X				
19	Solar Tech Int'l.	Glass	Neoprene	Neoprene	Aluminum	Box	Gray	51.3	5	X	X				
20	Arco Solar Inc.	Glass	PVB	Not required	Mylar	Sheet	Transparent	56.9	7	X				X	Box support creates void beneath substrate
21	Solarex (Block III)	RTV	RTV	Not required	Polyester	Sheet	Tan	46.5	15				X		
	JPL-Modified														
22	Solarex I (No. 3)	Sylgard	Sylgard	Not required	Fiche/G-10 board	Sheet	Green	55.1	10				X		1/2-in. fiberboard bonded to back side
23	Solar Power I (No. 4)	Sylgard	Sylgard	G-10 board	Aluminum	Sheet	Green	50.6	8		X				1/8-in. aluminum bonded to back side
24	Sensor Tech I	Sylgard	Sylgard	Sylgard	Aluminum	Sheet	Aluminum	41.7	3		X				Fins removed
25	EDS (Xerox) (No. 14)	Glass	RTV 615	Circuit board	Aluminum	Voidless extruded	Blue	45.6	4		X				Void beneath cell filled
26	M-7 (No. 5)	Plexiglas	RTV 615	Not required	Plexiglas	Sheet	Transparent	54.1	6					X	Void between cell and cover filled
27	M-7 (No. 26)	Plexiglas	RTV 615	Not required	Painted Plexiglas	Sheet	White	57.2	10				X		Back side painted white, void filled
28	Spectrolab Mini (No. 7)	Glass	PVB	Not required	Painted polyester	Sheet	White	44.6	8				X		Back side painted white
29	Solar Power I (No. 23)	Sylgard	Sylgard	G-10 board	Aluminum	Sheet	Green	49.6	10		X		X		Aluminum painted white

(2) RTV silicone rubber was the most effective pottant and sealing material. Water intrusion into PVB-encapsulated modules caused electrical failures.

(3) Glass covers with glass, aluminum, or stainless-steel back panels withstood the 2-yr tests without failure.

In these tests, the newer FSA candidate pottants, such as EVA, EMA, and PnBA, were not available for evaluation, and the module cost and performance goals for their application were different from the FSA Project objectives.

Module failure mechanisms identified during qualification and field testing of FSA Block I, II, and III modules that have resulted in degraded module performance or limited module life, or have required module replacement for safety reasons, have included:

(1) Module surface soiling, reversible and non-reversible.

(2) Solar-cell cracking from pre-existing cell-edge flaws and stressing by various mechanical and thermal loads.

(3) Interconnect failures from thermal-cycle fatigue fractures or disbonds between the interconnect and cell surface; disbonds from solder melting have been observed.

(4) Structural failure of glass-sheet superstrates due to mechanical mounting forces, thermally induced loads, and hail or object impact; glass failure due to wind forces alone have not been reported.

(5) Electrical-isolation breakdown at 1500 V or less has been observed and has been attributed mainly to manufacturing flaws, such as metal projections and sharp edges, voids, contamination or mislocated cells and wires.

(6) Excess leakage current (>50 μA) through the encapsulant to ground at 1500 V, especially during salt-fog exposures.

(7) Visible deterioration of electrical termination hardware, metal conductors and insulating polymers.

(8) Degradation of the physical-chemical properties of polymeric encapsulants as manifested by color change, shrinkage, splits and cracks, embrittlements, softening, surface tackiness, or bubble formation.

(9) Delamination of encapsulant layers from cells and substrates producing visible interface voids and direct exposure of cells to moisture and dirt.

(10) Corrosion of module and array structural hardware exposed to the atmospheric elements and corrosion of solar-cell circuit components within the module, due to the combined effects of an electrical field and electrolytes formed by contaminants and intrusive moisture;

contaminants may come from the environment (sulfur dioxide), from manufacturing (solder flux), or polymer degradation reactions (acetic acid).

(11) Wrinkling of polymer film and aluminum foils used as back covers, due to thermal distortion and yielding during temperature and humidity cycling.

Note that hot-spot cell heating is not listed above as a failure mechanism; rather, it is the normal response of a solar-cell module to several fault conditions leading to cell reverse bias. Fault conditions include cracked or mismatched cells, open-circuit interconnect failures, or non-uniform illumination (partial shadowing). Under these conditions, a back-biased cell dissipates power equal to the product of the current and the reversed voltage that develops across the cell. Depending on the cell characteristics, the circuit design and the thermal characteristics of the encapsulant, the cell may be heated to an elevated temperature sufficient to melt solder, ignite the pottant, or cause gas-bubble evolution from the pottant with consequent cell bulging and cracking.

Control of hot-spot heating and testing for resistance to damage from hot-spot heating is covered in References 45 and 46.

The hot-spot temperature limits placed on a specific module will generally be determined by the long-term photothermal stability of the polymer pottant candidates. This information is being compiled by the FSA Encapsulation Task for the materials of interest under expected exposure conditions.

D. LIFE ASSESSMENT BASED ON POLYMER LONG-TERM STABILITY

After designing a PV module to pass the appropriate qualification test reliably and with sufficient design margin to survive exposure extremes with a low failure probability, the next step is to assess its life potential based on resistance to wear-out phenomena.

A review of the experimental data on the foregoing 11 module-failure mechanisms reveals that most of these failures have occurred during qualification testing or after a relatively short field test (less than 2 yr).

Initial evaluation of the effects of encapsulant-material aging on bulk-material properties revealed very little change (e.g., in the silicone rubber). However, changes in surface character and interfaces were noted. The bare silicone surface became more tacky and now retained more dirt than do glass or other plastic films. Delamination that occurred between silicone rubber and aluminum or polyester-glass-fiber substrates were related to UV exposure, moisture, and the surface preparation or priming methods used. These specific material combinations will have limited application in future module designs.

A prominent module-failure mode has developed, however, as a significant wear-out mechanism in interconnect cyclic fatigue. Recent analysis and experimental work at JPL has quantitatively related the interconnect materials and configuration to failure probability under specific field exposure conditions (Figure 6-3). The encapsulant material property that relates directly to this wear-out failure is the thermal-expansion coefficient of the substrate panel.

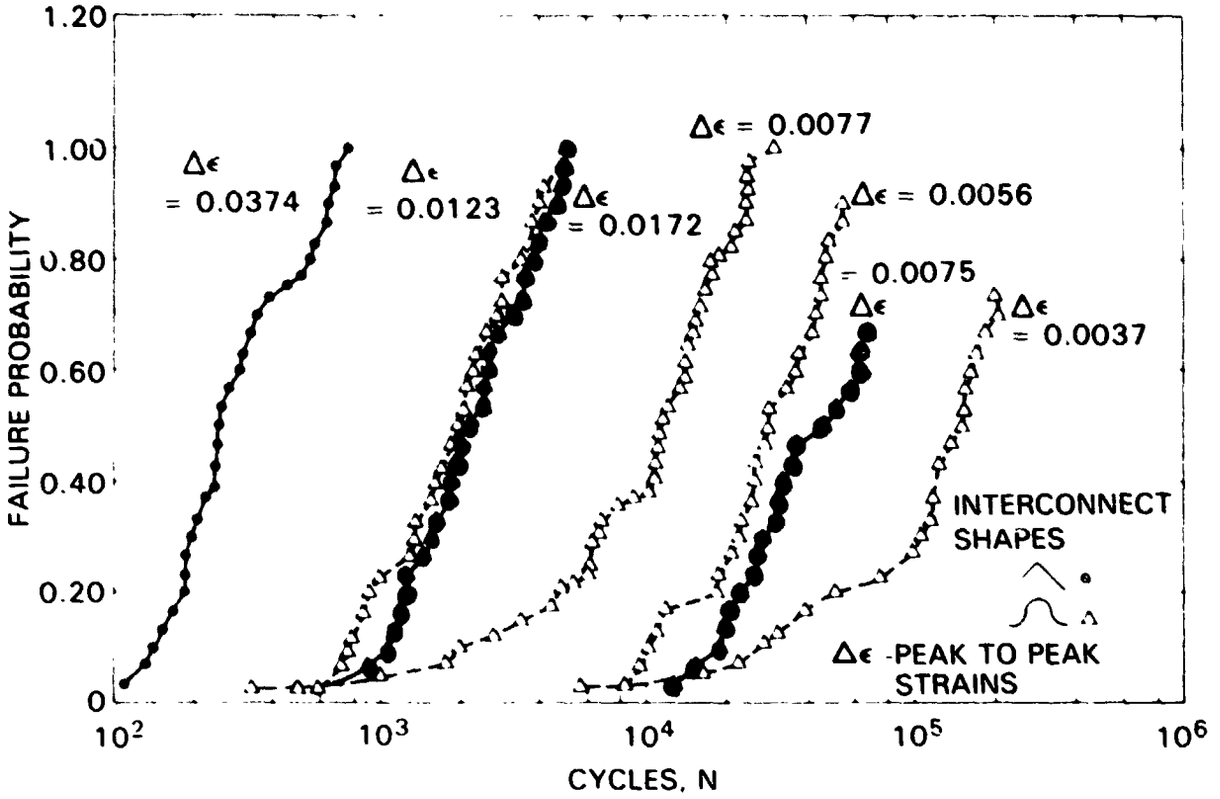

Figure 6-3. Interconnect Strain-Cycle Failure Test Data Fatigue and Failure

Failures have occurred in modules with either organic (polymer-glass-fiber) or aluminum panels. Glass-superstrate modules have not experienced this problem because of the much closer match between the thermal expansion of glass and the silicon solar cells.

In reviewing the critical encapsulant properties that must be retained over long times to achieve a 20-yr service life, they may be divided into five encapsulation-package classifications:

(1) Optical transmission.

(2) Environmental isolation.

(3) Mechanical integrity.

(4) Dielectric properties.

(5) Chemical inertness.

These are the encapsulant material characteristics that must be measured for present candidate encapsulant materials and material combinations as a function of exposure time, temperature, and various environmental exposure stresses under normal and accelerated testing conditions.

Polymer aging-mechanism models are being developed and validated that will: (1) facilitate extrapolation of property-degradation data to 20 yr, (2) define limits on the levels of test acceleration that may be used in verifying long-term effects, and (3) identify the material properties that can be monitored to track the aging process.

The candidate encapsulant materials for which photothermal stability data are being measured with some initial results available include:

(1) Cover Materials:

  (a) Fluorocarbon film (Tedlar UTB-300).

  (b) Acrylics:

    1) Korad.

    2) PMMA (3M).

    3) Stabilized copolymers.

(2) Pottants:

  (a) Silicone rubber (RTV 615).

  (b) Ethylene vinyl acetate (EVA).

  (c) Polyvinyl butyral (PVB-Saflex).

  (d) Poly-n-butyl acrylate (PnBA).

  (e) Et'.ylene methyl acrylate (EMA).

Physical properties being measured as a function of exposure and aging time include:

(1) Spectral transmission.

(2) Weight loss.

(3) Tensile elongation.

(4) Elastic modulus.

(5) Molecular weight.

(6) Differential scanning calorimetry (DSC).

(7) Creep.

The range of exposure conditions includes UV radiation from a mercury source (equivalent to 7 suns in a selected wavelength region) at temperatures of 30°C, 55°C, 70°C, 85°C, and 105°C. Material specimens were exposed to

these temperatures in the absence of radiation, and to combinations of UV and no air access. Data were thus obtained on the mechanisms of thermal degradation, thermal oxidation, photooxidation and photolysis.

Future data will be available on the change in dielectric properties as a function of photothermal aging.

A JPL report on the results of the photothermal stability measurement program is being compiled. A summary of the initial results is presented below.

In addition to evaluating and understanding the long-term stability characteristics of individual encapsulant materials, it is necessary to assess the stability of complete encapsulant packages and the effect of the encapsulant on the performance and stability of the solar cells. Data in this area for current and advanced designs are limited. JPL is working to develop and validate appropriate accelerated durability tests and provide a basis for potential life assessment.

E. PHOTOTHERMAL STABILITY OF POLYMER CANDIDATES, POTTANTS

The photothermal charcterization results in the following paragraphs indicate initial results and trends to be futher investigated and documented.

1. Silicone Rubber (RTV)

Crosslinked silicone rubbers (polydimethyl-siloxane, RTV 615), used as pottants, undergo very little change in bulk properties when exposed directly for long periods to UV and air, or exposed behind glass. During material sample tests for 800 h in the presence of oxygen under 7 suns of UV at 105°C, RTV 615 was stable in terms of its optical transmission (less than 0.5% change), and of its mechanical integrity, as measured by tensile modulus. Chemically, Si-H bonds were cleaved and large hydroxyl and carbonyl functionalities were formed due to thermal oxidation and photooxidation. Temperature coefficients of the rate of change of optical and mechanical properties indicate that the lifetime of this pottant at 55°C and 1 sun (AM1) in a non-hermetic design can be expected to be 20 yr or more for these two types of failure mechanisms. Surface chemical changes noted above may cause delamination and may increase power loss due to soil retention.

2. Ethylene Vinyl Acetate (EVA)

EVA without UV stabilizer and antioxidants (Elvax 150) undergoes chain scission and loss of optical transmission when exposed to UV, due to formation of carbonyl-containing chromophores and incomplete saturation. Samples of EVA Formulation A9918, as shown in Table 4-4, were tested under 7 suns of UV, 70°C to 105°C, and under hermetic (no oxygen access) and non-hermetic designs. Formulated EVA is chemically and physically stable at temperatures up to 80°C in hermetic designs. In non-hermetic designs, photothermal oxidation begins to dominate at temperatures above 80°C, as evidenced by the detection of hydroxyl formation in Fourier transform infrared (FTJR) analysis.

Loss of additives also takes place in non-hermetic designs. The time scale of substantial loss (50%) of additives on outdoor exposure of non-hermetic modules is expected to be 10 to 15 yr. Because EVA without additives undergoes relatively rapid degradation on outdoor exposure (1 to 2 yr) to UV and oxygen, leading to yellowing, cracking, and onset of creep, modules containing EVA will require an effective UV-screening cover and oxygen barrier (e.g., glass) to provide a life potential of 20 yr with daily peak temperatures of 80°C. The temperature coefficient of the rate of loss of additives is about 5 $\pm$2 kcal/mole. In non-hermetically sealed modules operating at 55°C, EVA will lose 50% of the additives in 15 to 20 yr. An initial estimate of module life potential of greater than 17 to 22 yr can be made at this temperature with an effective UV screen outer cover or oxygen barrier.

Recent work by the University of Toronto on chemical and physical property changes in EVA exposed to UV shows a substantial inhibition period, followed by a rapid autocatalytic loss of chemical and physical integrity. One method of ensuring stability of EVA would be to extend the inhibition period to 20 yr by using advanced stabilization techniques. However, during this inhibition period, harmful chemicals (e.g., alcohols, acids) may gradually build up in the pottant, even in the presence of additives, as shown by the University of Toronto. These chemicals could cause corrosion of the interconnects, metallization and delamination. These slow chemical processes during the inhibition period may be retarded by using either a hermetic design (no oxygen) or advanced stabilization techniques being developed. Research in this area is in progress.

3. Polyvinyl Butyral (PVB Saflex)

PVB Saflex has long been used in automobile safety glass, in which it is hermetically sandwiched between two sheets of glass. In this application, it has lasted for over 20 yr without serious degradation. However, tests in non-hermetic configurations indicated loss of stabilizers at 55°C, corresponding to a 15% loss within 2 to 4 yr of exposure. Stabilized PVB is chemically stable at 55°C for up to 1.5 yr of outdoor exposure. At 70°C, stabilized PVB undergoes rapid chemical (thermal and photothermal) oxidation leading to loss of transmission, weight loss and formation of voids, chemical crosslinking, and increase in equilibrium tensile modulus (an initial decrease in apparent modulus was observed).

4. Poly-n-Butyl Acrylate (PnBA)

Tests have been initiated on JPL-developed uncrosslinked PnBA. Room-temperature photolysis data indicate that photooxidation takes place, leading to crosslinking. A stabilized PnBA is being developed and further tests will be made.

5. Ethylene Methyl Acrylate (EMA)

Preliminary photolysis data indicate surface photooxidation when EMA is exposed to UV at room temperature. More extensive photothermal tests have been initiated.

6. Aliphatic Polyurethane (PU)

Samples tested were linear aliphatic polyurethane, manufactured by H.S. Quinn. These PU samples degraded readily at 55°C during photothermal aging in nonhermetic designs. With 400 h of UV aging time at 70°C (equivalent to 1.5 yr of outdoor exposure), PU suffered a weight loss of 16% due to formation of volatile photoproducts and a rapid loss of optical transmission (400 to 800 nm). Furthermore, chain scission occurred, leading to a 20% decrease in tensile modulus measured at 10% strain. Limited data on our sample of PU indicate that the pottant will undergo rapid degradation leading to yellowing, gradual loss of materials leading to void formation, and decrease of mechanical integrity leading to creep after 5 to 7 yr of service.

F. COVER MATERIALS

Because the function of the outer cover of a module includes protection of the module pottant and solar cells from water, soil, and solar UV, mechanical integrity of the cover film and maintenance of a high level of UV-screening property during service life are key concerns. Surface polarity and hydrophilicity have also been measured in some cases as a function of aging time, because these properties will affect the soiling character of the outer cover film.

1. Ultraviolet-Screening Polymethyl Methacrylate (PMMA) Films (X22416/17, from 3M Corp.)

Tests have been initiated on PMMA. Dimensional stability, optical transmission, and weight loss were monitored as a function of accelerated photothermal aging in air at 85°C, and thermal aging in a dark, stagnant oven at 85°C for up to 800 h (equivalent to 3.0 years). No change in direct and hemispherical transmission occurred during this period, and there was no dimensional change. Less than 0.5% weight change had been detected. These results indicate that the UV absorber was not being lost to a significant extent, and dimensional stability is good under these conditions. Further tests are being initiated on this material.

2. Acrylic Copolymer Films

Different kinds of acrylic copolymer films with UV absorbers have been evaluated. They were copolymers of methyl methacrylate and: (1) 5-vinyl, 2-hydroxyphenyl benzotriazole, (2) a JPL-developed additive: 4,4' dimethoxy 3-allyl, 2-hydroxybenzophenone, and (3) Permasorb MA.

a. 5-Vinyl 2-Hydroxyphenyl Benzotriazole. The hydroxyphenyl benzotriazole class of UV stabilizers-absorbers are marketed under the general trade name Tinuvin (e.g., Tinuvin P), by Ciba Geigy; and Cyasorb, by American Cyanamid. The methacrylate copolymer film has been subjected to accelerated UV (295 to 370 nm) exposure up to 4000 h at 35°C, equivalent to more than 18 yr of outdoor UV exposure.

Figure 6-4 shows that the chemical structure of the UV absorber group remains unchanged, hence the UV protective properties of the film remains unchanged. Molecular weight measurements indicate that the polymeric network undergoes both chain scission and crosslinking processes, but at a rate that will not significantly affect mechanical properties after the 4000-h test. Surface tension measurements were done as a function of exposure period.

These data indicate that the exposed (sun-side) surface gradually becomes more polar and hydrophilic, but the other surface does not change. Chemical changes in surface structure were also detected by FTIR-attenuated total reflectance spectroscopy. Water-soaking tests and extraction with boiling solvents were performed; they failed to extract the UV absorber from the polymer.

These aging data demonstrate the possibility of having a chemically and physically stable weatherable acrylic film that is transparent and retains its UV-screening properties for up to 20 yr of deployment.

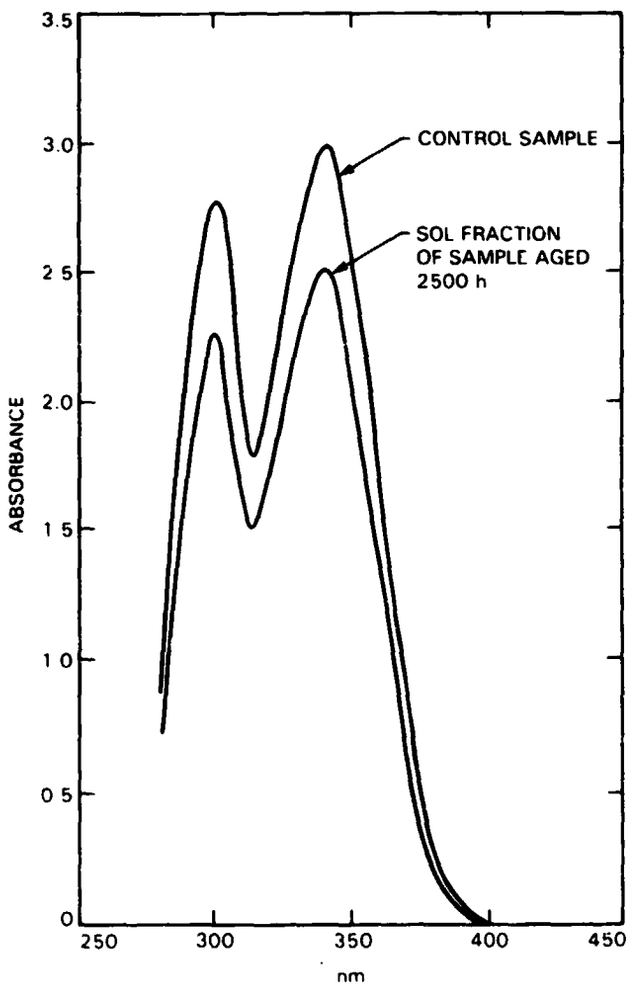

Figure 6-4. Electronic Absorption Spectra of Fluid Solutions of 5-Vinyl 2-Hydroxyphenyl Benzotriazole Co (MMA) Solvent CH_2Cl_2

b. 4,4'-Dimethoxy-3-Allyl-2-Hydroxy Benzophenone. Tests on the copolymer films of this additive, formulated at JPL with acrylics, show that complete physical stability has been achieved, and no chemical change in the UV-absorber chromophore can be detected. However, the polymer matrix undergoes a slow photodegradation process caused by synergistic energy transfer from the chromophore to the polymeric network. This rate of degradation corresponds to about 10-yr outdoor life expectancy.

c. Permasorb MA. Copolymerization studies done with Permasorb and acrylics indicate that this material has very poor polymerization reactivity; it was rarely attached to the polymeric network, but did oligomerize to form dimers and trimers that are almost insoluble in solvents such as methanol, which dissolve the monomer.

The oligomerized Permasorb MA remains fugitive, as shown in Figure 6-5. For this test, prototype candidate encapsulation film materials such as PMMA

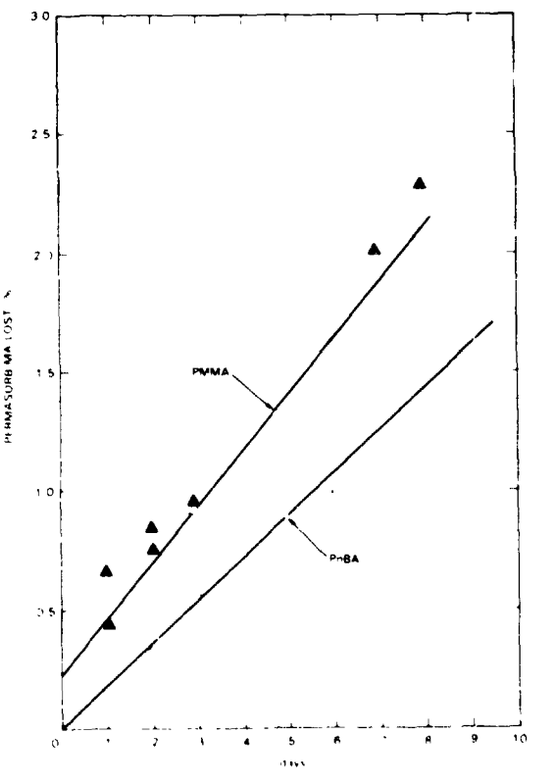

Figure 6-5. Oligomerization of Permasorb MA Blended with Polymethyl Methacrylate and Poly-n-Butyl Acrylate

(for outer-cover application) and PnBA (for application as pottant) were blended with Permasorb MA oligomers, and then exposed to distilled water at room temperature for periods of up to 14 days. As shown in Figure 6-5, significant leaching rates could be measured in both cases.

3. Tedlar UTB-300

This UV-screening form of Tedlar film is supplied by Du Pont as a candidate outer-cover film material. UV-visible absorption spectra (Figure 6-6) show that the UV absorber is lost from this material at 85°C, presumably because it is presented in a physically blended state. No systematic photodegradation studies have been performed on this material, although there are some indications that in free-standing films, photodegradation does take place at 55°C and causes a change (increase) in absorbance of the film. Similar results have been reported by Boeing after their tests on Tedlar (Reference 47).

4. Korad

Korad is an acrylic copolymer of butyl acrylate and other acrylic comonomers. Photothermal and thermal aging of Korad films at 55°C and 105°C resulted in a large decrease of absorbance in the 300 to 400 nm region (Figure 6-7). This shows that the UV-absorber component evaporates from Korad under these conditions.

An activation energy can be calculated from these rates of loss of UV absorbers. The temperature coefficient was determined to be 5 to 7 kcal/mole,

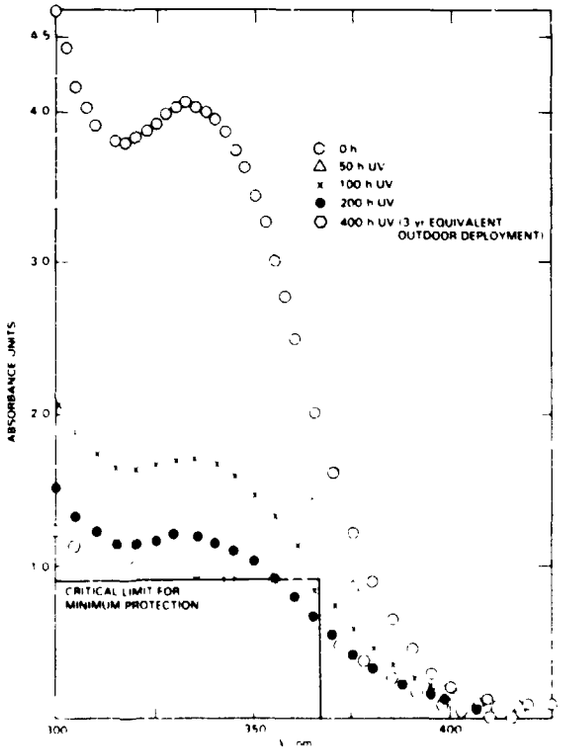

Figure 6-6. Loss of Ultraviolet Absorber from Tedlar at 85°C

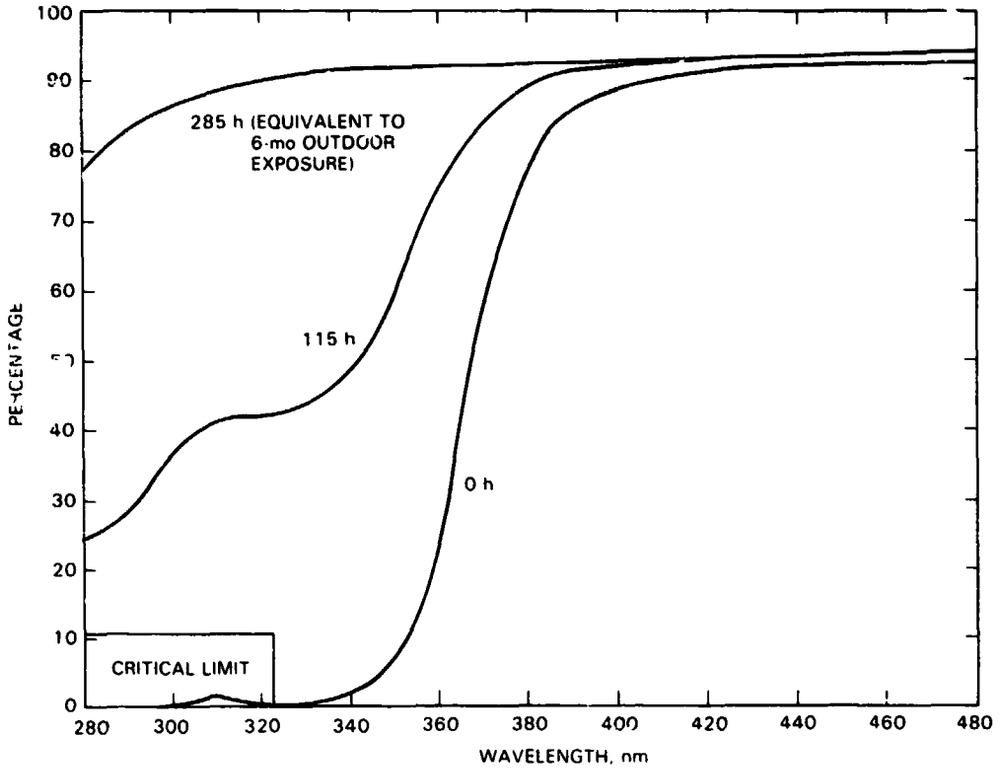

Figure 6-7. Loss of Ultraviolet Absorber from Korad Film at 85°C

a typical value for a physical process. Photodegradation of Korad results mainly in chain scission, a process that eventually leads to film cracking. The rate of chain scission was estimated at 55°C from a 295 to 350 nm wavelength.

In accelerated tests on two-cell modules, Korad films cracked after 14 to 28 days (308 to 616 h of UV exposure). This period of exposure is equivalent to 1.5 to 3 yr of outdoor exposure in the spectral range of 295 to 370 nm. Photodegradation of Korad is found to be caused chiefly by UV absorption, with oxygen and water playing secondary roles. Thus a good prediction of outdoor life could be obtained by performing a high-UV service-temperature test, as shown in Figure 6-8.

A synergistic mode of photodegradation appeared to be dominant in the early stage of the test, when most of the UV was being absorbed by the absorber. The electronic energy picked up the absorber molecules helped to catalyze a degradative process in the polymer matrix. Consequently, the presence of the UV absorber did not stabilize Korad from photodegradation, but there was a small enhancement in the rate.

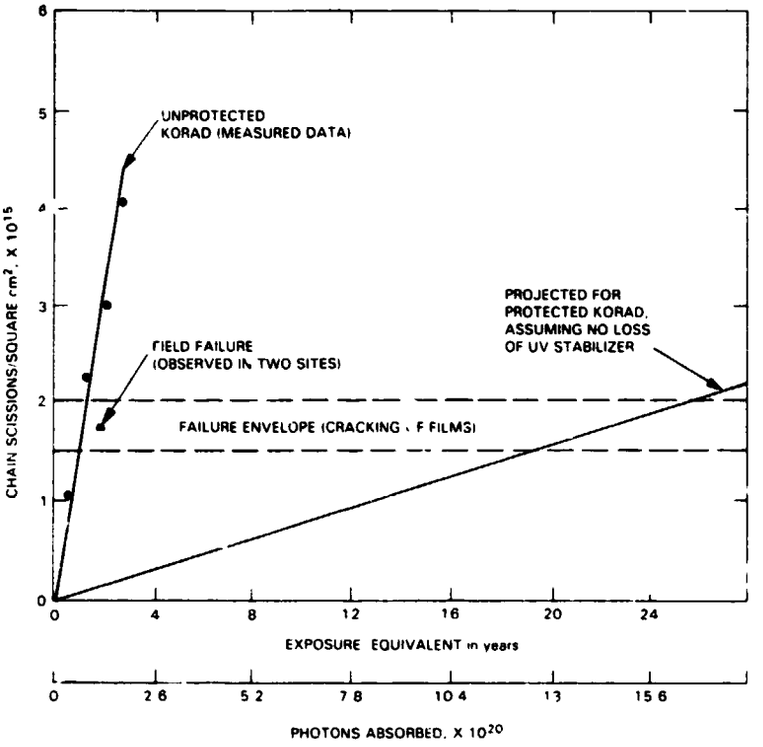

Figure 6-8. Summary of Test Results on Korad Films

SECTION VII

REFERENCES

1. Interim Standard for Safety: Flat-Plate Photovoltaic Modules and Panels, JPL Internal Document No. 5101-164, Jet Propulsion Laboratory, Pasadena, California, February 20, 1981.

2. Terrestrial Service Environments for Selected Geographic Locations, ERDA/JPL-954328-76/5, Battelle Columbus Laboratories, Columbus, Ohio, June 24, 1976.

3. Wind Loads on Flat-Plate Photovoltaic Array Fields, DOE/JPL 954833-81/3, Boeing Engineering and Construction Co., Seattle, Washington, April 1981.

4. Moore, D. M., and Wilson, A. H., Photovoltaic Solar Panel Resistance to Simulated Hail, JPL Project Document No. 5101-(DOE/JPL-1012-78/6, Jet Propulsion Laboratory, Pasadena, California, October 15, 1978.

5. Hoffman, A. R., and Maag, C. R., Photovoltaic Module Soiling Studies, JPL Publication No. 80-87, DOE/JPL-1012-49, Jet Propulsion Laboratory, Pasadena, California, November 1, 1980.

6. Ross, R. G., Jr., "Photovoltaic Design Optimization for Terrestrial Applications," presented at the 13th IEEE Photovoltaic Specialists Conference, Washington, D.C., June 5-8, 1978.

7. Ross, R. G., Jr., "Flat-Plate Photovoltaic Array Design Optimization," presented at the 14th IEEE Photovoltaic Specialists Conference, San Diego, California, January 7-10, 1980.

8. Stultz, J. W., and Wen, L. C., Thermal Performance Testing and Analysis of Photovoltaic Modules in Natural Sunlight, JPL Internal Document No. 5101-31, Jet Propulsion Laboratory, Pasadena, California, July 29, 1977.

9. Stultz, J. W., Thermal and Other Tests of Photovoltaic Modules Performed in Natural Sunlight, JPL Project Document No. 5101-76, DOE/JPL-1012-78/9, Jet Propulsion Laboratory, Pasadena, California, July 31, 1978.

10. Willis, P., et al., Investigations of Test Methods, Material Properties, and Processes for Solar-Cell Encapsulants, Annual Report, ERDA/JPL-954527, Springborn Laboratories, Inc., Enfield, Connecticut, July 1977.

11. Willis, P., Baum, B., and White, R., Investigations of Test Methods, Material Properties, and Processes for Solar-Cell Encapsulants, Annual Report, ERDA/JPL-954527, Springborn Laboratories, Inc., Enfield, Connecticut, July 1978.

12. Design and Analysis of Advanced Encapsulation Systems for Terrestrial Photovoltaic Modules, Interim Report Covering Work Performed from 1 December 1979 to 1 October 1980, Spectrolab, Inc., Sylmar, California, (in press).

13. Griffith, J. A., Rathod, M. S., and Paslaski, J., "Some Tests of Flat Plate Photovoltaic Module Cell Temperatures in Simulated Field Conditions," presented at 15th IEEE Photovoltaic Specialists Conference, Kissimmee, Florida, May 12-15, 1981.

14. Chen, C. P., Fracture Strength of Silicon Solar Cells, JPL Project Document No. 5101-137, JPL Publication No. 79-102, DOE/JPL-1012-32 Jet Propulsion Laboratory, Pasadena, California, October 15, 1979.

15. Mon, G. R., "Defect Design of Insulation Systems for Photovoltaic Modules," presented at 15th IEEE Photovoltaic Specialists Conference, Kissimmee, Florida, May 12-15, 1981.

16. Phillips, C. J., Glass: Its Industrial Applications. Reinhold Publishing Co., New York, 1960.

17. Cuddihy, E. F., Encapsulation Materials Status to December 1979, JPL Internal Document No. 5101-144, Jet Propulsion Laboratory, Pasadena, California, January 15, 1980.

18. Cuddihy, E. F., Encapsulation Material Trends Relative to 1986 Cost Goals, JPL Internal Document 5101-61, Jet Propulsion Laboratory, Pasadena, California, April 13, 1978.

19. Willis, P., et al., Investigations of Test Methods, Material Properties, and Processes for Solar-Cell Encapsulants, Annual Report, ERDA/JPL-954527, Springborn Laboratories, Inc., Enfield, Connecticut, July 1980.

20. Cuddihy, E. F., Baum, B., and Willis, P., Low-Cost Encapsulation Materials for Terrestrial Solar Cell Modules, JPL Internal Document 5101-78, Jet Propulsion Laboratory, Pasadena, California, September 1978, and Solar Energy, Vol. 22, p. 389, 1979.

21. Develop Silicone Encapsulation Systems for Terrestrial Silicon Solar Arrays, Final Report, DOE/JPL 945995-80/6, Dow Corning Corp., December 1979.

22. Carmichael, D. C., et al., Review of World Experiences and Properties of Materials for Encapsulation of Terrestrial Photovoltaic Arrays, Final Report, Battelle Columbus Laboratories, Columbus, Ohio, July 21, 1976.

23. Brendlay, W. H., Jr., "Fundamentals of Acrylic Polymers," Paint and Varnish Production, Vol. 63, No. 7, pp. 19-27, July 1973.

24. Rainhart, L. G., and Schimmel, W. P., Jr., "Effect of Outdoor Aging on Acrylic Sheet," Solar Energy, Vol. 17, pp. 259-264, 1975.

25. Longo, F. N., and Durman, G. J., "Corrosion Prevention with Thermal-Sprayed Zinc and Aluminum Coatings," Atmospheric Factors Affecting the Corrosion of Engineering Metals, ASTM STP 646, pp. 97-114, Edited by S. K. Coburn, American Society for Testing and Materials, Philadelphia, Pennsylvania, 1978.

26. White, M.L., "Encapsulation of Integrated Circuits," in Proceedings of the IEEE, Vol. 57, p. 1610, 1969.

27. Jaffe, D., "Encapsulating Integrated Circuits Containing Beam Leaded Devices with a Silicone RTV Dispersion, IEEE Transactions on Parts, Hybrids, and Packaging, Vol. 12, p. 182, 1976.

28. White, M. L., "Encapsulating Integrated Circuits," Bell Laboratories Record, Vol 52, p. 80, March 1974.

29. Shar, N. L., and Feinstein, L. G., "Performance of New Copper-Based Metallization Systems in an 85°C, 80% RH, Cl_2 Contaminated Environment," in Proceedings of 1977 Electronic Components Conference, Arlington, Virginia, May 16-18, 1972, pp. 84-95.

30. Pleuddemann, E. P., Chemical Bonding Technology for Terrestrial Solar Cell Modules, JPL Internal Document 5101-132, Jet Propulsion Laboratory, Pasadena, California, September 1, 1979.

31. Eirls, James L., Use of Glass Reinforced Concrete (GRC) As a Substrate for Photovoltaic Modules, Final Report, Tracor MBA, San Ramon, California, March 12, 1980.

32. Gupta, A., Photodegradation of Polymeric Encapsulants of Solar Cell Modules, JPL Internal Document 5101-77, Jet Propulsion Laboratory, Pasadena, California, August 10, 1978.

33. Gupta, A., Effect of Photodegradation on Chemical Structure and Surface Characteristics of Silicone Pottants Used in Solar Cell Modules," JPL Internal Document 5101-79, Jet Propulsion Laboratory, Pasadena, California, August 18, 1978.

34. Runge, M. L., and Dreyfuss, P., "Effect of Interfacial Chemical Bonding on the Strength of Adhesion of Glass-Polybutadiene Joints," J. Polym. Sci., Vol. 17, p. 1067, 1979.

35. Conley, W. R., Ion-Plating of Solar-Cell Arrays Encapsulation Task: First Quarterly Progress Report, December 1979 to March 1980, Illinois Tool Works, Endurex Division, Elgin, Illinois, June 1980.

36. Hoffman, A.R., and Maag, C.R., "Airborne Particulate Soiling of Terrestrial Photovoltaic Modules and Cover Materials," in Proceedings of the Institute of Environmental Sciences, Philadelphia, Pennsylvania, May 11-14, 1980, Institute of Environmental Sciences, Mt. Prospect, Illinois, 1980.

37. Hoffman, A.R., and Maag, C.R., Photovoltaic Module Soiling Studies, May 1978 to October 1980, JPL Project Document No. 5101-131, JPL Publication No. 80-87, DOE/JPL-1012-49, Jet Propulsion Laboratory, Pasadena, California, November 1, 1980.

38. Cuddihy, E.F., "Theoretical Considerations of Soil Retention," Solar Energy Materials, Vol. 3, pp. 21-33, 1980.

39. Investigations of Test Methods, Material Properties, and Processes for Solar-Cell Encapsulants, Annual Report, Springborn Laboratories, Inc., Enfield, Connecticut, and DOE/JPL 954527-80-15, Jet Propulsion Laboratory Pasadena, California, July 1981.

40. Photovoltaic Module Design, Qualification and Testing Specification, JPL Project Document No. 5101-65, DOE/JPL-1012-7817A, Jet Propulsion Laboratory, Pasadena, California, March 24, 1978.

41. Jaffe, P., LSA Field Test Annual Report, August 1977 to August 1978, JPL Internal Document No. 5101-85, DOE/JPL-1012-78/12, Jet Propulsion Laboratory, Pasadena, California, September 15, 1978.

42. Jaffe, P., LSA Field Test Annual Report, August 1979 to August 1980, JPL Project Document No. 5101-166, JPL Publication No. 81-12, Jet Propulsion Laboratory, Pasadena, California, December 30, 1980.

43. Mihalkanin, P. A., and Anderson, R. T., A Program to Develop Elements of a Reliability Design Guidebook for Flat Plate Photovoltaic Modules/Arrays, Quarterly Report, DOE/JPL 955720-80, IIT Research Institute, Chicago, Illinois, October 1980.

44. Trenchard, S. E., Testing of Solar Photovoltaic Arrays for Utilization on Marine Aids to Navigation, U.S. Coast Guard Report No. CG-D-10-81, U.S. Coast Guard Research and Development Center, Avery Point, Groton, Connecticut, November 1980.

45. Block V Solar Cell Module Design and Test Specification for Residential Applications-1981, JPL Internal Document No. 5101-161, Jet Propulsion Laboratory, Pasadena, California, February 20, 1981.

46. Flat-Plate Photovoltaic Module and Array Circuit Design Optimization Workshop Proceedings - May 19-20, 1980, JPL Internal Document No. 5101-170, Jet Propulsion Laboratory, Pasadena, California.

47. Mavis, C. L., The Status and Recommended Future of Plastic-Enclosed Heliostat Developments, Sandia 80-80320, Boeing Engineering and Construction Co., Seattle, Washington, October 1980.

APPENDIX

A MASTER-CURVE METHOD OF ESTIMATING TENSILE STRESSES IN ENCAPSULATED SOLAR CELLS BY MODULE DEFLECTION AND THERMAL EXPANSION

APPENDIX

INTRODUCTION

Structural analyses of silicon-solar-cell stress in modules with glass, wood, and steel panels were described in Section III, and Figures 3-11 through 3-18 review these findings. These computer-predicted stress curves are applicable where the structural panel is the generator of stress, resulting from either panel deflection or thermal expansion, with the pottant acting to damp the transmission of the generated stress to the solar cells. The computer analysis indicates that the efficiency of a pottant in damping stress transmission increases with increasing pottant thickness and with decreasing pottant modulus. However, the computer findings are not immediately as informative for the panels as they are for the pottants. Stress generation by a structural panel can be expected to involve panel properties, such as Young's modulus, thermal expansion, panel thickness and area, and loading conditions (the magnitude of the wind loads and temperature excursions). But inspection of the figures in Section III does not readily reveal trends or directions that would enable a general assessment or estimation for panels other than glass, wood, or steel. Also, several of the structural computer runs involved analysis for only a single Young's modulus of a pottant, primarily because of computer cost, running time, and demands on the computer for other Phase I calculations. This yields upper-bound information for pottants with a lower Young's modulus, but is not much help in assessing pottants with higher values of Young's modulus.

To generate computer traces for any combination or choice of pottant and panel is impractical, not only because of cost, but also, more important, from the necessity of maintaining the computer capability and operators in a virtual readiness mode whenever the information is desired or new pottants or panel candidates are identified in the future. Accordingly, an effort was made to determine if the structural computer traces plotted in Figures 3-11 to 3-18 could be used to generate a composite, reduced-variable master curve that could be used to estimate or approximate solar-cell tensile stresses from any combination or choice of pottant and panel. This appendix describes the development of cell-stress master curves for thermal expansion and wind deflection, using the structural computer traces generated from the Phase I analytical activities.

A. THERMAL-EXPANSION MASTER-CURVE ANALYSIS

To facilitate generation of a reduced-variable master curve, the computer traces for thermal-expansion stresses, Figures 3-14, 3-15, and 3-18, were replotted on log-log graph paper, and these log-log traces for glass and steel are plotted in Figures A-1 and A-2. A trial operation involving horizontal and vertical shifting of these separate data traces revealed that a composite master curve could be developed.

Given this observation, the remaining activity was to identify reduced-variable expressions for the ordinate and abscissa that would achieve mathematical merging of all the segments into the composite master curve. The log-log data traces for wood which could be generated from Figure 3-18 were not helpful in establishing the reduced-variable expression for the abscis· , because these data traces were essentially parallel with this axis. Thus, additional computer

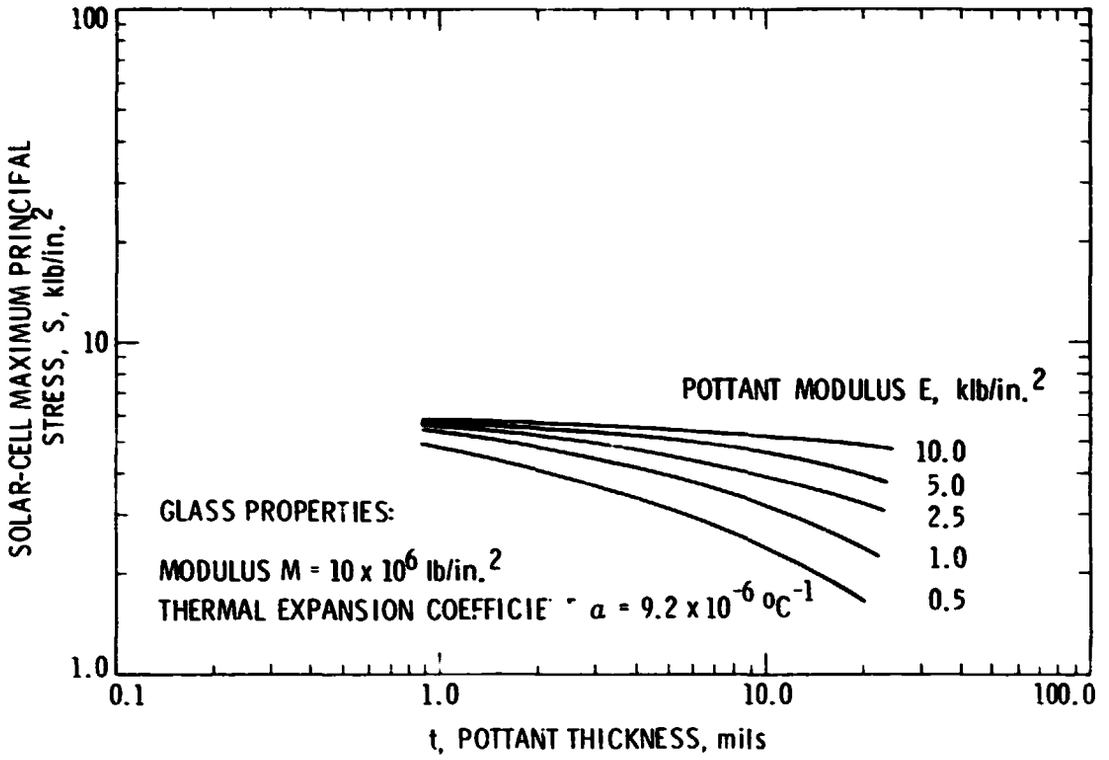

Figure A-1. Log-Log Plots of Computer Traces Given in Figure 3-14 for a Glas. -Superstrate Design

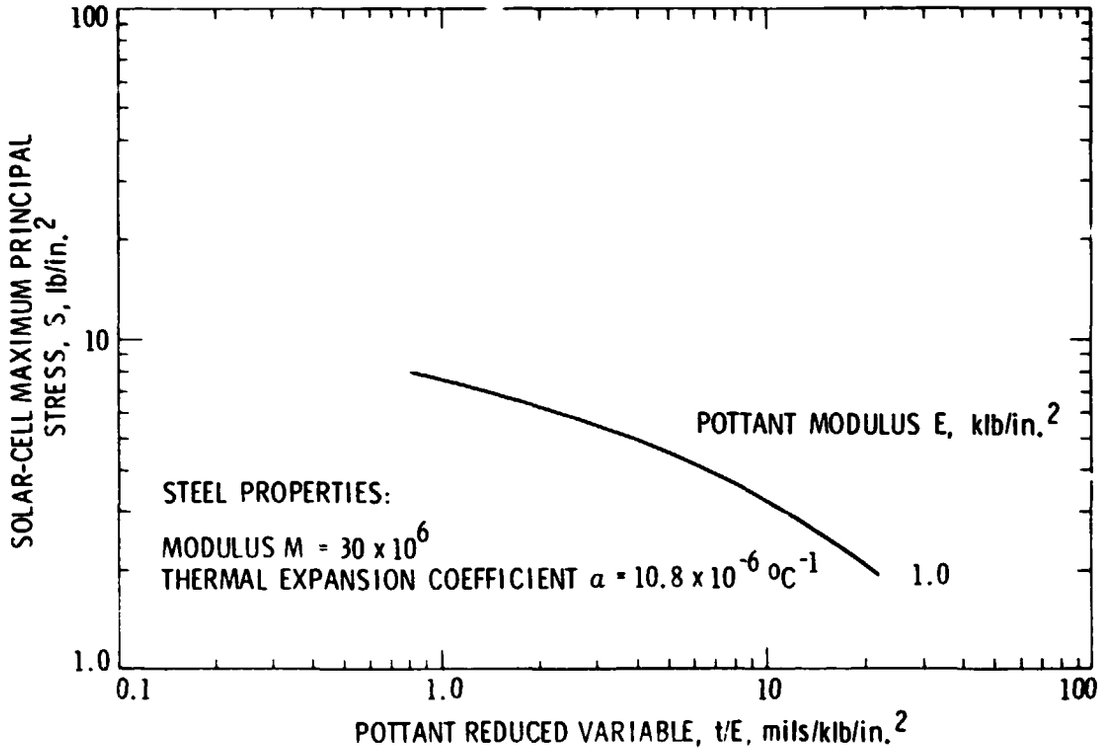

Figure A-2. Log-Log Plot of the Computer Trace Given in Figure 3-15 for a Steel-Substrate Design

runs were made to generate log-logdata traces for a wooden-panel module, using an artificial thermal-expansion value 10 times higher than the actual value, i.e., 7.2×10^{-5} $^{o}C^{-1}$ compared to the actual value of 7.2×10^{-6} $^{o}C^{-1}$. Log-log computer traces for wood with this artificial expansion value, and for two levels of Young's modulus for the pottant, 1 klb/in.^{2} and 50 klb/in.^{2}, are plotted in Figure A-3. The use of the artificial-expansion coefficient develops curvature in the computer traces, which enables both horizontal and vertical positioning of these traces into a composite master curve.

To develop the master curve, the log-log traces for glass, Figure A-1, can be shifted horizontally to a composite curve, Figure A-4, and from the relative magnitudes of the shift ratios, a reduced-abscissa variable, t/E, is generated. The terms in the variable are t, thickness of the pottant in mils, and E, Young's modulus of the pottant in units of klb/in.^{2}. Accepting t/E as a valid reduced variable for the abscissa, the two computer traces for wood that were calculated with the artificial thermal-expansion coefficient, Figure A-3, were appropriately shifted horizontally. The shifted plots are shown in Figure A-5.

For steel (Figure A-2) there is only a single computer trace for E = 1.0 klb/in.^{2}. Assuming that t/E is valid, then this computer trace is properly positioned along the horizontal axis for the reduced variable t/E.

The composite curves for steel, glass, and wood, plotted with the reduced-abscissa variable t/E (Figures A-2, A-4, and A-5, respectively) are still separated horizontally and vertically, although trial shifting of these composite

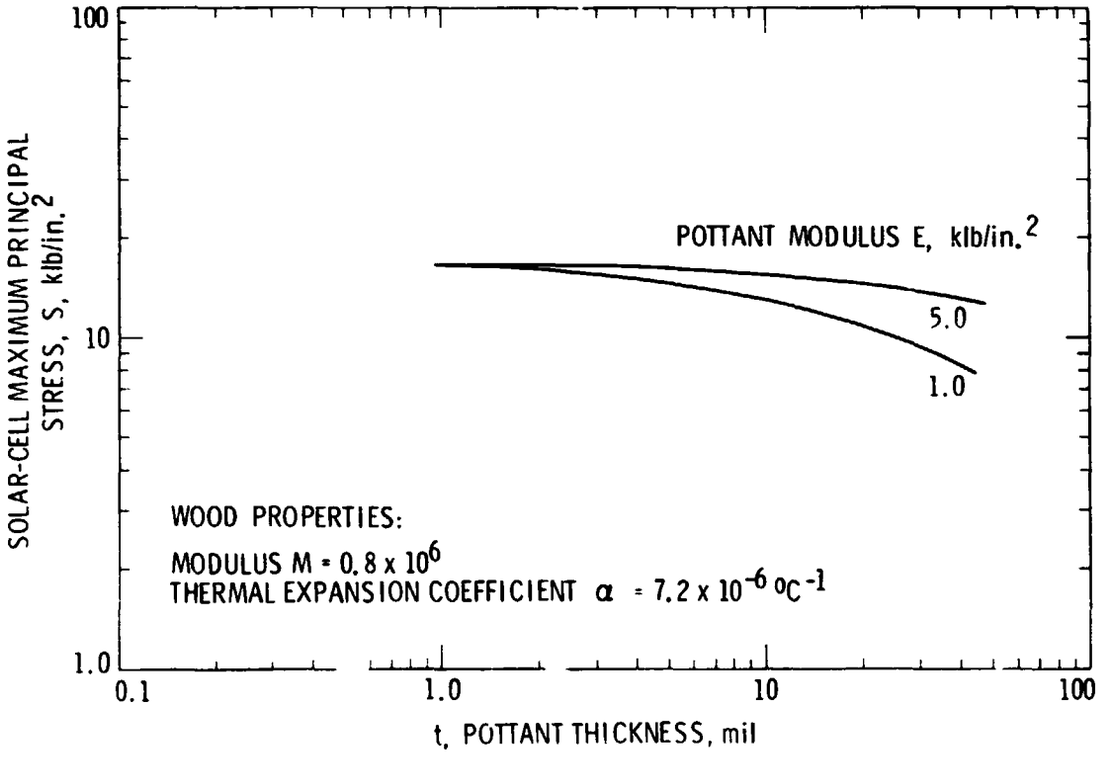

Figure A-3. Computer-Predicted Stresses of Encapsulated Silicon Solar Cells Resulting from Thermal Expansion Differences in a Wooden-Substrate Module for a ΔT of 100°C, Using an Artificial Thermal Expansion Coefficient

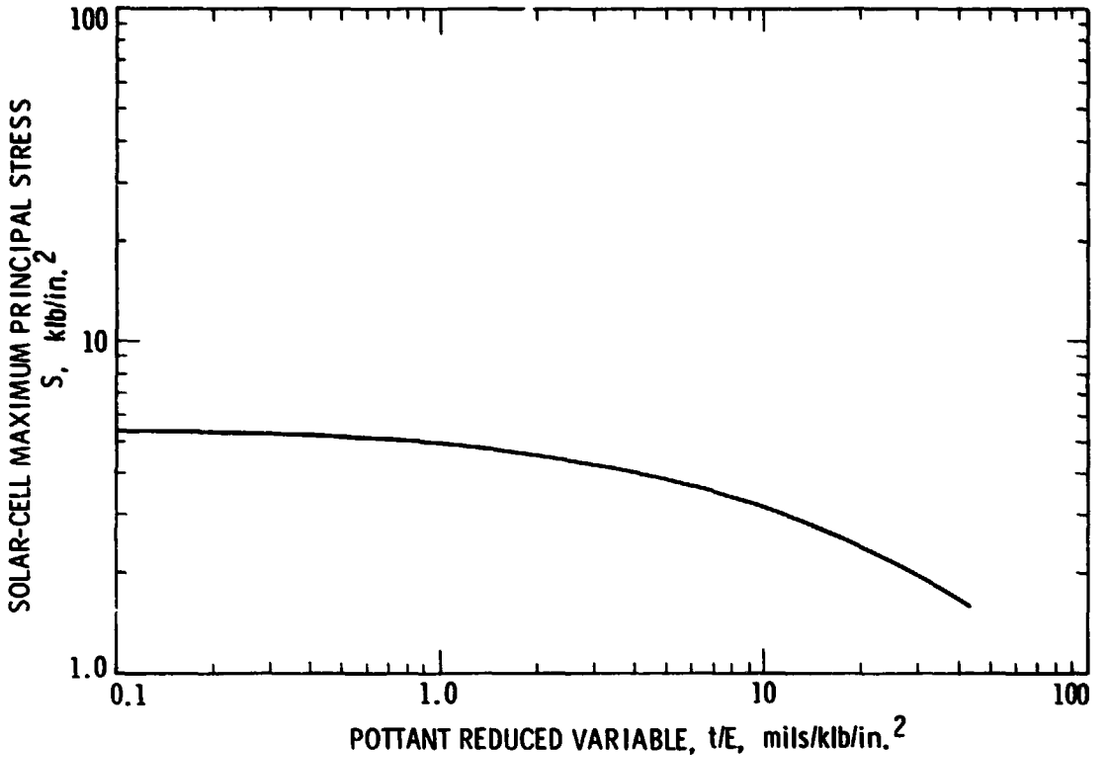

Figure A-4. Horizontally Shifted Computer Traces of Figure A-1 for Glass, Using Reduced Variable, t/E

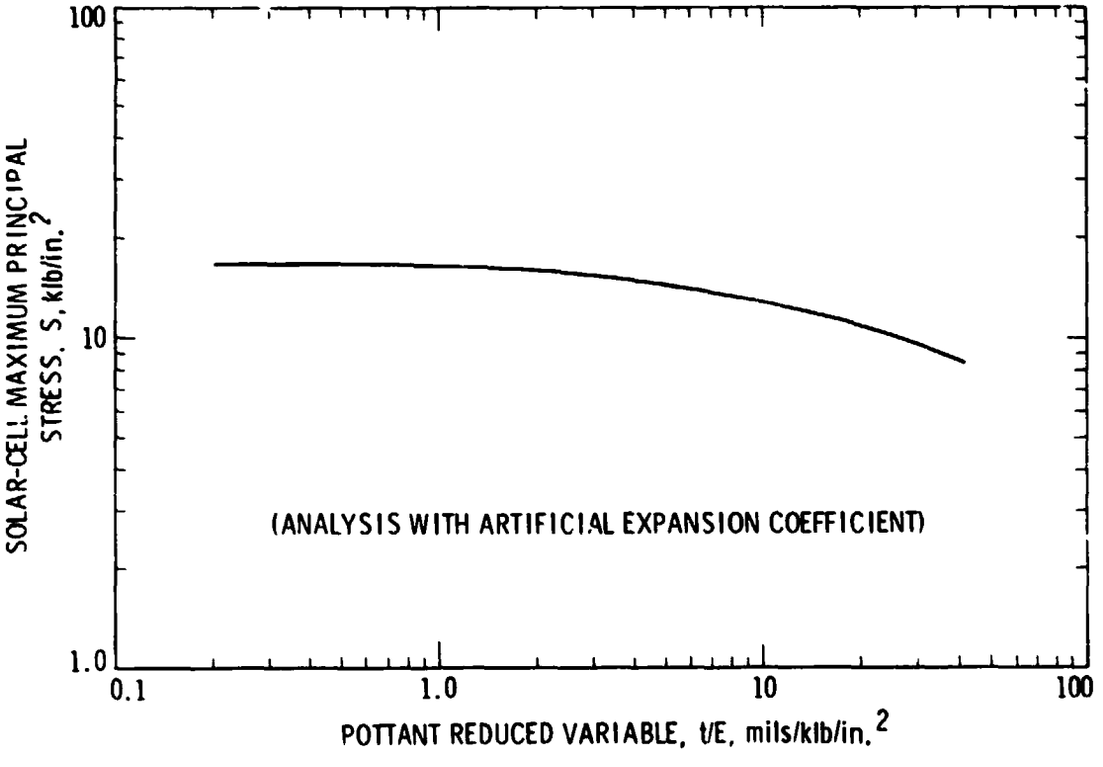

Figure A-5. Horizontally Shifted Computer Traces of Figure A-3 for Wood, Using Reduced Variable, t/E

curves reveals that they are still three segments of a common master curve. In earlier work at JPL, using computer techniques to predict stress distributions throughout modules generated by thermal-expansion differences, a term called thermal stiffness was observed to be a variable in the computer programs. For any given material, the thermal stiffness is the product of its Young's modulus and thermal-expansion coefficient. As a trial term for the reduced-variable scheme, the thermal stiffness of each of the three structural panels (glass, wood, and steel) were calculated, with the product term expressed as $M\alpha$, where M is the Young's modulus of the structural panel and α is its corresponding expansion coefficient.

Using the thermal-stiffness values, four trial reduced-parameter terms were calculated, two for the ordinate and two for the abscissa: $S\alpha M$, $S/\alpha M$, $t\alpha M/E$, and $t/\alpha ME$. The best fit occurred with the third term, $t\alpha M/E$, which resulted in a horizontal shifting of the three composite curves (Figures A-2, A-4, and A-5) to the vertical alignment shown in Figure A-6.

Finally, to merge these three curves vertically into a common master curve, it was observed from the two computer calculations done on the wooden panel that the asymptotic levels of the solar-cell tensile stress S were essentially different by a multiple of 10. Because the only difference between these two calculations for the wooden panel involved the use of expansion coefficients α, which differed by a multiple of 10, it was reasoned that the reduced-variable term for the ordinate involved at least the form S/α. Use of this reduced-ordinate variable helped, but did not completely achieve the

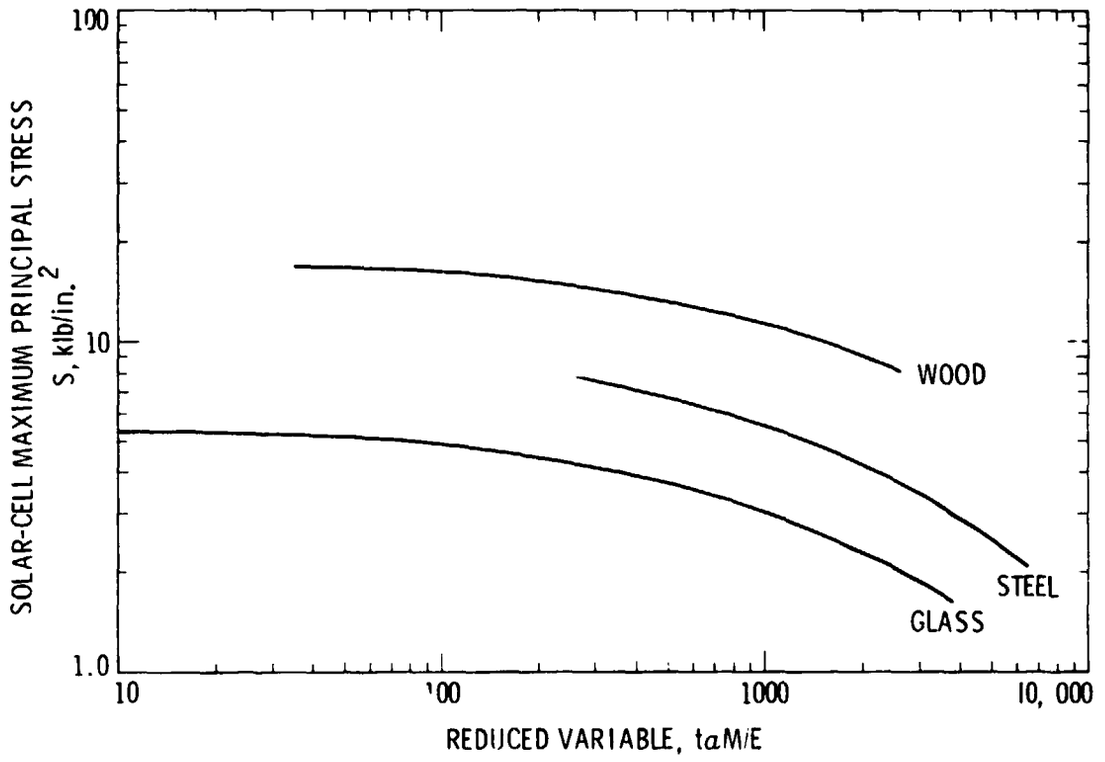

Figure A-6. Horizontally Shifted Computer Traces of Figures A-2, A-4, and A-5 for Steel, Glass, and Wood Using the Reduced Variable $t\alpha M/E$

desired vertical merging of the three curves. Thereafter, the effort involved trial-and-error combinations of parameters, finally resulting in identification of the term $S/\alpha M^{1/3}$, which did achieve a vertical merging of the three curves into a common master curve.

The resulting master curve, plotted with the reduced variables $S/\alpha M^{1/3}$ vs $t\alpha M/E$, is shown in Figure A-7. Although all of the computer-predicted log-log traces can be observed to be segments of this composite master curve, the validity of the reduced parameters has not been verified. The Spectrolab computer program also indicates that the level of the solar-cell tensile stress S is directly proportional to the temperature difference ΔT. Thus, the reduced-ordinate variable can be alternately expressed as $S/\alpha M^{1/3}\Delta T$, with appropriate rescaling on Figure A-7 of the numerical values of the ordinate (i.e., decreased by a multiple of 100).

The master curve, if valid, can be used to estimate solar-cell tensile stresses for two technical situations: aluminum panels and the hygroscopic expansion of wood.

1. Aluminum Panel

The Young's modulus M for aluminum is 10^7 lb/in.^{2}, and its expansion coefficient α is 24 x 10^{-6} $^oC^{-1}$. Using these values, log-log traces of solar-cell tensile stress S vs pottant thickness t can be generated from the

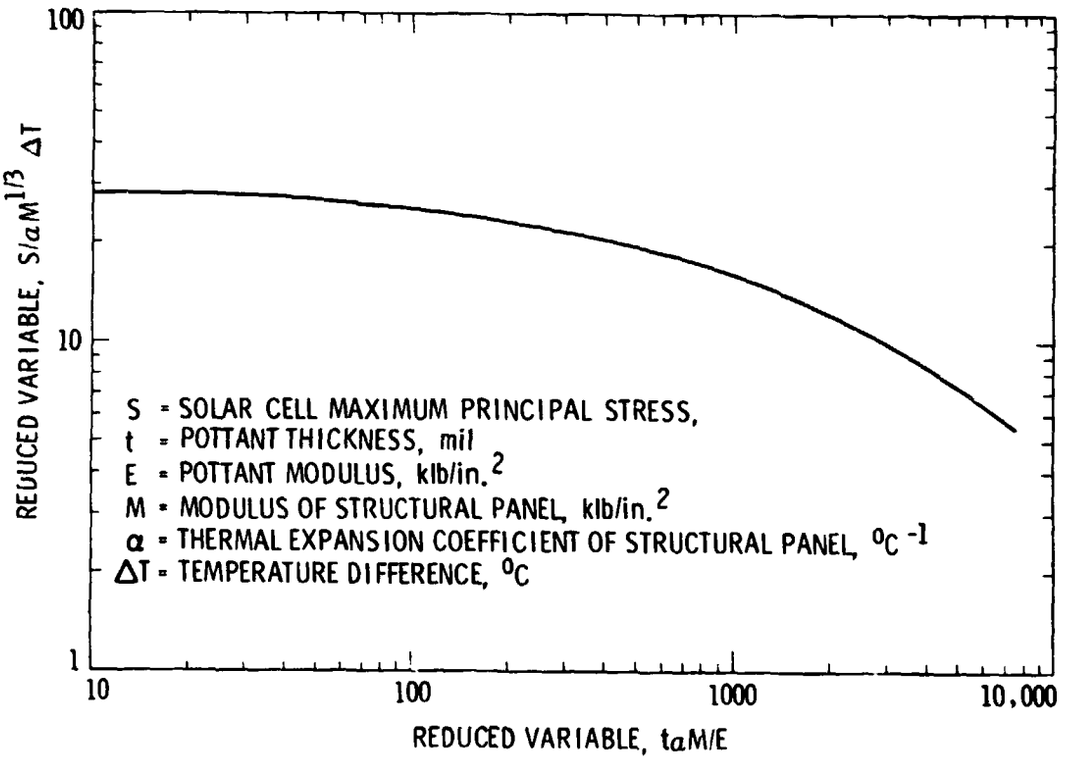

Figure A-7. Master Curve for Thermal Stress Analysis

master curve for a temperature difference of 100°C. The resulting log-log traces for four levels of the Young's modulus of the pottant, E = 500 lb/in.^{2}, 1000 lb/in.^{2}, 2000 lb/in.^{2}, and 5000 lb/in.^{2}, are shown in Figure A-8.

Examination of these predicted log-log traces indicates that aluminum is worse than glass, wood, or steel in the level of tensile stresses generated in solar cells from thermal-expansion differences. This is intuitively expected because of the high thermal expansion value for aluminum. Assuming that the allowed solar-cell tensile-stress-in-tension is 5000 lb/in.^{2}, it is predicted that almost 7 mils or more of a pottant with a Young's modulus of 500 lb/in.^{2} is needed. RTV silicones typically have a Young's modulus that is about this value, and these predicted results may suggest a partial explanation for the occurrences of solar-cell cracking in early-version commercial modules using RTV silicone pottants and aluminum panel substrates. Lastly, the use of a pottant with a Young's modulus of 1000 lb/in.^{2}, such as EVA, would require that the pottant thickness be at least 14 mils, and higher-modulus pottants would have to be used in correspondingly higher thicknesses.

2. Hygroscopic Expansion of Wood

The hygroscopic-expansion coefficient of hardboard is reported to be 50 x 10^{-6} in. % RH, compared with its thermal-expansion coefficient of 7.2 x 10^{-6} in.°C. Sections III and IV described how unprotected hardboards

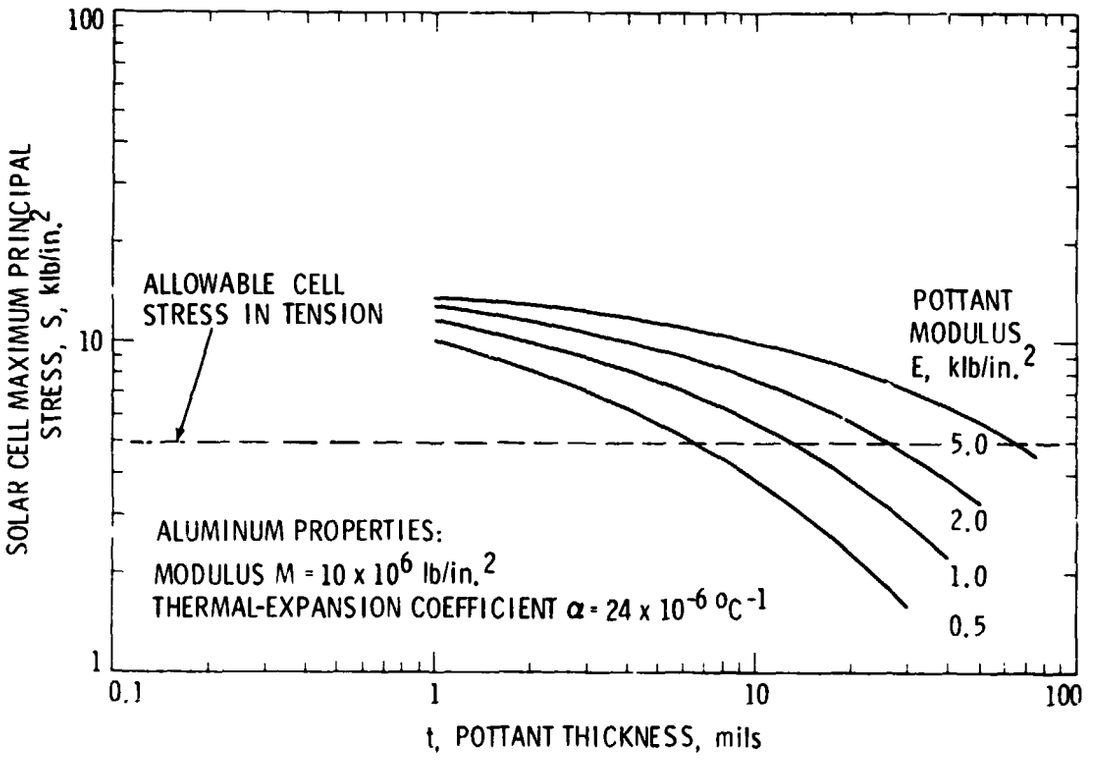

Figure A-8. Predicted Stresses of Encapsulated Silicon Solar Cells Using the Figure A-7 Master Curve Resulting from Thermal-Expansion Differences in an Aluminum Substrate Module for a ΔT of 100°C

dry out and shrink during vacuum-bag lamination, and regain moisture and expand with exposure to the ambient atmosphere. Actual experiences with hardboard modules fabricated with EVA ($E \approx 1000$ lb/in.^{2}) with vacuum-bag lamination are yielding a high incidence of solar-cell cracking.

A prediction of the tensile stresses developed in solar cells from the hygroscopic expansion of wood can be generated from the master curve by using the hygroscopic-expansion coefficient and 100% RH instead of 100°C. Formally, this is equivalent to considering that the wooden panel has a thermal-expansion coefficient α of 50×10^{-6}°C^{-1}.

The predicted log-log traces for three levels of Young's modulus of the pottant, E = 500 lb/in.^{2}, 1000 lb/in.^{2}, and 2000 lb/in.^{2}, are plotted in Figure A-9 for a relative-humidity excursion of 100% RH (i.e., dry wood to saturated wood).

The predicted solar-cell tensile stresses tend to be high, requiring very thick layers of pottant material to reduce the generated tensile stresses to acceptable levels. A pottant with a Young's modulus of 500 lb/in.^{2} would have to have a predicted thickness of about 33 mils; a pottant, such as EVA, with a Young's modulus of about 1000 lb/in.^{2} would have to be at least 66 mils thick. Even if the relative-humidity excursion after vacuum-bag lamination were only up to 50% RH, which is more realistic, the thickness of a pottant, such as EVA,

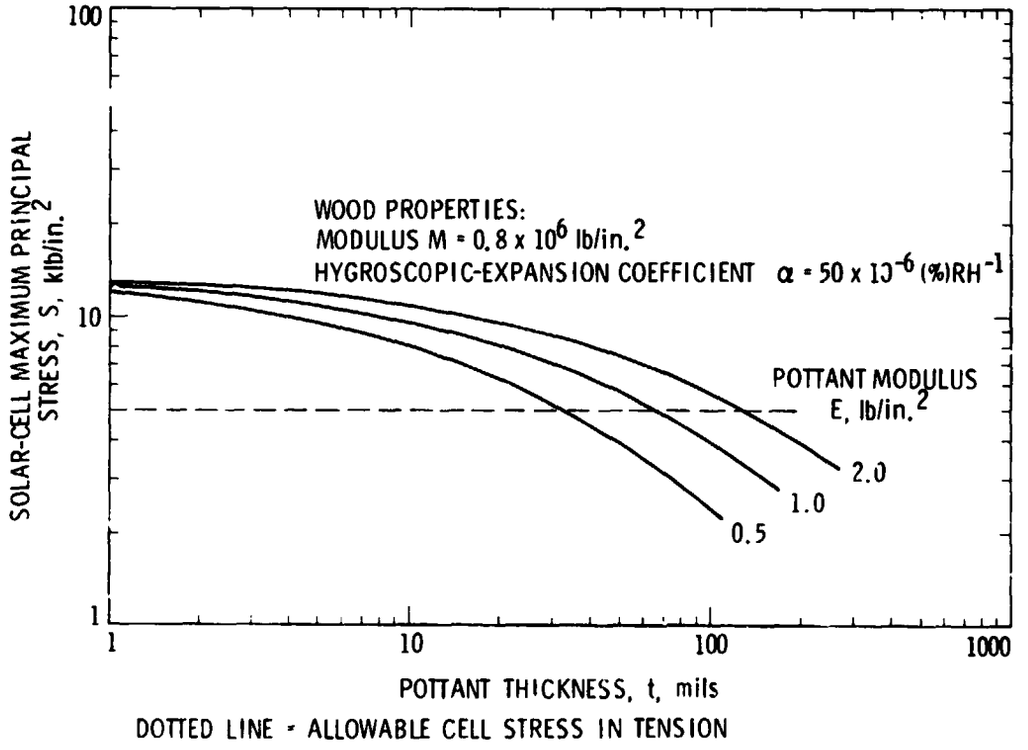

Figure A-9. Predicted Stresses in Encapsulated Silicon Solar Cells, Using the Figure A-7 Master Curve, Resulting from Hygroscopic Expansion of a Hardboard Panel from 0% to 100% Relative Humidity

would still have to be at least 33 mils. The experimental hardboard modules, presently fabricated with EVA, use no more than 18 mils of EVA between the cells and the wood.

The predicted results and actual observations of a high incidence of solar-cell cracking with EVA-hardboard modules fabricated by vacuum-bag lamination, is the main thrust behind Encapsulation Task activities to find practical methods of protecting the wood against dry-out during vacuum-bag lamination.

3. Deflection Master-Curve Analysis

The linear computer traces for deflection analysis, Figures 3-13, 3-16, and 3-17, are replotted log-log in Figures A-10, A-11, and A-12 for glass, steel, and wood, respectively. Trial shifting of all of the log-log traces, horizontally and vertically, showed that a composite master curve could be generated, but unlike the computer traces for thermal expansion, it was not found readily possible to establish a set of reduced-variable parameters that achieves mathematical merging of the deflection traces into a composite master curve. Partial clues for some of the terms in the reduced-variable parameters could be determined.

Three of the four log-log traces for glass, associated with a Young's modulus for the pottant of 0.5 ks, 1.0 ks, and 2.5 ks± could be shifted horizontally into a composite curve, using the reduced variable t/E, as shown in

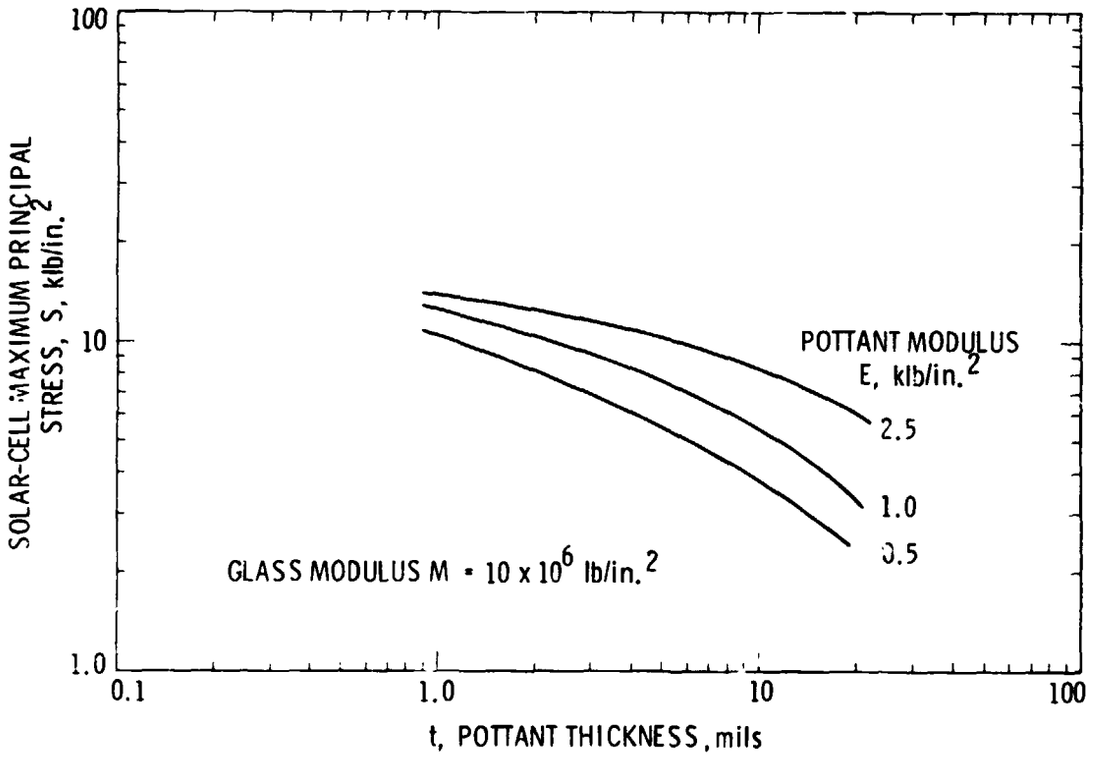

Figure A-10. Log-Log Plots of the Computer Traces Given in Figure 3-13 for a Glass-Superstrate Module

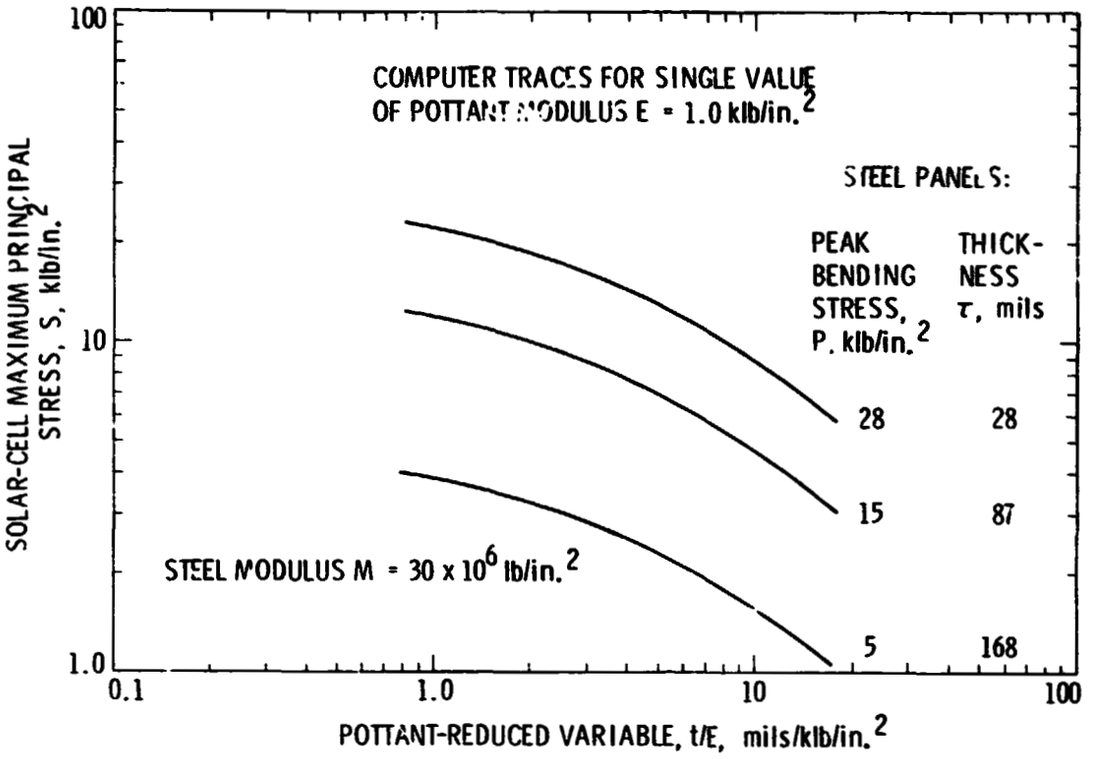

Figure A-11. Log-Log Plots of the Computer Traces Given in Figure 3-16 for a Steel-Substrate Module

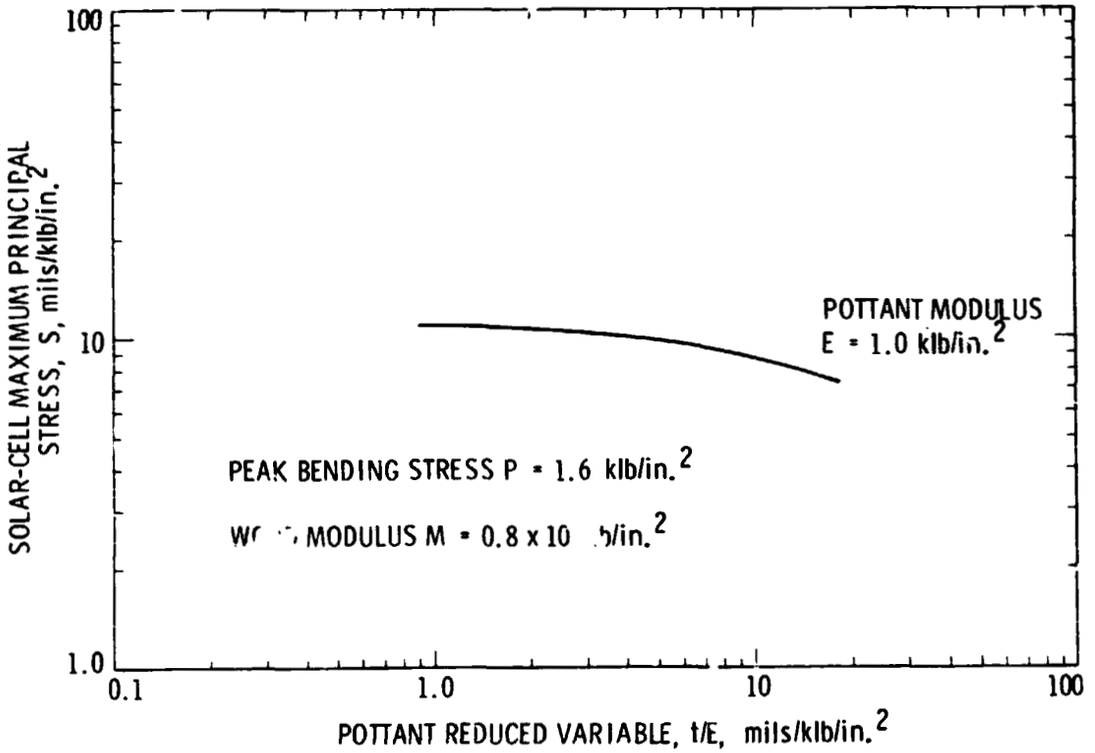

Figure A-12. Log-Log Plot of the Computer Trace Given in Figure 3-17 for the Unribbed Wooden-Substrate Module

Figure A-13. The fourth trace, associated with a Young's modulus for the pottant of 50 klb/in.^{2}, shifted to the left and did not merge with the other three. From observation of the behavior of this fourth trace, it is inferred that at this level of modulus, the pottant contributes deflection stress to the solar cells, rather than damping stress generated by deflection of the glass.

For steel (Figure A-11), the three log-log traces are associated with solar-cell deflection stresses for three different thicknesses of steel plate, and for a single and constant Young's modulus of the pottant of 1.0 klb/in.^{2}. The reduced variable t/E is assumed to be valid for the abscissa, and therefore for a value of E = 1.0 klb/in.^{2}, the log-log trace is properly positioned horizontally for the reduced variable t/E. Vertical merging of these three log-log traces into a composite curve was done in Figure A-14, by using a reduced parameter S/P, where S is the solar-cell stress in klb/in.^{2} and P is the peak bending stress of the steel plate, also in klb/in.^{2}. The plate thicknesses τ associated with the peak bending stresses are included in Figure A-11. Trial and error identified a simple connective relationship between P and τ:

$$P = 43.8 - 3\tau^{1/2} \qquad (1)$$

where P is expressed in klb/in.^{2} and τ is the plate thickness in mils.

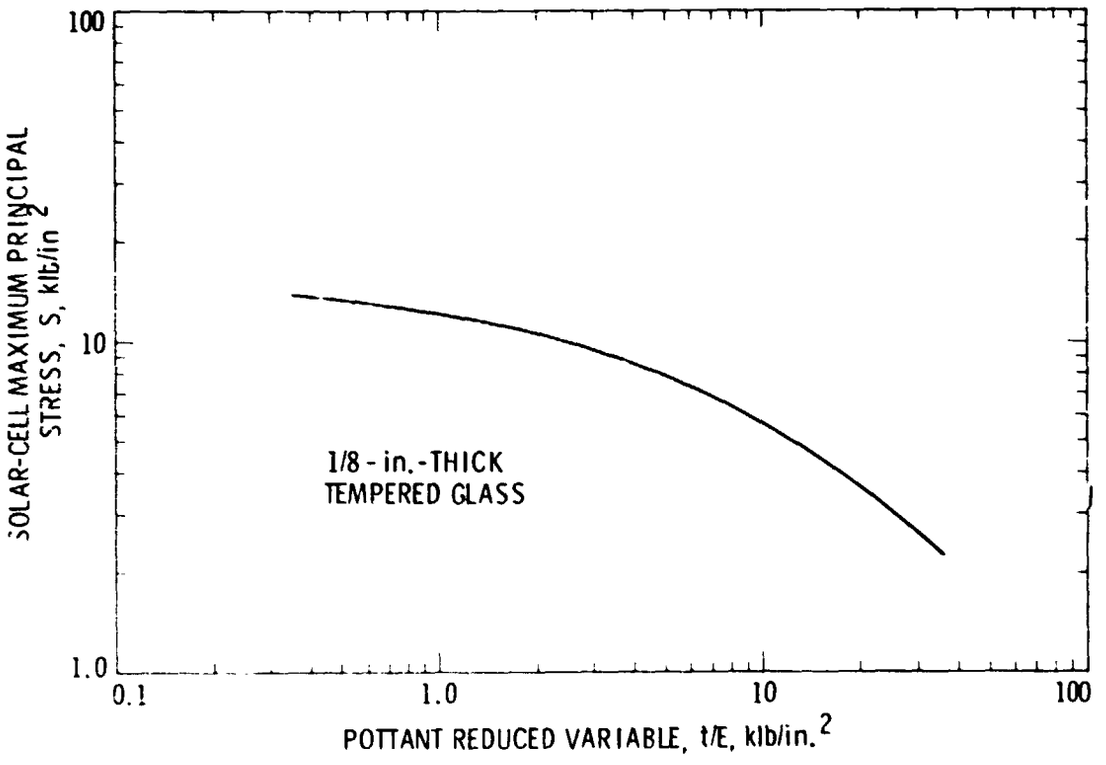

Figure A-13. Horizontally Shifted Computer Traces of Figure 3-13 for Glass Using the Reduced Variable, t/E

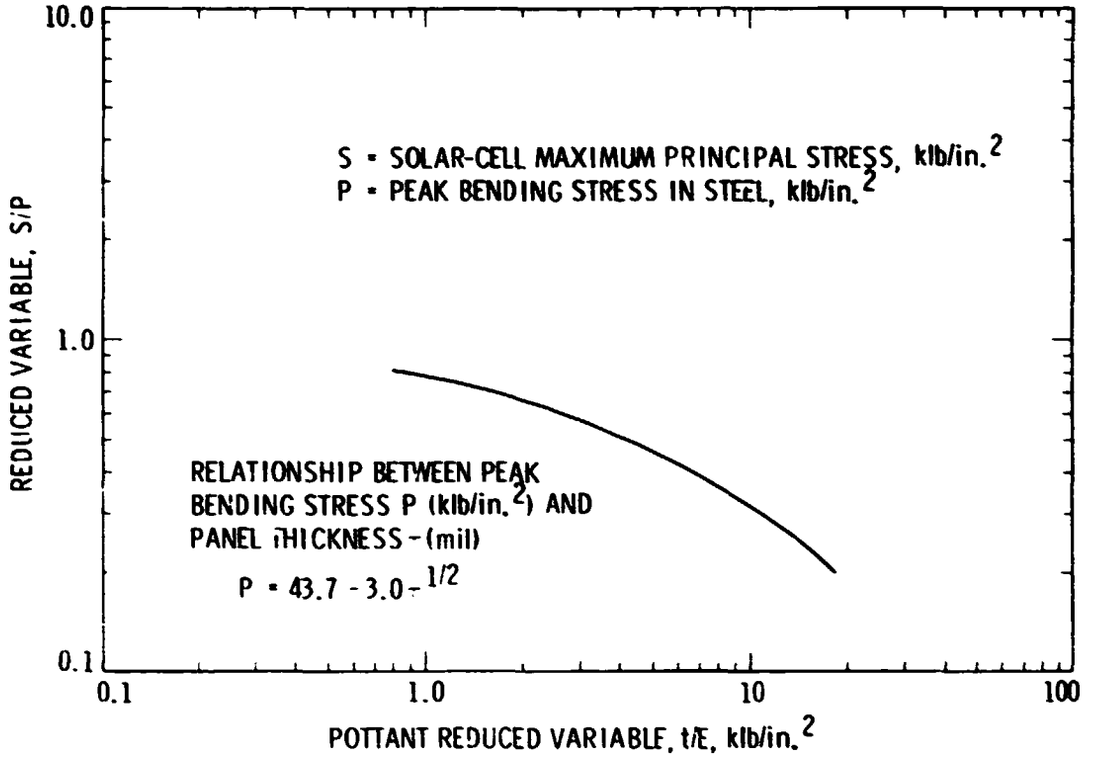

Figure A-14. Vertically Shifted Computer Traces of Figure A-11 for Steel Using the Reduced Variable, S/P

Further efforts to identify trends for the reduced-variable expressions were not rewarding. This was primarily due to lack of sufficient parametric studies on the comptuer, and also to an ignorance of key terms and/or combinations of terms for deflection analysis that would be expected in reduced-variable schemes for deflection (e.g., the thermal-stiffness term $M\alpha$ which was used in the thermal-stress mater curve).

To illustrate that the three composite traces for wood, glass, and steel (Figures A-12, A-13, and A-14) are segments of a common master curve, the curves were first shifted horizontally (Figure A-15), and then vertically to a common curve in the master curve of Figure A-16, so this curve could be used to broaden the t/E scale for each of the three panels. For example, using Figures A-14, Figure A-16, and Equation (1) for unribbed steel panels, predictions of solar-cell-bending stresses can be generated for any combintations of pottant modulus and thickness, and thickness of the steel panel.

4. Future Work

The concept of generating reduced-variable master curves to enable desktop predictions of stresses developed in encapsulated solar cells that results from thermal expansion and contraction and out-of-plane deflections of modules is an attractive objective. The preliminary efforts described in this

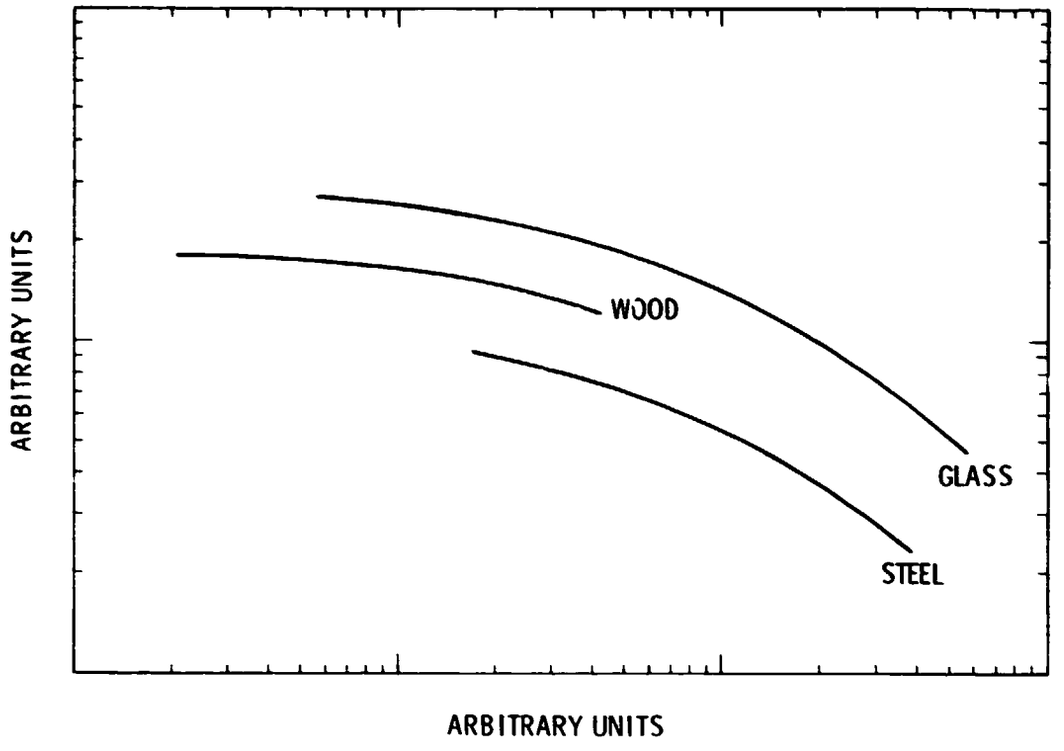

Figure A-15. Horizontally Shifted Composite Computer Traces of Figures A-12, A-13, and A-14 for Wood, Glass, and Steel to Demonstrate Potential of Superposition to a Master Curve

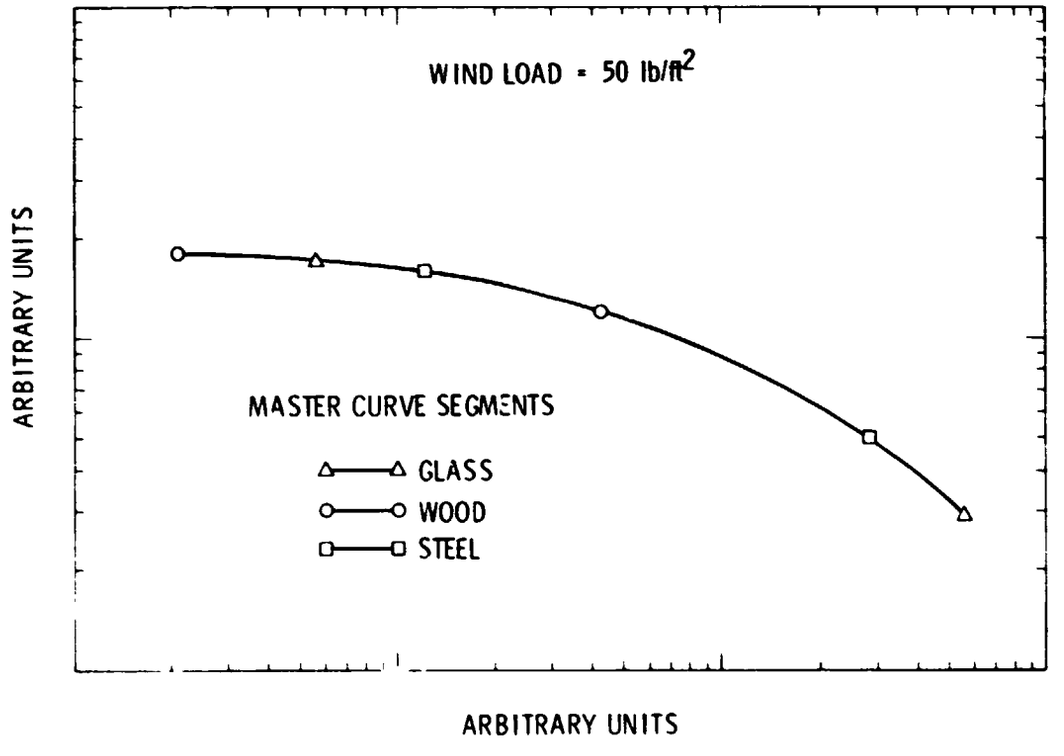

Figure A-16. Master Curve for Deflection Stress Analysis

appendix, using computer traces of predicted stresses for a few test cases, indicated that such an objective may be possible. Plans include expansion of the computer studies to investigate more fully some of the parameters previously studied, and to introduce new parameters of technical interest into the computer programs. The parameter studies will be preferentially directed toward master-curve development to assess expeditiously the proper placement of the parameters into reduced-variable terms. Table A-1 shows the parameters being considered for study; some of the parameters given in this table have already been assessed, as reported in this appendix.

Table A-1. Structural Parameters Considered for Reduced-Variable Master-Curve Studies

Component	Parameter
Pottants	Modulus Thickness Thermal-expansion coefficient Hygroscopic-expansion coefficient
Solar cells	Modulus Dimensions (thickness, width, length) Thermal-expansion coefficient Intercell spacing Geometry (i.e., round, square, rectangle, etc.)
Panels	Modulus Dimensions (thickness, width, length) Thermal-expansion coefficient Hygroscopic-expansion coefficient